ORNL-5893
ENDF-330

ornl

OAK
RIDGE
NATIONAL
LABORATORY

UNION
CARBIDE

Neutron Transmission and Capture Measurements and Analysis of ^{60}Ni from 1 to 450 keV

C. M. Perey
J. A. Harvey
R. L. Macklin
R. R. Winters
F. G. Perey

OPERATED BY
UNION CARBIDE CORPORATION
FOR THE UNITED STATES
DEPARTMENT OF ENERGY

Printed in the United States of America. Available from
National Technical Information Service
U.S. Department of Commerce
5285 Port Royal Road, Springfield, Virginia 22161
NTIS price codes—Printed Copy: A05; Microfiche A01

This report was prepared as an account of work sponsored by an agency of the United States Government. Neither the United States Government nor any agency thereof, nor any of their employees, makes any warranty, express or implied, or assumes any legal liability or responsibility for the accuracy, completeness, or usefulness of any information, apparatus, product, or process disclosed, or represents that its use would not infringe privately owned rights. Reference herein to any specific commercial product, process, or service by trade name, trademark, manufacturer, or otherwise, does not necessarily constitute or imply its endorsement, recommendation, or favoring by the United States Government or any agency thereof. The views and opinions of authors expressed herein do not necessarily state or reflect those of the United States Government or any agency thereof.

ORNL-5893
ENDF-330

Engineering Physics Division

NEUTRON TRANSMISSION AND CAPTURE MEASUREMENTS AND ANALYSIS OF ^{60}Ni FROM 1 TO 450 keV

C. M. Perey, J. A. Harvey, R. L. Macklin, R. R. Winters,* and F. G. Perey

Manuscript Completed - September 30, 1982
Date Published - November 1982

*Denison University, Granville, Ohio

Prepared by the
OAK RIDGE NATIONAL LABORATORY
Oak Ridge, Tennessee 37830
operated by
UNION CARBIDE CORPORATION
Under Contract No. W-7405-eng-26
for the
Division of Basic Energy Sciences
U.S. DEPARTMENT OF ENERGY

CONTENTS

NEUTRON TRANSMISSION AND CAPTURE MEASUREMENTS AND ANALYSIS OF ^{60}Ni FROM 1 TO 450 keV

C. M. Perey, J. A. Harvey, R. L. Macklin, R. R. Winters, and F. G. Perey

ABSTRACT

High-resolution transmission and capture measurements of ^{60}Ni-enriched targets have been made at the Oak Ridge Electron Linear Accelerator (ORELA) from a few eV to 1800 keV in transmission and from 2.5 keV to 5 MeV in capture. The transmission data from 1 to 450 keV were analyzed with a multi-level R-matrix code which uses the Bayes' theorem for the fitting process. This code provides the energies and neutron widths of the resonances inside the 1- to 450-keV region as well as a possible parameterization for outside resonances to describe the smooth cross section in this region. The capture data were analyzed with a least-squares fitting code using the Breit-Wigner formula. From 2.5 to 450 keV, 166 resonances were seen in both sets of data. Correspondence between the energy scales shows a discontinuity around 300 keV which makes the matching of resonances at higher energies difficult. Eighty-nine resonances were seen in the capture data only. Average parameters for the 30 observed s-wave resonances were deduced. The average level spacing D_o was found to be equal to 15.2 $\pm$ 1.5 keV, the strength function, S_o, equal to (2.2 $\pm$ 0.6) $\times$ 10^{-4} and the average radiation width, Γ_γ, equal to 1.30 $\pm$ 0.07 eV. The staircase plot of the reduced level widths and the plot of the Lorentz-weighted strength function averaged over various energy intervals show possible evidence for doorway states. The level densities calculated with the Fermi-gas model for $\ell = 0$ and for $\ell > 0$ resonances were compared with the cumulative number of observed resonances, but the analysis is not conclusive . The average capture cross section as a function of the neutron incident energy is compared to the tail of the giant electric dipole resonance prediction.

---

1. INTRODUCTION

The cross sections of structural materials in the iron region are important in reactor applications because of the stainless steels that are used. The recent ENDF/B-V evaluation[1] of the nickel resonance parameters is based on measurements taken prior to 1971 and is identical to ENDF/B-IV and ENDF/B-III versions.

High-resolution total and capture measurements on the nickel isotopes were performed at ORELA in the resonance region. This report presents the analysis of the ^{60}Ni data and compares the results with previous measurements.

The experimental procedures used in the transmission measurements are reported in Sect. 2 along with a discussion of the various background and deadtime corrections. Details on the multilevel R-matrix analysis of the transmission data are given in Sect. 3. The code MULTI, used in a preliminary analysis of the data, is compared with the code SAMMY. Both codes make use of the multilevel R-matrix formalism. However, the code MULTI does a least-squares fit of the data whereas the code SAMMY uses Bayes' theorem.

The experimental conditions of the capture measurements are given in Sect. 4 with a discussion of the various corrections applied to the raw data. The capture data analysis made with a least-squares fitting code using the Breit-Wigner formalism is reported in Sect. 5.

Section 6 deals with problems encountered in the energy scales of the two sets of data. In Sect. 7, the resonance parameters obtained from the analysis of both data sets are reported and their uncertainties discussed. Comparisons with previously reported resonance parameters for ^{60}Ni are made in Sect. 8. The behavior of the average resonance parameters is analyzed in Sect. 9. Possible evidence for doorway states is discussed.

2. TRANSMISSION MEASUREMENTS AND DATA PROCESSING

The transmission measurements were made by the time-of-flight technique using neutron pulses from the ORELA water-moderated tantalum target and a 78.203-m flight path. Measurements were made on two samples of ^{60}Ni enriched to 99.7% with thicknesses of 0.00736 and 0.0744 atoms/barn. At the location of the samples 9 m from the neutron target, the neutron beam was collimated to a diameter of 2.4 cm. A neutron house monitor was used to normalize the sample-in sample-out data to compensate for variations in the neutron production rate during the runs which were of a few days duration. Two different neutron detectors and techniques were used to cover the energy region investigated.

For the energy region from 200 eV to 240 keV, transmission data were acquired using a 1.3-cm-thick, 11-cm-diam ^{6}Li glass scintillation detector. The electron beam burst was 40 nsec wide, producing a beam power on the target of 40 kW at 800 Hz and the moderator distance (for resolution) was 2.0 cm. Measurements were made on both samples, the thicker one mainly for the higher-energy region and the thinner one for the low-energy resonances. Two filters were inserted in the beam at 5 m: a 1-g/cm^2 ^{10}B filter (1/e transmission at $\sim$1 keV) to eliminate low-energy neutrons from preceding bursts, and a 0.6-cm-thick lead filter to reduce the gamma flash. The ^{6}Li glass scintillator was mounted on an RCA-4522 photomultiplier tube which was gated off during the gamma flash and the succeeding $\sim$8 μsec. During the measurements three sources of backgrounds were monitored: (1) a background arising from 2.2-MeV gamma rays produced by neutron capture in the water moderator of the target which has a 17.6-μsec half-life time dependence and is the main background at early times and amounts to $\sim$3%; (2) a time-independent room background which is the dominant background at long times; and (3) a background produced by neutrons scattered by the detector, air around the detector, and the concrete walls and floor of the detector station which later return to the detector. This background is estimated from blacking-out resonances in ^{60}Ni and, at lower energies, from an auxiliary measurement using a ^{238}U sample. Additional details on these backgrounds are reviewed in ref. 2.

By use of a 2-cm-thick, 7.5-cm-diam NE-110 proton recoil scintillation detector,[3] transmission data were obtained from 4 to 240 keV, overlapping the ^{6}Li data, and also extended upward to 1770 keV. The phototube was gated off for $\sim$5 μsec during and after the gamma flash to reduce interference from afterpulsing. The electron beam burst was 10-nsec wide producing a beam power of 16 kW at 1000 Hz. The energy resolution, $\Delta E/E$, obtained with the NE-110 scintillator was 0.1% below 100 keV and 0.35 $\sqrt{E(\mathrm{MeV})}$ % at higher energies. Both ^{60}Ni samples were measured under these conditions. Two filters were inserted in the neutron beam at 5 m: the 1-g/cm^2 ^{10}B filter and a 0.6-cm-thick ^{238}U filter. Three sources of background were present: (1) gamma rays in the beam produced by neutron capture in the water moderator, (2) a constant beam-independent background, and (3) a 478-keV gamma ray from the ^{10}B(n,$\alpha\gamma$) reaction produced from the absorption of neutrons by the boron in the Pyrex face of the photo-multiplier and moderated by the NE-110 plastic scintillator. To aid in the determination of these

backgrounds and to optimize the signal to background ratio, four separate pulse-height spectra were recorded. The first spectrum is for neutrons ≤200 keV and the second for neutrons from ~200 to ~600 keV. The 478-keV gamma background from $^{10}B(n,\alpha\gamma)$ is mostly seen in the third spectrum from 0.6 to 2 MeV. The time-dependent 2.2-MeV gamma rays from the water moderator falls mainly in spectrum 4. The contribution of these backgrounds to the lower pulse height spectra is determined by two auxiliary experiments: (1) using a ^{7}Be source which emits the 478-keV gamma ray, and (2) by inserting a thick polyethylene filter which removes neutrons but allows gamma rays from the target to be transmitted. The contribution of all these backgrounds was <1% over the energy region where the data are analyzed. Additional details on corrections for these backgrounds are given in refs. 2 and 4.

All time-of-flight data were acquired using an EG&G time digitizer and stored in one of the ORELA Data Acquisition Computers.[5] The data were first corrected for the deadtime (1104 nsec) of the time digitizer and then corrected for the backgrounds discussed above. The transmission and total cross section are computed from the background corrected sample-in sample-out ratio normalized to the same monitor counts. Results, up to 450 keV, are shown in Figs. 1 to 7.

3. TRANSMISSION DATA ANALYSIS

The transmission data were first analyzed with the multilevel R-matrix least-squares fitting code MULTI.[6] When this analysis and the analysis of the capture data described in Sect. 5 were completed, the code SAMMY,[7] a modified version of MULTI, became available and has been used to obtain the final fits to the transmission data and the corresponding neutron widths reported here. Because the results obtained with the code MULTI were used as input to the capture analysis and to the transmission analysis with the code SAMMY, some details of this preliminary analysis are given below.

In both codes the cross section is Doppler-broadened and resolution-broadened and is expressed as

$$\sigma_T = \Sigma\, \sigma_{nT} = 2\pi k^{-2} \sum_J g(J) Re(1-U^J_{nn}) \quad , \tag{3.1}$$

$$U^J_{nn} = e^{-2i\phi_\ell} \frac{1 - R^J_\ell(S_\ell - B^J_\ell - iP_\ell)}{1 - R^J_\ell(S_\ell - B^J_\ell + iP_\ell)} \tag{3.2}$$

and

$$R^J_\ell = \sum_\lambda \frac{\gamma_{\ell\lambda}\gamma_{\ell\lambda}}{E_\lambda - E - i\Gamma_{\gamma\lambda}/2} \quad . \tag{3.3}$$

Here R^J_ℓ is the R matrix; k is the neutron wave number, assuming that the only open channels are elastic neutron scattering and photon emission; and $\gamma_{\ell\lambda}$ and $\Gamma_{\gamma\lambda}$ are the neutron reduced width amplitude and the radiation width, respectively, for the λth resonance. The ϕ_ℓ, S_ℓ, B_ℓ, and P_ℓ represent the usual hard sphere phase shifts, shift factors, boundary conditions, and neutron penetrability, respectively. The codes used in this analysis give the neutron width, $\Gamma_{n\lambda}$, for each resonance which is related to the neutron reduced width amplitude, $\gamma_{\ell\lambda}$, by the relation

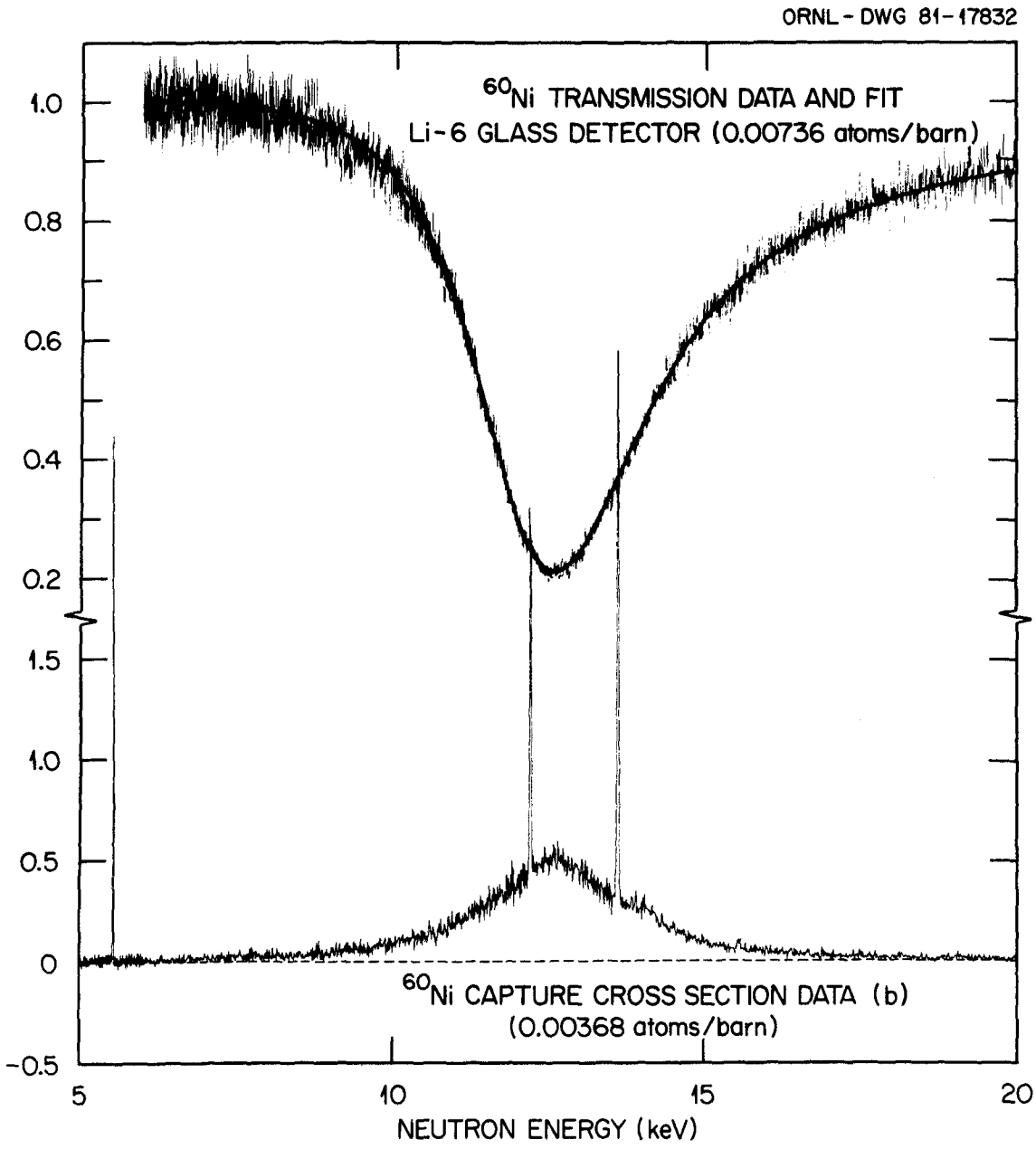

Fig. 1. Ni-60 transmission data and fit shown with the ^{60}Ni capture data from 5 to 20 keV.

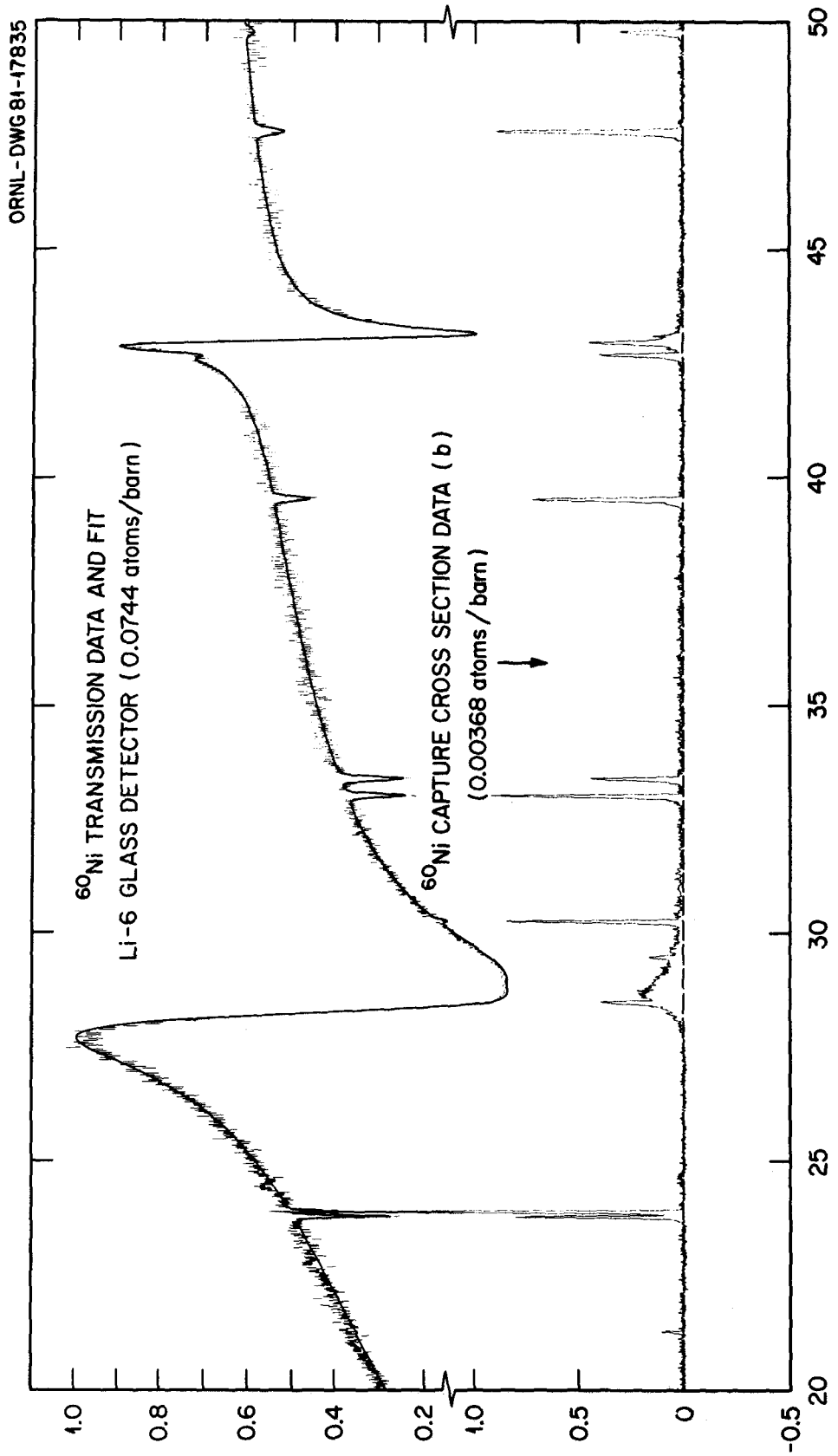

Fig. 2. Ni-60 transmission data and fit shown with the ^{60}Ni capture data from 20 to 50 keV.

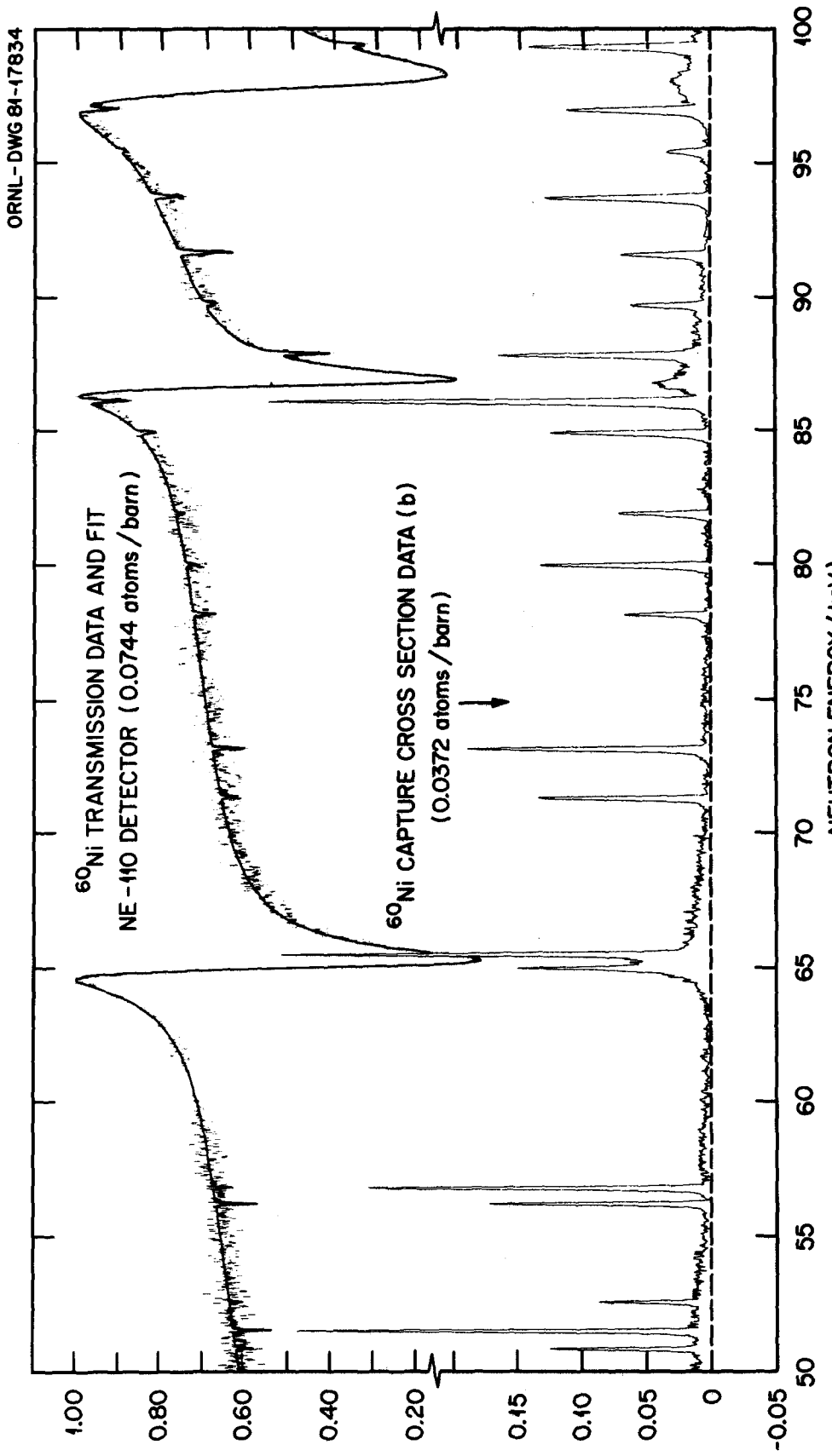

Fig. 3. Ni-60 transmission data and fit shown with the ^{60}Ni capture data from 50 to 100 keV.

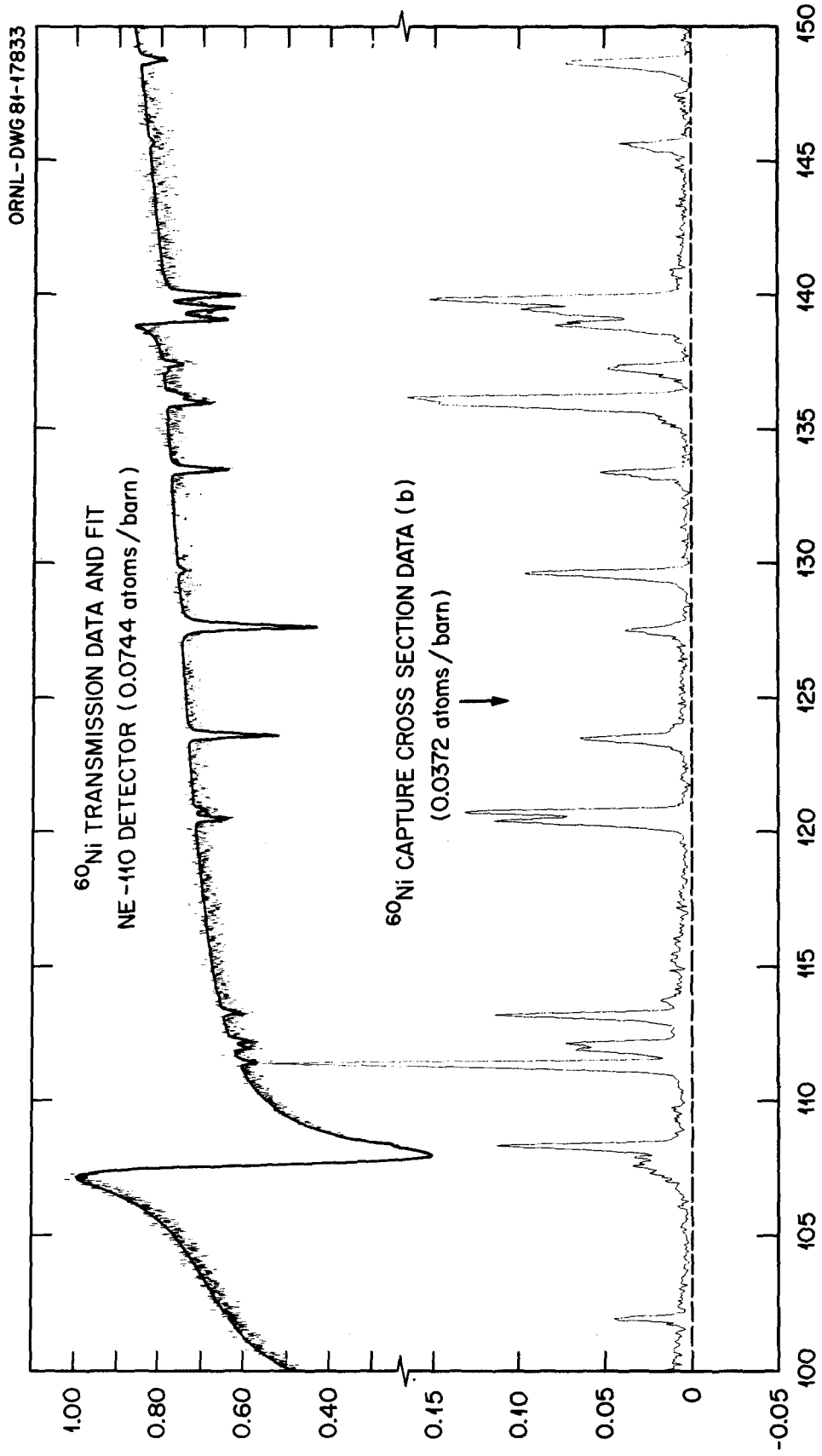

Fig. 4. Ni-60 transmission data and fit shown with the ^{60}Ni capture data from 100 to 150 keV.

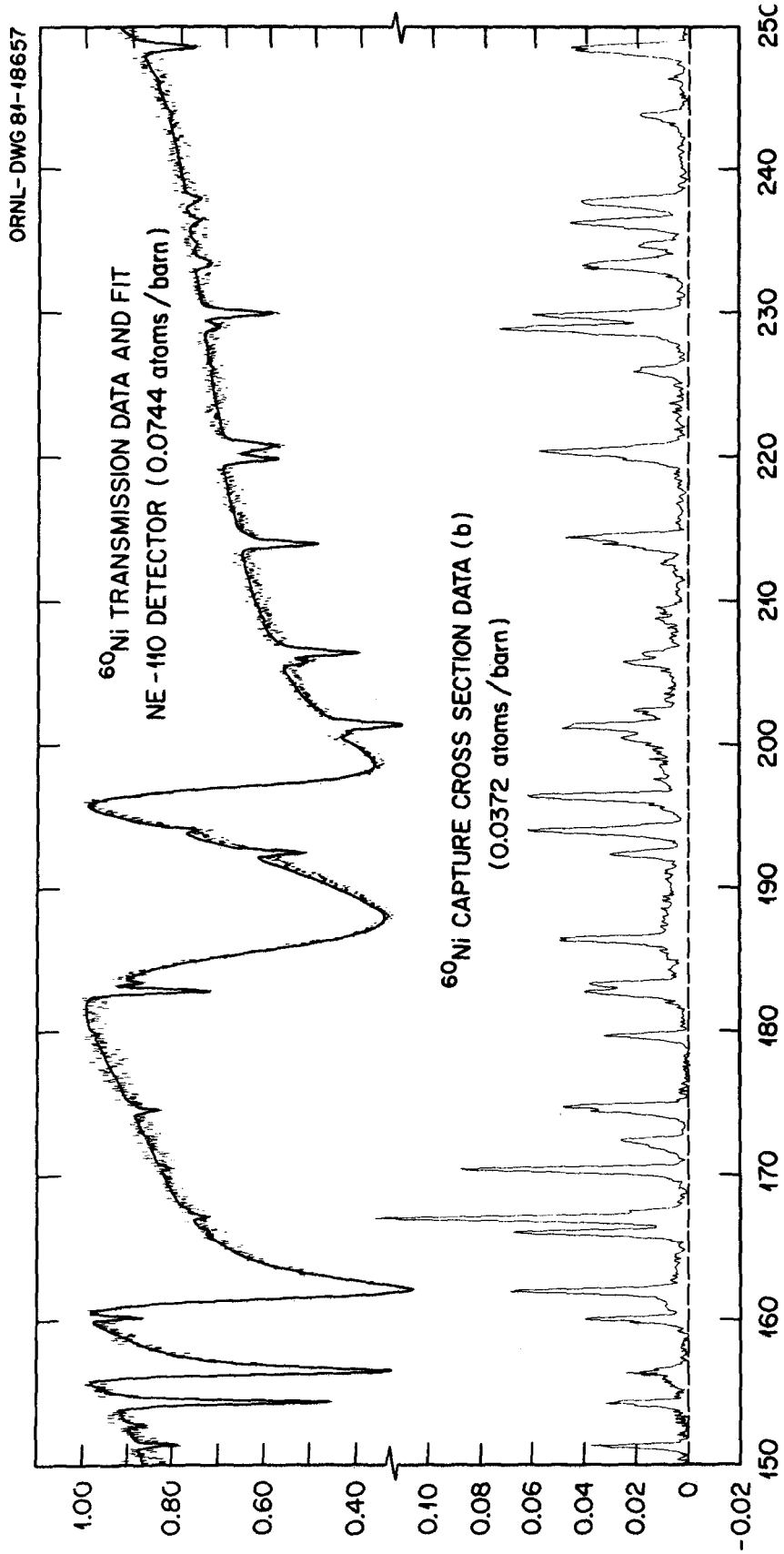

Fig. 5. Ni-60 transmission data and fit shown with the ^{60}Ni capture data from 150 to 250 keV.

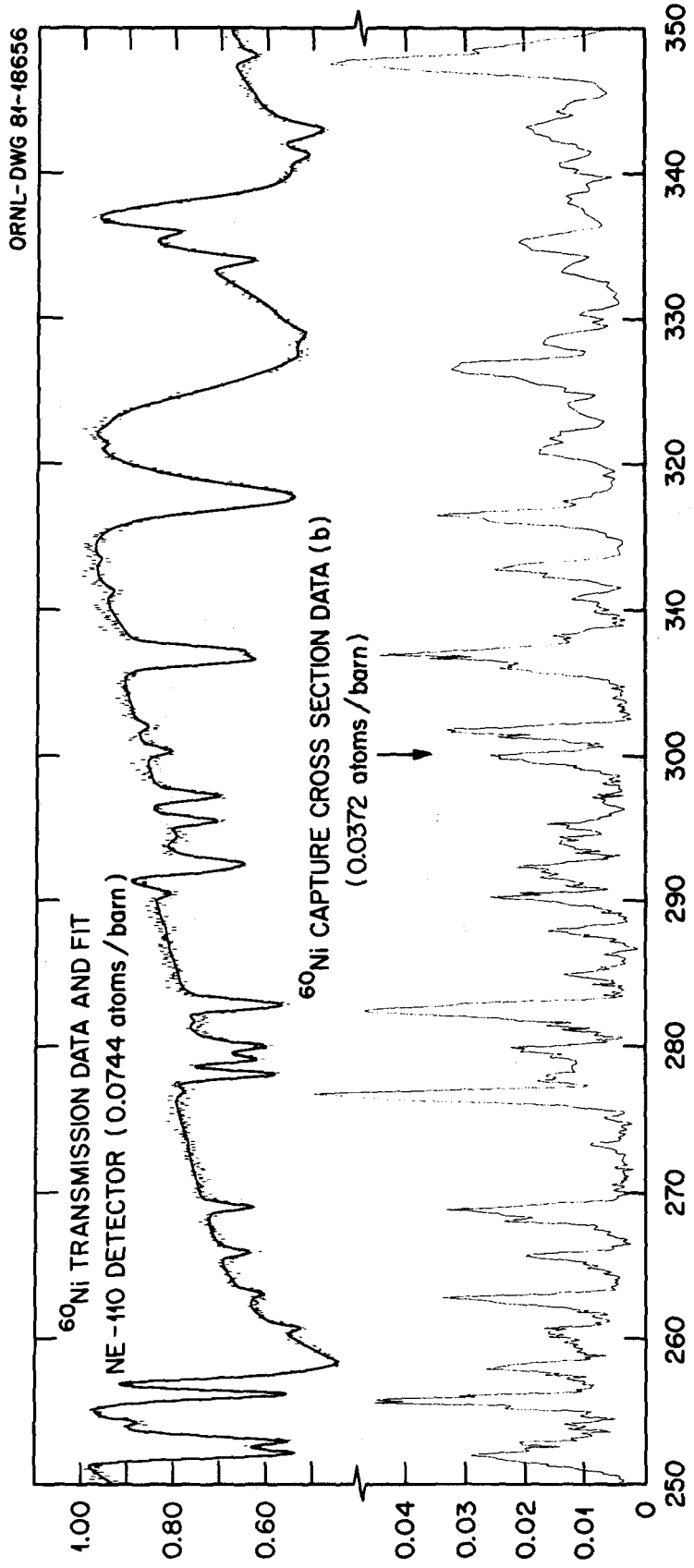

Fig. 6. Ni-60 transmission data and fit shown with the ^{60}Ni capture data from 250 to 350 keV.

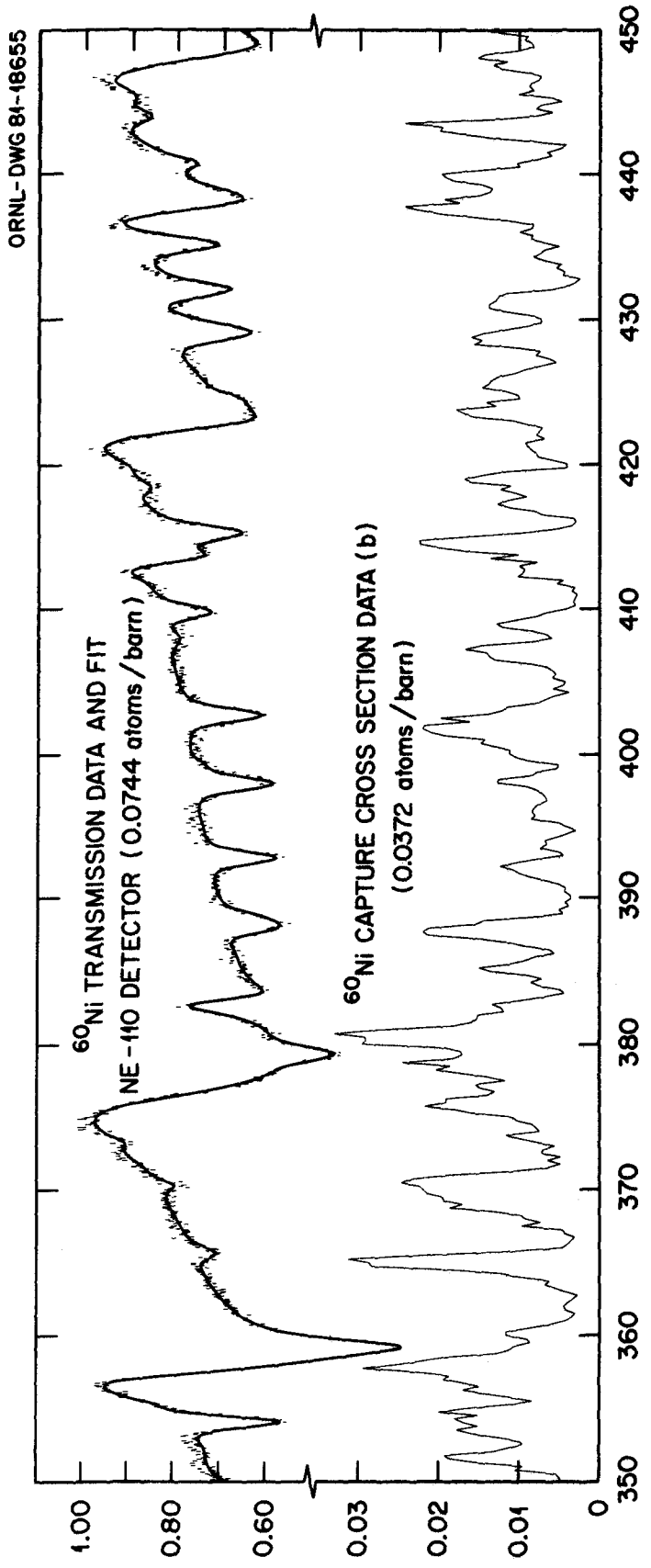

Fig. 7. Ni-60 transmission data and fit shown with the ^{60}Ni capture data from 350 to 450 keV.

$$\Gamma_{n\lambda} = 2\gamma_{\ell\lambda}^2 P_\ell \quad .$$

The first excited state at 1332.5 keV is well above the energy range of our analysis so inelastic scattering channels could be ignored.

In this work, S_ℓ and B_ℓ^J are set equal to zero as is conventionally done. The channel radius has been set equal to 6.0 fm from a preliminary analysis up to 150 keV where the radius was adjusted.

3.1 ANALYSIS WITH THE CODE MULTI

The transmission data were analyzed from 1 to 550 keV. In this energy range the original data files contained 25,000 channels. The uncertainties given are only the statistical ones. Uncertainties due to background and deadtime corrections were not included. These uncertainties would produce a correlation among the uncertainties in the data which could be handled by the code SAMMY but could not be handled by the code MULTI.

The transmission data analyzed between 1 and 50 keV were those obtained with the ^{6}Li detector. Data obtained with the thick sample of ^{60}Ni (0.0744 atoms/barn) were used from 1 to 6 keV and from 20 to 50 keV. From 6 to 20 keV, the data obtained with the thin sample (0.00736 atoms/barn) were analyzed. Above 50 keV, the data obtained with the NE-110 detector and the thick sample were analyzed.

Data files containing up to 1000 data points were generated through a data reduction averaging program[8] in which the averaging factor can be adjusted in any energy interval. This allows us to keep the minimum number of data points necessary to adequately define the resonances and also to greatly reduce the number of data points between resonances. Since all the data from 1 to 550 keV, even after averaging, could not possibly be fitted into a single run of the code MULTI, the data had to be broken up into data sets of various lengths, and the analysis performed iteratively.

Working with data sets of approximately 150-keV intervals, the parameters of the large s-waves and outside fictitious resonances were determined in order to approximately reproduce the main features of the transmission data. The fictitious resonances account for the tail of the unobserved resonances below 1 keV and above 550 keV. The detailed analysis was then conducted using smaller data sets (50 to 100 keV), which overlapped by 15 to 20 keV, in order to obtain a smooth theoretical curve in the complete range of energy. The energies of the fictitious resonances were kept at the values found earlier. However, their neutron widths, Γ_n, as well as the parameters of the resonances in the interval being analyzed were adjusted by the code for an optimum fit in each region.

The final set of parameters obtained with the code MULTI reproduced well the transmission data. However, this set is not unique since some of the uncertainties of these parameters are strongly correlated as shown in a quantitative manner in the results obtained with the code SAMMY and as reported in Sect. 7.

No attempt was made to determine the spin and parity of $\ell > 0$ resonances in the fitting process since the data resolution was always much larger than the neutron widths of the resonances required to fit the data. (See Table 1 for samples of neutron energy resolution.) Up to 260 keV, we were able to obtain good fits with any resonance having a statistical weight equal to one ($s_{1/2}$ and $p_{1/2}$ resonances). The shape of the $p_{1/2}$ and $p_{3/2}$ resonances are practically symmetrical and are very similar over all this energy range. Therefore the $\ell > 0$ resonances were all fitted as $p_{1/2}$ resonances. Above 260 keV, the tails of some resonances were better fitted by introducing $d_{3/2}$ resonances. As expected, the number of $d_{3/2}$ resonances found necessary for a

Table 1. Sample values of neutron energy resolution, ΔE, full width at half maximum, FWHM, in the transmission and capture experiments

E_n	Transmission Exp.		Capture Exp.
(keV)	Detector	ΔE (eV)	ΔE (eV)
10	Li-6	15	10
30	Li-6	75	46
50	Li-6	160	80
	Ne-110	50	
100	Ne-110	130	173
200	Ne-110	333	390
400	Ne-110	927	949

good fit increases as the energy goes up. Around 400 keV, as many d as p resonances are required. Higher resolution transmission data and measurements of the differential elastic scattering cross sections[9,10] would be necessary to assign spin and parity to $\ell > 0$ resonances.

3.2 THE CODE SAMMY

The code SAMMY was developed to cope with a practical problem encountered in the analysis of the data with the code MULTI which was reported in the Sect. 3.1. This problem developed because MULTI is a nonlinear least-squares code and because all the transmission data could not be fitted simultaneously. When analyzing a particular energy region of the data, if one allows all of the resonance parameters inside and outside the region to be adjusted to obtain a fit to this energy region, one obtains a good fit for this energy region, but the fit to the previously analyzed energy regions is destroyed. There is no way to communicate to MULTI how to vary resonance parameters to improve the fit in a particular energy region being analyzed in such a way that the fits to the data previously analyzed will not be destroyed. The code SAMMY solves this problem.

SAMMY is a constrained least-squares code which, in principle, produces an output of a sequential analysis of all the energy regions of the data the same as if all the energy regions had been analyzed simultaneously. SAMMY achieves this result by solving Bayes' equation which makes use of the covariance matrix of the parameters being varied (obtained as the output of the previously analyzed energy regions) to vary the parameters of the resonances to fit a new energy region. In contradistinction to MULTI where only the parameters of the resonance in the energy region being analyzed can safely be allowed to vary, in SAMMY the parameters of all the resonances are always adjusted when analyzing a particular energy region. The different energy regions need not overlap — in fact they must not — since this would amount to twice as much weight to the overlapped data. The major difference between the two codes from an operational point of view is that in SAMMY one must input not only a resonance parameter file but also a covariance matrix for these resonance parameters. It is this covariance matrix of the input parameters that allows SAMMY to vary the resonance parameters to fit a new energy region without destroying the fit to previously analyzed energy regions.

The other major improvement of SAMMY over MULTI is the option to handle off-diagonal elements in the covariance matrix of the data. These off-diagonal elements would be the correlation among the uncertainties due to background and deadtime corrections usually referred to as "systematic" uncertainties. These uncertainties, properly included and propagated in the data file, would give much more realistic uncertainties on the final resonance parameters adjusted by the code. The off-diagonal uncertainties were not computed for these transmission data; therefore, the uncertainties given in Table 2 for the neutron widths of the resonances seen in the transmission data and for the energies of the large s-wave resonances are not more realistic than the ones obtained with the code MULTI. How to deal with the off-diagonal uncertainties is shown in ref. 11.

3.3 ANALYSIS WITH THE CODE SAMMY

When the analysis with the code SAMMY was initiated, it was intended to cover the same energy range from 1 to 550 keV as previously analyzed with MULTI and to include the information obtained in the capture analysis from 2.5 to 450 keV.

The input parameter file was composed of 273 resonances: three fictitious outside resonances located at -50 keV ($\Gamma_n = 14$ keV), -0.5 keV ($\Gamma_n = 15$ eV), and 607 keV ($\Gamma_n = 71$ keV); 41 s-wave resonances; and 229 $\ell > 0$ resonances. A total of 203 parameters were allowed to be adjusted by the code during the analysis: two of the three energy parameters of the fictitious resonances, as well as their three neutron widths (the energy of the resonance at -50 keV was kept fixed); 30 of the 41 energy parameters of the s-wave resonances; all of their 41 neutron widths; and the neutron widths of the 127 $\ell > 0$ resonances well defined in the transmission data.

All of the resonances already analyzed with the code MULTI and defined in the transmission data were also seen in the capture data whose analysis had been completed up to 450 keV and is reported in Sect. 5. For the resonances seen in both data sets, the radiation widths are known without ambiguity and were included in the input parameter file of SAMMY, but they were not adjusted by the code. For most of these resonances, the neutron widths are much larger than the radiation widths. Therefore, the capture area was not affected by a small readjustment of Γ_n. However, when Γ_n and Γ_γ are of the same order of magnitude, if Γ_n is readjusted by the code, Γ_γ must be corrected in order to keep the capture area at the value found in the capture analysis.

The input parameter file included 101 small resonances, but none of these parameters were allowed to vary. Eighty-nine of these 101 resonances were seen only in the capture data. By including those 89 resonances in the parameter file a check could be made to see if the values assigned to Γ_n and Γ_γ were also consistent with the transmission data. Some were not and had to be readjusted by trial and error. For some of these resonances we were able to estimate the upper limit of Γ_n. For example, we can see in Fig. 3 that the parameters given in Table 2 for the resonances at 50.927, 56.880, 71.370, 78.217, and 84.990 keV give the maximum acceptable dip in the theoretical transmission to stay compatible with the data. It should be understood that the set of values for Γ_n and Γ_γ assigned to the resonances seen only in the capture data is not unique since only the capture area is well defined. When possible, a value of 0.5 eV was assigned to the radiation width of these resonances.

Above 450 keV, where no capture analysis was performed, an arbitrary value of 2 eV was assigned to the radiation widths of all resonances.

The input covariance matrix of the parameters has only diagonal elements. The starting uncertainties on all the neutron widths were 10%. The default uncertainty on the energy of the resonances is given by half the sum of the radiation, neutron, Doppler, and resolution widths. For the large s-wave resonances, the neutron width is the dominant term and would give too large uncertainties on the starting energy parameters which are already well defined from the previous analysis with MULTI. Instead,

Table 2. Resonance parameters for ^{60}Ni + n from 1 to 450 keV

(Columns are fully identified in Sect. 7.1.)

E_o [a] (keV)			$g\Gamma_n\Gamma_\gamma/\Gamma$	$g\Gamma_n$	Γ_γ	C	$\Gamma_{\gamma(cor)}$
$s_{1/2}$	$p_{1/2}$	$d_{3/2}$	(eV)	(eV)	(eV)	(10^{-3})	(eV)
-50				14,800(70)			
-0.15 (11)				0.86 (25)	1.5		
	2.253 (1)[e]			0.053 (1)	1.20 (8)		
	5.532 (1)		0.043 (3)	0.045 (3)	1.0 (6)		
	12.220 (1)[b]		0.201 (4)	0.34	0.50[d]		
12.487 (1)			4.3 (2)	2358 (3)	4.3 (2)	0.72	2.6 (9)
	13.624 (1)[b]		0.353 (6)	1.20	0.50[d]		
	21.274 (2)[b]		0.022 (2)	0.023	0.50[d]		
	23.788 (1)		0.24 (1)	4.5 (2)	0.25 (1)		
	23.898 (1)		0.54 (1)	1.17 (4)	1.0 (1)		
	[28.458 (2)[b]		0.04 (2)[c]	0.05	0.50[d]		
	[28.497 (2)[b]		0.11 (2)	0.14	0.50[d]		
28.709 (1)			1.6 (1)	698 (1)	1.6 (1)	1.3	0.7 (5)
	29.480 (2)[b]		0.061 (5)	0.069	0.50[d]		
	30.262 (1)		0.39 (1)	1.0 (3)[c]	0.63 (2)		
	33.017 (2)		0.56 (1)	7.7 (3)	0.60 (1)		
	33.393 (2)		0.29 (1)	10.0 (3)	0.30 (1)		
	39.534 (1)		0.57 (1)	2.3 (1)	0.76 (2)		
	42.705 (1)		0.35 (5)	1.6 (2)[c]	0.45 (3)		
	42.985 (2)[b]		0.37 (4)	2	0.50[d]		
43.105 (1)			0.26 (2)	104.4 (6)	0.26 (2)	0.58	0.20 (4)
	[47.567 (5)[b]		0.08 (1)[c]	0.1	0.50[d]		
	47.621 (3)		0.63 (6)[c]	1.1 (2)[c]	1.5		
	[47.637 (5)		0.31 (3)[c]	0.64 (10)[c]	0.60		
	49.801 (1)[b]		0.36 (1)	≤0.6	0.90		
	50.927 (2)[b]		0.185 (7)	≤0.29	0.50[d]		
	51.594 (1)		0.50 (1)	0.85 (5)[c]	1.21 (5)		
	52.658 (3)[b]		0.110 (7)	≤0.14	0.50[d]		
	56.290 (1)		0.32 (1)	0.69 (5)[c]	0.60 (2)		
	56.880 (1)[b]		0.52 (1)	≤0.62	3.2		
	[64.918 (10)[b]		0.05 (2)[c]	0.05	0.50[d]		
	[65.053 (6)[b]		0.24 (7)	0.47	0.50[d]		
65.228 (1)			1.10 (5)	443.0 (8)	1.10 (5)	0.35	0.94 (9)
	65.573 (2)[b]		1.09 (8)	≤2.4	2.0		
	71.370 (2)[b]		0.41 (1)	≤0.75	0.93		
	73.206 (1)		0.61 (1)	2.0 (1)	0.87 (3)		
	78.217 (2)[b]		0.24 (1)	≤0.80	0.34		
	80.048 (2)[b]		0.52 (1)	≤0.90	1.2		
	81.974 (3)[b]		0.27 (1)	0.45	0.66		
	84.990 (10)[b]		0.52 (2)	≤1.0	1.1		

Table 2. (Continued)

E_o [a] (keV)			$g\Gamma_n\Gamma_\gamma/\Gamma$	$g\Gamma_n$	Γ_γ	C	$\Gamma_{\gamma(cor)}$
$s_{1/2}$	$p_{1/2}$	$d_{3/2}$	(eV)	(eV)	(eV)	(10^{-3})	(eV)
	86.170 (2)		1.49 (10)	3.0 (2)[c]	2.9 (4)		
86.837 (1)			0.80 (5)	398 (1)	0.80 (5)	0.46	0.62 (10)
	87.891 (2)		0.9 (2)	11.6 (3)	1.0 (2)		
	89.751 (5)[b]		0.28 (1)	≤0.50	0.64		
	91.662 (5)		0.40 (1)	6.5 (2)	0.43 (1)		
	93.773 (5)		0.73 (2)	2.7 (5)[c]	1.01 (3)		
	95.504 (5)[b]		0.18 (1)	0.28	0.50[d]		
	97.059 (5)		0.62 (9)	2.9 (1)	0.8 (2)		
98.085 (1)			1.5 (1)	1002 (2)	1.5 (1)	0.60	0.9 (3)
	99.405 (5)		1.1 (1)	7.4 (3)	1.3 (1)		
	102.064 (7)[b]		0.25 (2)	≤0.5	0.50[d]		
107.85 (<1)			1.15 (6)	649 (1)	1.15 (6)	0.55	0.8 (2)
	108.453 (5)[b]		0.98 (10)	≤0.5	1.2		
	111.47 (1)		2.00 (5)	4.0 (5)[c]	4.0 (1)		
	112.00 (1)		0.39 (3)	2.5 (5)[c]	0.46 (4)		
	112.24 (1)		0.56 (3)	3.5 (5)[c]	0.66 (5)		
	113.320 (5)		0.90 (3)	3.0 (5)[c]	1.27 (7)		
	113.87 (2)[b]		0.08 (2)[c]	0.10	0.50[d]		
	120.52(1)		0.98 (3)	7.5 (3)	1.13 (4)		
	120.85 (1)		1.25 (3)	2.6 (2)	2.39 (8)		
	123.618 (5)		0.78 (4)	31.5 (5)	0.80 (4)		
	127.66 (1)		0.48 (2)	67.4 (5)	0.49 (2)	0.48	0.46 (3)
	129.77 (1)[b]		1.02 (3)	≤2.5	1.7		
	133.52 (1)		0.63 (3)	20.9 (4)	0.65 (3)		
	135.46 (2)[b]		0.12 (2)	0.16	0.50[d]		
	[136.03 (1)		1.34 (5)	15.5 (4)	1.45 (8)		
	[136.29 (1)		1.93 (8)	6.7 (3)	2.7 (1)		
	[137.21 (2)[b]		0.10 (1)	≤1.0	0.11		
	[137.47 (1)		0.58 (3)	5.6 (3)	0.65 (5)		
139.03 (<1)			1.14 (6)	30.7 (5)	1.18 (6)		
	139.56 (2)		1.22 (6)	26.2 (5)	1.28 (7)		
	140.01 (1)		2.23 (6)	31.6 (5)	2.4 (1)		
	145.72 (1)[b]		0.50 (2)	1.0	1.0[d]		
	147.53 (2)[b]		0.09 (2)[c]	0.1	0.50[d]		
	148.80 (1)		1.13 (4)	8.5 (3)	1.30 (5)		
	151.40 (1)		0.49 (2)	14.6 (4)	0.51 (2)		
	152.78 (5)[e]		≤0.05	5.9 (5)[c]			
	154.35 (1)		0.62 (3)	162.6 (8)	0.62 (3)	0.32	0.57 (4)
[156.36 (<1)			0.5 (1)[c]	472 (1)	0.5 (1)	0.31	0.35 (13)
[	156.48 (2)[b]		0.2 (1)[c]	0.3	0.50[d]		

Table 2. (Continued)

E_o [a] (keV)			$g\Gamma_n\Gamma_\gamma/\Gamma$	$g\Gamma_n$	Γ_γ	C	$\Gamma_{\gamma(cor)}$
$s_{1/2}$	$p_{1/2}$	$d_{3/2}$	(eV)	(eV)	(eV)	(10^{-3})	(eV)
	160.22 (1)		0.67 (15)	20.4 (5)	0.70 (16)		
161.74 (<1)			0.9 (1)[c]	1325 (2)	0.9 (1)	0.33	0.46 (25)
	162.15 (2)[b]		1.4 (2)	10	1.7[d]		
	166.22 (1)[b]		1.34 (4)	≤3	2.5		
	167.21 (1)		2.60 (5)	7.4 (8)[c]	4.0 (1)		
	167.69 (2)[b]		0.35 (2)	1.2	0.50[d]		
	170.57 (1)		1.82 (5)	4 (1)[c]	3.3 (2)		
	172.10 (2)[b]		0.22 (2)	0.39	0.50[d]		
	172.63 (2)[b]		0.53 (3)	1.1	1.0[d]		
	174.59 (2)		0.46 (4)	12.3 (5)	0.48 (4)		
	174.99 (2)		0.93 (4)	2.0 (5)[c]	1.7 (1)		
	179.90 (2)[b]		0.62 (3)	1.6	1.0[d]		
	182.92 (2)		0.91 (8)	77.2 (8)	0.92 (8)		
	183.52 (2)		0.83 (6)	12.7 (5)	0.89 (7)		
186.51 (<1)			4.0 (5)[c]	5237 (6)	4.0 (5)	0.21	2.9 (8)
	186.67 (1)[b]		1.1 (1)	≤2	2.4		
	191.07 (10)[b]		0.13 (6)[c]	0.25	0.25[d]		
	192.59 (2)		0.78 (6)	62.2 (8)	0.79 (6)		
	194.19 (1)		1.65 (7)	19.9 (6)	1.8 (1)		
	194.54 (3)[b]		0.25 (10)[c]	0.5	0.50[d]		
	196.58 (1)[b]		1.7 (2)	≤5	2.5		
197.64 (<1)			1.8 (2)	3025 (5)	1.8 (2)	0.205	1.2 (4)
	199.87 (6)[6]		0.2 (1)	0.4	0.50[d]		
200.59 (3)			0.6 (2)	9.8 (3)	0.6 (2)		
	201.02 (3)		0.10 (5)[c]	7.4 (5)	0.10 (5)		
	201.50 (3)		2.0 (3)	156 (2)	2.1 (3)		
	202.54 (3)[b]		0.43 (14)	3	0.50[d]		
	205.93 (3)		0.64 (5)	36 (1)	0.65 (6)		
	206.51 (3)		0.56 (5)	141 (1)	0.56 (5)	0.20	0.53 (5)
	208.93 (5)[b]		0.20 (3)	0.33	0.50[d]		
	209.68 (5)[b]		0.18 (3)	0.29	0.50[d]		
	212.89 (5)[b]		0.21 (3)	0.35	0.50[d]		
	214.10 (3)		0.76 (5)	120 (1)	0.77 (5)	0.19	0.75 (5)
	214.69 (2)		1.36 (6)	4 (1)[c]	2.0 (1)		
	220.03 (3)		0.28 (5)	76 (1)	0.28 (5)	0.19	0.26 (5)
	220.60 (2)		1.85 (9)	33 (1)	1.96 (10)		
	220.93 (2)		0.67 (7)	65 (1)	0.68 (7)		
	226.28 (2)[b]		0.65 (4)	≤2	0.96		
	229.20 (2)		2.62 (8)	16.0 (8)	3.2 (1)		
		230.15 (2)	2.64 (8)	106 (1)	1.35 (4)		

Table 2. (Continued)

E_o [a] (keV)			$g\Gamma_n\Gamma_\gamma/\Gamma$	$g\Gamma_n$	Γ_γ	C	$\Gamma_{\gamma(cor)}$
$s_{1/2}$	$p_{1/2}$	$d_{3/2}$	(eV)	(eV)	(eV)	(10^{-3})	(eV)
	233.51 (3)		1.04 (7)	15.0 (7)	1.12 (8)		
	233.85 (3)		0.93 (7)	9 (2)[c]	1.04 (12)		
	235.03 (3)[b]		0.67 (4)	≤2	1.0		
	236.62 (2)		1.73 (6)	12 (2)[c]	2.0 (1)		
	237.84 (3)[b]		0.73 (7)	≤2	1.15		
	238.16 (3)		1.29 (8)	16 (2)[c]	1.4		
	244.07 (3)[b]		0.71 (4)	2.5	1.0[d]		
	246.62 (5)[b]		0.13 (3)	0.25	0.25[d]		
	248.72 (3)		2.33 (9)	75 (1)	2.4 (1)		
251.99 (<1)			1.37 (12)	536 (4)	1.37 (12)	0.17	1.28 (13)
	252.32 (5)		0.59 (8)	5 (1)[c]	0.66 (10)		
	253.07 (5)		1.03 (7)	264 (3)	1.04 (7)	0.17	1.00 (7)
	254.35 (5)		0.34 (5)	32 (5)[c]	0.34 (5)		
	255.84 (5)[b]		0.77 (8)	3.3	1.0[d]		
256.12 (<1)			0.70 (7)[c]	870 (6)	0.70 (7)	0.165	0.56 (10)
	256.27 (5)		1.21 (9)	11 (1)	1.32 (10)		
	257.49 (5)		0.20 (4)[c]	23 (3)	0.20 (4)		
257.63 (<1)			0.68 (15)	1826 (7)	0.68 (15)	0.165	0.38 (21)
	258.42 (5)		1.06 (7)	13 (1)	1.14 (9)		
	260.0 (1)[b]		0.40 (5)	2	0.50[d]		
	260.77 (5)		0.79 (5)	52 (2)	0.80 (5)		
	262.61 (5)[b]		0.37 (4)[c]	≤6	0.39		
	263.11 (5)		1.37 (7)	44 (4)[c]	1.42 (8)		
	265.30 (5)[b]		0.08 (4)	0.10	0.50[d]		
	265.94 (5)		0.80 (6)	56 (1)	0.81 (6)		
	268.35 (5)[b]		0.59 (5)	1.5	1.0[d]		
		269.09 (5)	1.89 (8)	98 (1)	0.97 (4)		
	273.55 (5)[b]		0.25 (4)	0.5	0.50[d]		
	276.63 (5)[b]		0.54 (9)	1.2	1.0[d]		
	277.05 (5)		2.77 (12)	17.2 (8)	3.4 (2)		
	278.18 (5)		1.01 (9)	367 (3)	1.01 (9)	0.16	0.95 (10)
278.93 (1)			0.45 (7)	225 (2)	0.45 (7)	0.16	0.41 (7)
	280.05 (5)		1.27 (7)	145 (2)	1.28 (7)		
	281.85 (5)		0.28 (6)	15.1 (6)	0.28 (6)		
	282.74 (5)		2.7 (2)	175 (3)	2.8 (2)		
		283.15 (5)	1.15 (13)	108 (1)	0.58 (6)		
	285.28 (5)[b]		0.42 (4)	0.7	1.0[d]		
	288.30 (5)[b]		0.64 (4)	1.7	1.0[d]		
	290.60 (5)		1.30 (6)	35 (4)[c]	1.35 (6)		
291.92 (1)			0.70 (6)	140 (3)	0.71 (6)	0.155	0.69 (6)
	292.65 (5)		1.21 (7)	142 (3)	1.22 (7)		

Table 2. (Continued)

E_o [a] (keV)			$g\Gamma_n\Gamma_\gamma/\Gamma$	$g\Gamma_n$	Γ_γ	C	$\Gamma_{\gamma(cor)}$
$s_{1/2}$	$p_{1/2}$	$d_{3/2}$	(eV)	(eV)	(eV)	(10^{-3})	(eV)
	294.35 (7)		0.62 (7)	15 (2)[c]	0.65 (7)		
	294.75 (7)		0.20 (6)	9 (1)	0.20 (7)		
		295.60 (7)	0.81 (6)	136 (2)	0.41 (3)		
	297.2 (1)		0.12 (4)	130 (3)	0.12 (4)	0.15	0.10 (4)
		297.5 (1)	0.20 (5)	22 (2)	0.10 (4)		
	299.80 (7)[b]		0.40 (5)[c]	2	0.50[d]		
		300.40 (7)	1.44 (7)	52 (1)	0.74 (4)		
		302.11 (5)	2.13 (7)	16 (2)	1.23 (5)		
	306.6 (1)		1.46 (9)	400 (4)	1.47 (9)	0.15	1.4 (1)
		307.36 (5)	3.10 (11)	210 (1)	1.57 (6)		
	308.7 (1)[b]		0.75 (8)[c]	3	1.0[d]		
	311.3 (1)		0.60 (8)	12.7 (7)	0.61 (9)		
	313.5 (1)		2.26 (13)	10 (2)[c]	2.9 (2)		
317.02 (<1)			1.5 (2)[c]	2788 (9)	1.5 (2)	0.15	1.1 (3)
	317.2 (1)[b]		2.8 (1)	⩽12	3.6		
	321.5 (1)		1.22 (12)	20 (5)[c]	1.3 (1)		
	322.8 (1)		1.01 (10)	5.2 (5)	1.25 (14)		
	324.6 (1)[b]		0.67 (10)	2	1.0[d]		
325.52 (<1)			2.5 (5)[c]	7084 (17)	2.5 (5)	0.14	1.5 (7)
	326.5 (1)[b]		0.75 (8)[c]	3	1.0[d]		
		327.4 (1)	2.7 (1)	16 (1)	1.6 (1)		
	329.0 (1)		0.94 (11)	40 (2)	0.96 (11)		
	329.6 (1)[b]		0.69 (7)[c]	2.2	1.0[d]		
	331.1 (1)[b]		0.57 (4)[c]	1.3	1.0[d]		
	334.1 (1)		1.2 (1)	230 (2)	1.2 (1)		
		336.1 (1)	2.2 (1)	162 (3)	1.12 (5)		
338.48 (<1)			3.0 (5)[c]	3563 (14)	3.0 (5)	0.13	2.5 (6)
	338.9 (1)[b]		0.41 (7)	⩽7	0.44		
	341.4 (1)		1.00 (10)	105 (3)	1.01 (10)		
	342.7 (1)		0.20 (3)[c]	110 (10)[c]	0.20 (3)		
	343.1 (1)		1.01 (12)	210 (4)	1.01 (12)		
	344.1 (1)[b]		1.49 (10)	4	2.5[d]		
	345.4 (1)[b]		0.86 (8)[c]	2	1.5[d]		
	348.17 (1)		5.2 (2)	94 (3)	5.5 (2)		
	349.1 (1)		2.3 (1)	27 (1)	2.6 (2)		
		350.0 (1)	1.5 (1)	20 (5)[c]	0.81 (8)		
		352.37 (7)	1.62 (10)	9 (3)[c]	1.0 (1)		
		354.27 (10)	1.82 (13)	493 (4)	0.91 (6)	0.13	0.87 (6)
		355.4 (1)	1.14 (8)	30 (10)[c]	0.60 (6)		
357.65 (<1)			3.0 (5)[c]	1619 (10)	3.0 (5)	0.13	2.8 (5)
	358.7 (1)[b]		1.34 (12)	10	1.5[d]		
		359.3 (1)	2.0 (2)[c]	1256 (7)	1.0 (1)	0.13	0.9 (1)

Table 2. (Continued)

E_o [a] (keV)			$g\Gamma_n\Gamma_\gamma/\Gamma$	$g\Gamma_n$	Γ_γ	C	$\Gamma_{\gamma(cor)}$
$s_{1/2}$	$p_{1/2}$	$d_{3/2}$	(eV)	(eV)	(eV)	(10^{-3})	(eV)
	361.1 (1)[b]		0.88 (13)	7	1.0[d]		
	365.6 (1)		0.8 (2)	60 (5)[c]	0.8 (2)		
		366.1 (1)	3.7 (2)	15 (2)[c]	2.5 (2)		
	369.7 (1)[b]		1.22 (11)	≤7	1.5		
		370.48 (1)	1.37 (11)	56 (15)[c]	0.7 (1)		
		371.68 (1)[b]	3.1 (2)	6.5	3.0[d]		
	373.4 (1)		0.17 (11)	30 (5)[c]	0.18 (11)		
	374.6 (1)[b]		0.37 (3)[c]	1.4	0.50[d]		
	376.8 (1)[b]		1.39 (11)	7	1.6[d]		
376.84 (<1)			3.5 (5)[c]	3865 (18)	3.5 (5)	0.13	3.0 (6)
	378.0 (2)[b]		0.45 (10)	4.5	0.50[d]		
	379.4 (1)		2.7 (2)	478 (7)	2.7 (2)	0.13	2.6 (2)
	381.1 (1)		2.07 (13)	30 (2)	2.22 (15)		
	381.8 (1)[b]		2.6 (2)	≤10	3.5		
383.13 (5)			1.86 (13)	370 (5)	1.87 (13)	0.13	1.82 (13)
	386.2 (1)[b]		1.85 (11)	≤5	2.9		
		388.2 (1)	0.78 (13)	260 (5)	0.39 (6)	0.13	0.37 (6)
	388.8 (1)		2.82 (13)	160 (5)	2.88 (13)		
		393.0 (1)	1.60 (11)	375 (5)	0.80 (6)	0.13	0.78 (6)
	394.8 (1)[b]		0.48 (9)	0.9	1.0[d]		
	397.0 (1)[b]		0.57 (7)	1.3	1.0[d]		
		398.1 (1)	0.40 (14)	460 (4)	0.20 (7)	0.12	0.17 (7)
	399.2 (1)		1.27 (11)	40 (6)[c]	1.38 (13)		
	401.0 (1)[b]		0.43 (10)	3	0.50[d]		
	401.6 (1)[b]		0.54 (8)	5.4	0.60[d]		
		402.8 (1)	3.3 (2)	443 (5)	1.65 (8)		
	404.0 (1)[b]		1.10 (11)	4	1.5[d]		
	407.9 (1)		1.4 (3)	30 (6)[c]	1.5 (3)		
	408.3 (1)		0.8 (2)	15 (5)[c]	0.9 (3)		
		409.9 (1)	0.6 (3)	220 (5)	0.30 (14)		
	410.2 (1)		1.0 (3)	13 (1)	1.1 (3)		
413.44 (5)			0.97 (14)	344 (6)	0.97 (15)	0.12	0.93 (15)
		415.4 (1)	1.5 (3)	400 (6)	0.77 (16)	0.12	0.75 (16)
		415.7 (1)	2.3 (3)	34 (3)	1.2 (2)		
418.3 (1)			1.28 (10)	68 (3)	1.30 (11)		
	419.9 (1)		2.29 (12)	20 (5)[c]	2.6 (2)		
422.49 (<1)			2.3 (3)[c]	1861 (15)	2.3 (3)	0.12	2.1 (3)
		424.6 (1)	2.32 (12)	70 (14)[c]	1.20 (7)		

Table 2. (Continued)

E_o [a] (keV)			$g\Gamma_n\Gamma_\gamma/\Gamma$	$g\Gamma_n$	Γ_γ	C	$\Gamma_{\gamma(cor)}$
$s_{1/2}$	$p_{1/2}$	$d_{3/2}$	(eV)	(eV)	(eV)	(10^{-3})	(eV)
	426.1 (1)[b]		0.84 (8)	5	1.0[d]		
	427.0 (1)[b]		1.5 (2)[c]	10	1.75[d]		
	429.1 (1)		0.7 (2)	600 (10)	0.7 (2)	0.12	0.6 (2)
		429.9 (1)	1.84 (14)	27 (2)	0.99 (8)		
	431.9 (1)		1.3 (2)	240 (10)	1.3 (2)		
		432.4 (1)	1.2 (2)	180 (8)	0.63 (8)		
		435.3 (2)	0.6 (2)	510 (5)	0.31 (9)	0.12	0.28 (9)
	436.5 (2)[b]		0.43 (15)[c]	3	0.50[d]		
437.73 (1)			1.5 (3)[c]	1219 (4)	1.5 (3)	0.12	1.35 (30)
		438.9 (1)	3.1 (2)	30 (6)[c]	1.72 (12)		
		440.9 (1)	3.3 (2)	180 (5)	1.68 (10)		
443.9 (2)			2.0 (2)	177 (7)	2.0 (2)		
	444.4 (2)[b]		1.0 (2)[c]	3	1.5[d]		
	445.5 (2)		0.25 (5)[c]	95 (4)	0.25 (5)		
	447.1 (2)[b]		0.5 (2)	1.0	1.0[d]		
448.00 (1)			2.0 (5)	2733 (36)	2.0 (5)	0.12	1.7 (5)
	448.9 (1)		1.7 (2)	24 (2)	1.8 (2)		
		451.2 (1)	1.9 (2)	150 (10)	0.95 (9)		
454.19 (7)				788 (80)			
463.5 (1)				1600 (200)			
485.9 (1)				3100 (400)			
498.6 (1)				3400 (400)			
522.2 (1)				3600 (500)			
527.0 (1)				2800 (300)			
540 (2)				79,000 (1000)			
555 (3)				1700 (200)			

[a] Resonance energy after all corrections discussed in Sect. 6 were applied. Within parentheses are statistical uncertainties. The notation is such that -0.15 (11) stands for -0.15 ± 0.11. Same notation is used elsewhere in the table.

[b] Resonance seen in capture only. If an upper bound of $g\Gamma_n$ is given, it is clearly seen as such on the theoretical fit to the transmission data and must be kept associated with the corresponding value of Γ_γ.

[c] Parameter adjusted by trial and error. The uncertainty was estimated from the sensitivity of the fit to the variation of this parameter.

[d] Assigned value of Γ_γ (see Sect. 3.3 for details).

[e] Resonance seen in transmission only.

an uncertainty of 0.02% was adopted for the starting energy parameters of the large s-wave resonances between 10 and 550 keV. On the contrary, the energies of the fictitious resonances are uncertain. Starting uncertainties for these parameters were chosen at 40% and 2% for the two resonances at −0.5 keV and 607 keV, respectively.

Running the code SAMMY with these input parameter and covariance files (or similar ones obtained at the end of each run) and with data files of about 300 points (~50-keV range) took an average of 1 h of computing time on the ORELA PDP-10. As new information was fed to the code through the data, the resonance parameters became better known and more correlated. The covariance matrix of the parameters increased in size (up to 13 print-out pages) as more non-diagonal elements were determined. Because of its size, the complete covariance matrix of the parameters cannot be given here. The main results are discussed in Sect. 7.

Above 300 keV the smooth behavior of the transmission between the sharp resonances is due mostly to the tail of the large fictitious resonance originally set at 607 keV. As the analysis was progressing from the lowest energy regions to the highest, the energy of this resonance was readjusted by the code towards lower energies. At the end of the 400- to 450-keV region analysis, the parameters of this resonance were $E_n = 540 \pm 2$ keV and $\Gamma_n = 79 \pm 1$ keV. At that point, difficulties in fitting the data up to 550 keV were anticipated. However, a satisfactory fit to the data up to 500 keV was obtained because the three s-wave resonances at 522, 527, and 555 keV acted as fictitious resonances beside the large one which, in the process of fitting this region, moved from 540 to 567 keV. Too many constraints were built in the system and a fit to the 500- to 550-keV region could not be achieved. More than one resonance above the range of energy to be analyzed is probably necessary. In view of this problem and since the capture data was not analyzed above 450 keV, it was decided to limit the transmission data analysis at 450 keV. In addition to the large resonance at 540 keV, the seven resonances reported in Table 2 above 450 keV also contribute to the calculated theoretical transmission below 450 keV and must be kept as part of the parameter file obtained from the analysis of the transmission data from 1 to 450 keV. Therefore, our final parameter file contains 257 resonances between 1 and 450 keV, two negative resonances, and eight fictitious resonances above 450 keV.

3.4 CONSISTENCY TEST ON SAMMY

The claim was made in Sect. 3.2 that SAMMY produces as output of a sequential analysis of all the energy regions of the data the same result that would have been obtained if all the energy regions were analyzed simultaneously. That is to say, the end results of two analyses proceeding through two different sequences of data regions should be identical, or at least equivalent, over the complete range of data analyzed. Such a test has been performed for the 6- to 150-keV energy range. The interval of energy was broken up into four regions: (1) Region A from 6 to 20 keV, (2) Region B from 20 to 50 keV, (3) Region C from 50 to 100 keV, and (4) Region D from 100 to 150 keV.

Two sets of runs were conducted, both starting from the same parameter and covariance files described in Sect. 3.3. The sequences were B1, A1, C1, and D1 in the first series of runs; C2, B2, D2, and A2 in the second series. The neutron widths up to 200 keV of the s-wave resonances obtained at the end of these two sequences of runs are given in Table 3 along with the parameters of the large fictitious resonance around 600 keV. The uncertainty of the neutron width of this large fictitious resonance is strongly correlated to the uncertainties of the parameters of the resonances at −50, 186.51, and 197.64 keV [cor (1, 76) is 0.72 in set D1, 0.35 in set A2; cor (25 or 27, 76) are about −0.30 in both sets of parameters].

Table 3. Consistency test on SAMMY[a]

E_n (keV)	Γ_n (eV) of s-wave resonances: 6 to 150 keV analyses D1	6 to 150 keV analyses A2	1 to 450 keV analysis: Final set as in Table 2	Variable identification number
-50.	10870 (130)	12450 (90)	14800 (70)	1
-0.31	6.3 (8)	5.2 (8)		
-0.15			0.9 (3)	3
12.487	2380 (3)	2374 (3)	2358 (3)	5
28.709	696 (1)	695 (1)	698 (1)	7
43.105	103.1 (6)	103.1 (6)	104.4 (6)	9
65.228	438.6 (8)	443.1 (8)	443.0 (8)	11
86.837	394 (1)	395 (1)	398 (1)	13
98.085	995 (2)	991 (2)	1002 (2)	15
107.85	650 (1)	641 (1)	649 (1)	17
139.03	31.5 (5)	38.2 (6)	30.7 (5)	19
156.36	481 (38)	535 (41)	472 (1)	21
161.74	1400 (92)	2807 (97)	1325 (2)	23
186.51	7649 (183)	413 (74)	5236 (6)	25
197.64	1849 (210)	3727 (278)	3025 (5)	27
↓	↓	↓	↓	
600	27600 (2700)			
557		79900 (3400)		76
540			79000 (1000)	

[a]Neutron widths of s-wave resonances up to 200 keV and of the large fictitious resonance are obtained from the analysis of the transmission data from 6 to 150 keV through two different sequences (see Sect. 3.4 for details). Also given are the corresponding neutron widths obtained from the complete analysis of the data from 1 to 450 keV (see Sect. 3.3). The last column gives the numbers associated in the code with the Γ_n's and used for notation purposes in Sect. 3.4 when discussing the correlations between neutron widths. The uncertainties on the last significant figures are given in parentheses.

The variations in the energy parameters between sets D1, A2, and the final set (from Table 2) were less than 2 eV except for the small negative resonance at −0.15 keV and the large resonance around 600 keV as shown in the first column in Table 3. The other energy parameters are the same as in Table 2.

The parameters of the $\ell > 0$ resonances were very similar, and their correlations with the nearest s-wave resonance parameters were identical in both sets. The resonances at 139.56 and 140.01 keV were the only $\ell > 0$ resonances with discrepancies in their neutron widths larger than the sum of the respective uncertainties in Γ_n. This results from a slightly different smooth average theoretical transmission in this region.

Table 3 shows the s-wave resonance parameters of the final set (from Table 2) in the region where the consistency tests were conducted to illustrate how the parameters and their uncertainties were readjusted when more data were included in the analysis. In fact, the final set is obtained through the continuation of the first sequence given above: the energy regions above 150 keV were analyzed successively up to 450 keV, and the parameter and covariance files of run D1 were progressively readjusted and completed up to the final set. It should be pointed out that in sets D1 and A2 all the resonances above 150 keV are fictitious resonances relative to the small energy region analyzed. There are many more fictitious resonances than the four s-wave resonances given here, but these four are the ones which are the most correlated to the resonances inside the analyzed energy region in addition to the two large ones at −50 and 600 keV. The neutron widths of these four resonances have large uncertainties which are very strongly correlated. For example, cor (21, 23) is −0.80 in both sets D1 and A2 compared to 0.02 in the final set. This sharp difference is not always true. For example, cor (25, 27) is 0.30 in the three sets, but, in general, parameters of outside resonances are more correlated than the ones of the better defined inside resonances.

The discrepancies between the neutron widths given in parameter sets D1 and A2 for the resonances at 65.228 and 107.85 keV were about four times larger than was expected from the uncertainties on these parameters given by the code. This can be partially justified by the fact that the uncertainties of these resonances are correlated by 0.07 to 0.19 to the 186.51-keV resonance whose neutron width is 18 times smaller in set A2 than in set D1. The resonance at 12.487 keV is similarly correlated to this resonance but much more (0.40) to the large fictitious resonance at −50 keV. The small s-wave resonance at 139.03 keV shows a different situation where the uncertainties on Γ_n are undoubtedly unrealistic.

The theoretical transmissions calculated with the parameter sets D1 and A2 were plotted on the same graph and compared to the data. Up to 70 keV, the two lines are indistinguishable from one another. The fit to the data is the same as the fit shown in Figs. 1 and 2 and in part of Fig. 3 (slightly better in the 20- to 27-keV region). Above 70 keV and up to 148 keV, the discrepancy between the theoretical transmissions is less than 1%. These transmissions are always smaller than the ones calculated with the final parameter set; therefore they give a better fit to the data than the one shown in Figs. 3 and 4 where the fit is slightly too high. From 148 to 150 keV, the theoretical transmission calculated with the parameter set A2 becomes too large. This is an "edge" effect, probably due to the drastic change in the parameters of the nearby fictitious resonances, especially the one at 186.51 keV.

The uncertainties in the theoretical transmissions calculated by the code are 10 to 20 times smaller than the differences between the transmissions calculated with the parameter sets D1 and A2. Can we still claim that this consistency test is conclusive? Here we must point out again that these high-resolution neutron transmission measurements have small uncertainties and the code calculates the theoretical uncertainties as if these thousands of data points had no systematic uncertainties (as if they were totally uncorrelated). As a result, the uncertainties given in the theoretical transmissions and on the resonance parameters are unrealistically small.

In conclusion, this test showed (1) that the set of resonance parameters and their correlations inside the range of energy analyzed is fairly well reproduced when two different sequences are followed in the analysis, and (2) that the fits to the data obtained with each parameter set, D1 and A2, are less than 1% apart, are well inside the spread of the data points, and give as good or better fit than the one obtained with the final parameter set shown in Figs. 1 to 4.

This test would probably have been even more conclusive if it had been conducted on a larger range of energy so that the "edge" effects would have been relatively less important. It would also be interesting to see the effects of taking data regions of various sizes.

4. CAPTURE MEASUREMENTS

Neutron capture measurements made from 2.5 keV to ~5 MeV were based on 4.955- and 49.11-g enriched metal samples containing 99.79% ^{60}Ni. While the capture yield depends primarily on weight and purity, the resonance self-protection and multiple-scattering corrections depend on the dimensions of the samples which were approximately 26 mm by 52 mm with a thickness of 0.50 mm for one and 4.65 mm for the other. These thicknesses correspond to 0.00368 and 0.0372 atoms/barn, respectively.

The samples were exposed to the collimated ORELA neutron flux at 40.12 m from the electron target and moderator. Capture gamma rays were detected by a pair of C_6F_6-based liquid scintillators, one on each side of the sample, outside the beam. Accelerator conditions were 1000 pulses of 4 ns each per second and an average power of 7 kW. The run was completed in 78 hours with partial results recorded four times during the run for consistency checks. The time resolution of the scintillation detectors and associated electronics, as determined with coincident ^{60}Co gamma rays, was 2.1 ns full width at half maximum flux (FWHM). More important at most energies was the neutron slowing-down time in the moderator. Expressed as an equivalent spread in flight path, this was found to be about 28 mm FWHM by fitting the narrowest resonance peaks.

The total gamma-ray energy emitted as a function of neutron time-of-flight was derived by pulse-height weighting[12] and was corrected for a calculated 2.0% energy loss in the thin sample and 12.4% in the thick sample. The neutron flux was monitored by a 0.5-mm ^{6}Li glass scintillator[13] located 0.4 m upstream from the sample position. Above 70 keV this monitor had been calibrated against a ^{235}U fission chamber.[14] The capture efficiency was calibrated at 4.9 eV with a 50-micron gold foil sample using the saturated resonance technique.[15]

The raw capture data were corrected for electronic deadtime losses, amplifier gain standardization, environmental backgrounds, average scattered-beam background, and the excitation energy reached in ^{61}Ni. The time-of-flight data were rebinned to a set of neutron-energy scales, and the capture yield was expressed as millibarns per nucleus of ^{60}Ni in the target. The estimated various systematic uncertainties reported in Table 4 give a global systematic uncertainty of 3.4 to 4% on the capture yield in the range of energy analyzed in this report.

Table 4. Systematic uncertainties on the capture yield in percent

Saturated resonance calibration	3
Shape of the ^{6}Li(n,α) cross section at 50 keV	1
Shape of the ^{6}Li(n,α) cross section at 250 keV	2
Shape of the ^{6}Li(n,α) cross section at $\geq$500 keV	3
Pulse height weighting technique	1
Gamma-ray self absorption of thin sample	0.4
Gamma-ray self absorption of thick sample	1.0
Detector bias extrapolation (E_{bias} = 153 keV)	0.4
Misalignment of sample or neutron beam	<0.2
Uncertainty in detector efficiency from gain drifts of electronics	<0.4

5. CAPTURE DATA ANALYSIS

The capture data have been analyzed with a least-squares fitting program[16] LSFIT using the Breit-Wigner formula

$$\sigma_{n\gamma} = \pi k^{-2} \frac{g\Gamma_n\Gamma_\gamma}{(E - E_c)^2 + (\Gamma/2)^2} \tag{5.1}$$

where g is the statistical weight factor; Γ_n, Γ_γ, and Γ are the neutron, radiation, and total width, respectively, for each resonance; and E_c is the resonance energy.

5.1 METHOD OF ANALYSIS

A field encompassing up to 500 data points and up to 16 resonances is evaluated at one time. The program iterates upon trial parameters applying corrections for systems resolution, Doppler width, resonance self-protection, and multiple scattering.

Analysis of the thin sample data was conducted from 2.5 to 82 keV. The thick sample data were analyzed starting at 32 keV and going up to 450 keV. The capture kernels reported in Table 2 are from the thin sample data analysis up to 50 keV and from the thick sample data at higher energies.

If the resonance has not been previously seen and analyzed in the transmission data, the neutron width, Γ_n, is not known and only the capture area $A_\gamma = (2\pi^2/k^2)(g\Gamma_n\Gamma_\gamma/\Gamma)$ is determined. About 30% more resonances are seen in capture than in transmission. Therefore, after the capture data analysis was completed, we went back to the transmission data. Knowing now, from the capture

analysis, where the resonance should be seen, it was possible to adjust the neutron width to a reasonable value which would show a small resonance on the theoretical curve fitting the transmission data where there was none before. These small resonances in transmission are smaller than the statistical spread of the data points, and the corresponding neutron widths given in Table 2 are probably close to the maximum acceptable value of Γ_n.

The parameters of the overlapping resonances were not all adjusted by the code simultaneously but were adjusted separately in successive runs until the best set of parameters was obtained which would give the most satisfactory fit to the capture and transmission data simultaneously.

5.2 ASYMMETRIC RESOLUTION FUNCTION

Since these data showed a small low-energy (i.e., time delayed) tail on the usual Gaussian resolution function, a resolution shape modification was added to the code. The fraction of the neutrons which shows an asymmetric resolution function (up to 40% at 145 keV) is plotted in Fig. 8 as a function of the neutron incident energy. The asymmetric part is convoluted with a negative exponential whose time constant is given as a fraction of the Gaussian resolution (FWHM). Here the decay constant is 68% of the resolution and corresponds to about 7 ns.

5.3 OFF-RESONANCE SCATTERING

In order to evaluate properly the part of the multiple scattering due to the attenuation of the neutron flux in the sample, one needs to know the off-resonance scattering cross section, σ_{off}, in the region of each resonance. For s-wave resonances and for $\ell > 0$ resonances not on top of s-wave resonances, σ_{off} is equal to the effective potential scattering which decreases smoothly from 8 to 3 b as the neutron energy increases from 12 to 450 keV. At low energy (below 100 keV) for resonances which are on top of large s-wave resonances, σ_{off} can vary drastically. For example, for the $\ell > 0$ resonances at 12.220 and 13.624 keV on top of the large 12.487-keV s-wave resonance, σ_{off} is as large as 200 b and 120 b, respectively. These resonances as well as the $\ell > 0$ resonances at 28.497, 29.480, and 65.573 keV have been analyzed individually using the proper σ_{off} given by the transmission data and taking as background the capture cross section of the s-wave resonance at the corresponding energy. The fit of the data for the resonance at 12.220 keV is shown in Fig. 9. The value of $g\Gamma_n\Gamma_\gamma/\Gamma$ given by the code is 0.201 $\pm$ 0.004 eV. To illustrate the importance of choosing the correct σ_{off} in this energy region, this resonance was reanalyzed using different values of σ_{off}. All the fits were equivalent to the one in Fig. 9. The values of $g\Gamma_n\Gamma_\gamma/\Gamma$ obtained for five different values of σ_{off} are given in Table 5. The 40% increase seen in the capture kernel when the value of the non-resonant scattering varies from 8 to 200 b is due to the neutron attenuation in the sample because of its finite size. The corresponding correction factors for the multiple scattering, which vary from 3 to 52% of the capture area, are also given in Table 5.

5.4 BACKGROUND CORRECTION

A background term having a $E^{-1/2}$ energy dependence can be adjusted by the code if necessary. This background term includes the direct capture, if any, and the capture in the tails of the faraway s-wave resonances as well as the incompletely subtracted background from various sources. For these ^{60}Ni capture data, the optimum background for good fits to well-isolated resonances appeared to be roughly uniform — about 5 $\pm$ 2 mb up to 50 keV where the data taken with the thin sample (0.00368 atoms/barn) were analyzed, and 2.5 $\pm$ 1 mb above 50 keV. The optimum value of the background can

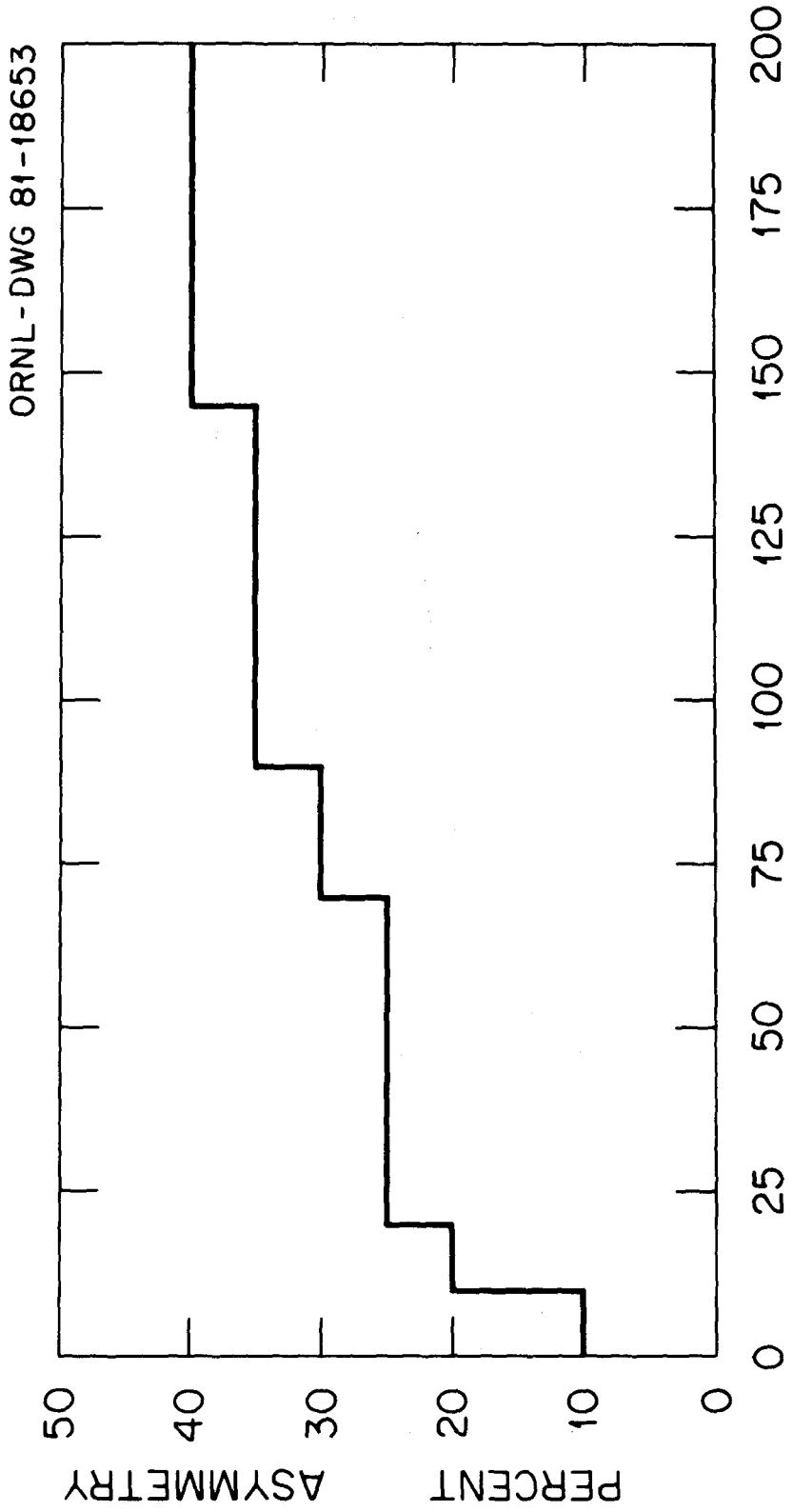

Fig. 8. Percentage of the neutrons showing an asymmetric resolution function which has been calculated by the code as explained in Sect. 5.2.

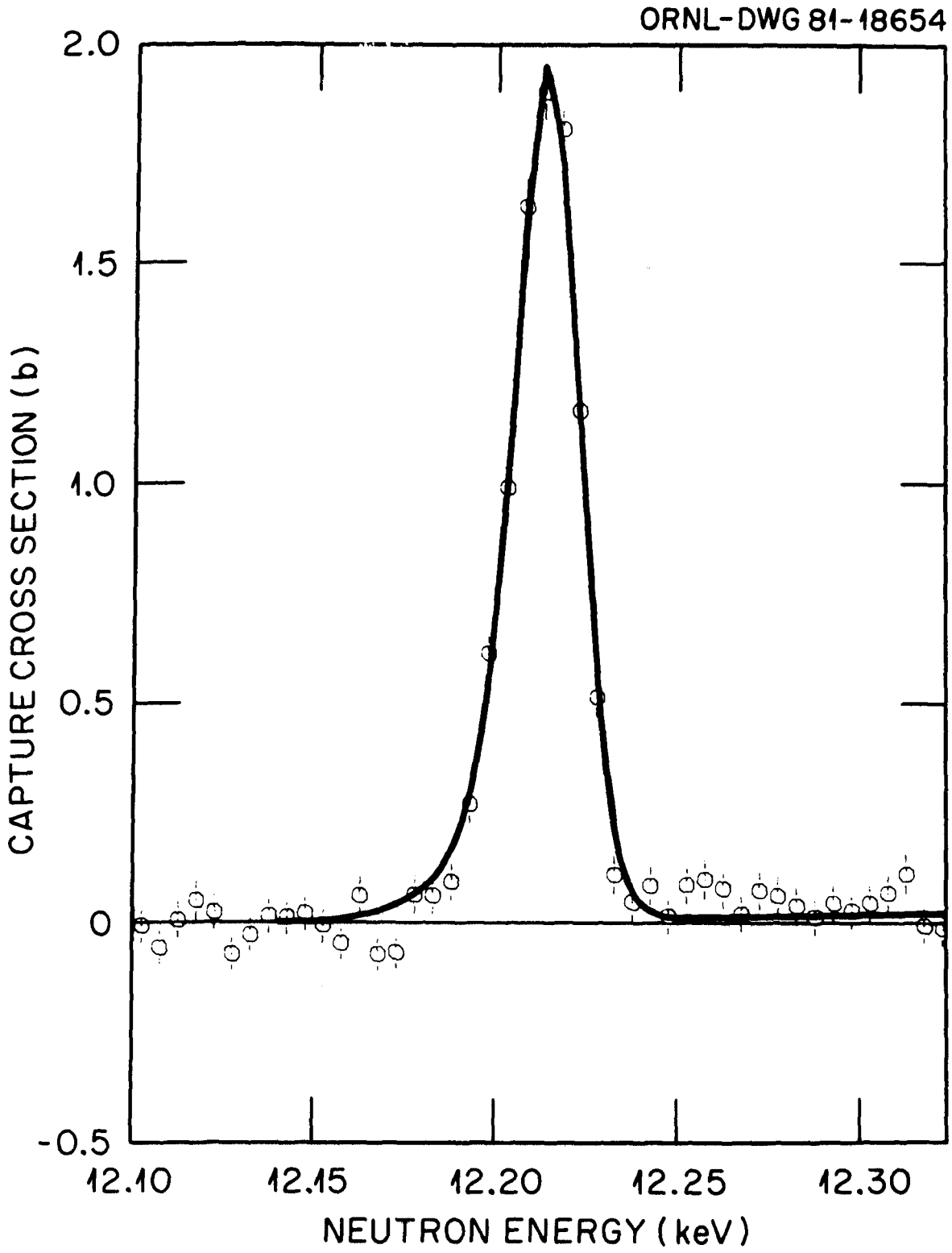

Fig. 9. The resonance at 12.22 keV. The code readjusted the various parameters to give this fit with any of the off-resonance scattering values given in Table 5.

Table 5. Illustration of the effect of the value of σ_{off} used in the code on the kernel $g\Gamma_n\Gamma_\gamma/\Gamma$ and on the multiple scattering correction factor f_o for the $\ell > 0$ resonance at 12.220 keV

σ_{off} (b)	$\frac{g\Gamma_n\Gamma_\gamma}{\Gamma}$ (eV)	f_o (%)
200	0.201 ± 0.004	52
150	0.186 ± 0.004	42
100	0.170 ± 0.003	31
50	0.155 ± 0.003	17
8	0.144 ± 0.003	3

be checked on a few well-separated individual resonances up to 250 keV. At higher energy, the overlap of the resonances does not permit picking up the background between the resonances. Satisfactory fits were obtained using the uniform value of 2.5 mb found earlier, but above 250 keV a 2-mb uncertainty on the background is more realistic. Figures 1 to 7 show the capture data before the background corrections were applied, whereas these background corrections have been subtracted from the capture data shown in Figs. 10 to 15.

5.5 NEUTRON SENSITIVITY OF THE DETECTOR

A correction for the capture in the detector environment of neutrons scattered from discrete resonances in the sample is required.[17] This prompt neutron sensitivity can be formulated as a correction to Γ_γ such that

$$\Gamma_{\gamma(cor)} = \Gamma_\gamma - C\Gamma_n \quad , \tag{5.2}$$

where C is dependent on the amounts and distribution of absorber in the vicinity of the detector. This correction factor is energy dependent and varies from 10^{-3} to 10^{-4} over the energy range of this analysis as shown in Fig. 16. Values of C are considered accurate to ~50%. This correction has been applied and C is given in Table 2 if $C\Gamma_n$ is 3% or more of Γ_γ. Below 200 keV, this correction is responsible for most of the uncertainty on the capture width of large s-wave resonances where $C\Gamma_n$ can be as large as half of the capture width given by the code.

6. ENERGY SCALE CALIBRATION

The energies of the resonances in the transmission data are systematically larger than those in the capture data. The difference between the two energy scales, E_T - E_c, varies smoothly from 0.01 to 0.06% of the neutron-incident energy from 20 to 300 keV but at a much higher rate above 300 keV as shown by the points plotted in Fig. 17. When the resonances are well separated in both sets of data, it is possible to match them with good confidence. This is true up to 250 keV as shown in Figs. 2 to 5

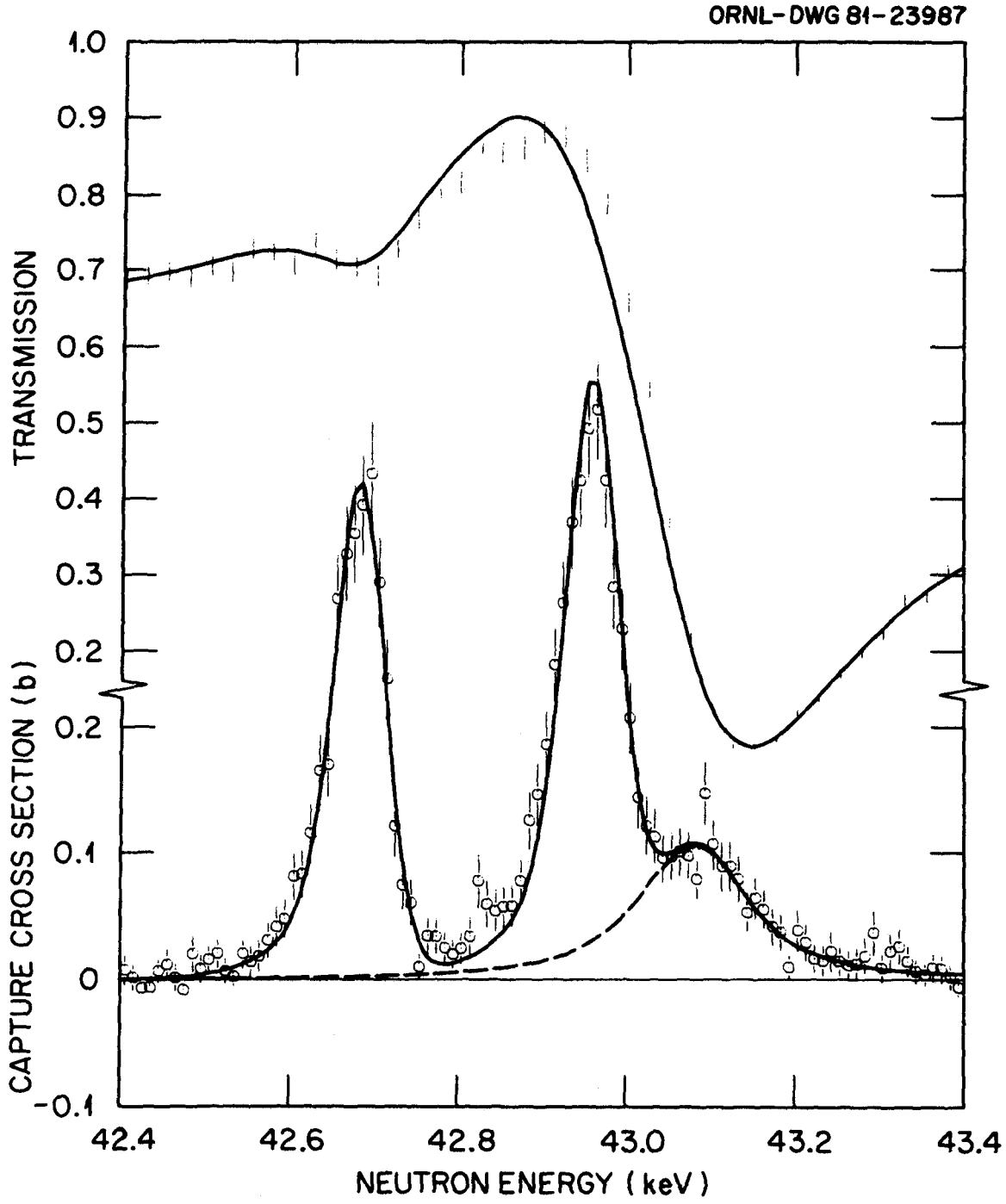

Fig. 10. Fits to the transmission and capture data in the region of the 43.1-keV s-wave resonance. The dashed curve is the s-wave resonance contribution to the capture cross section.

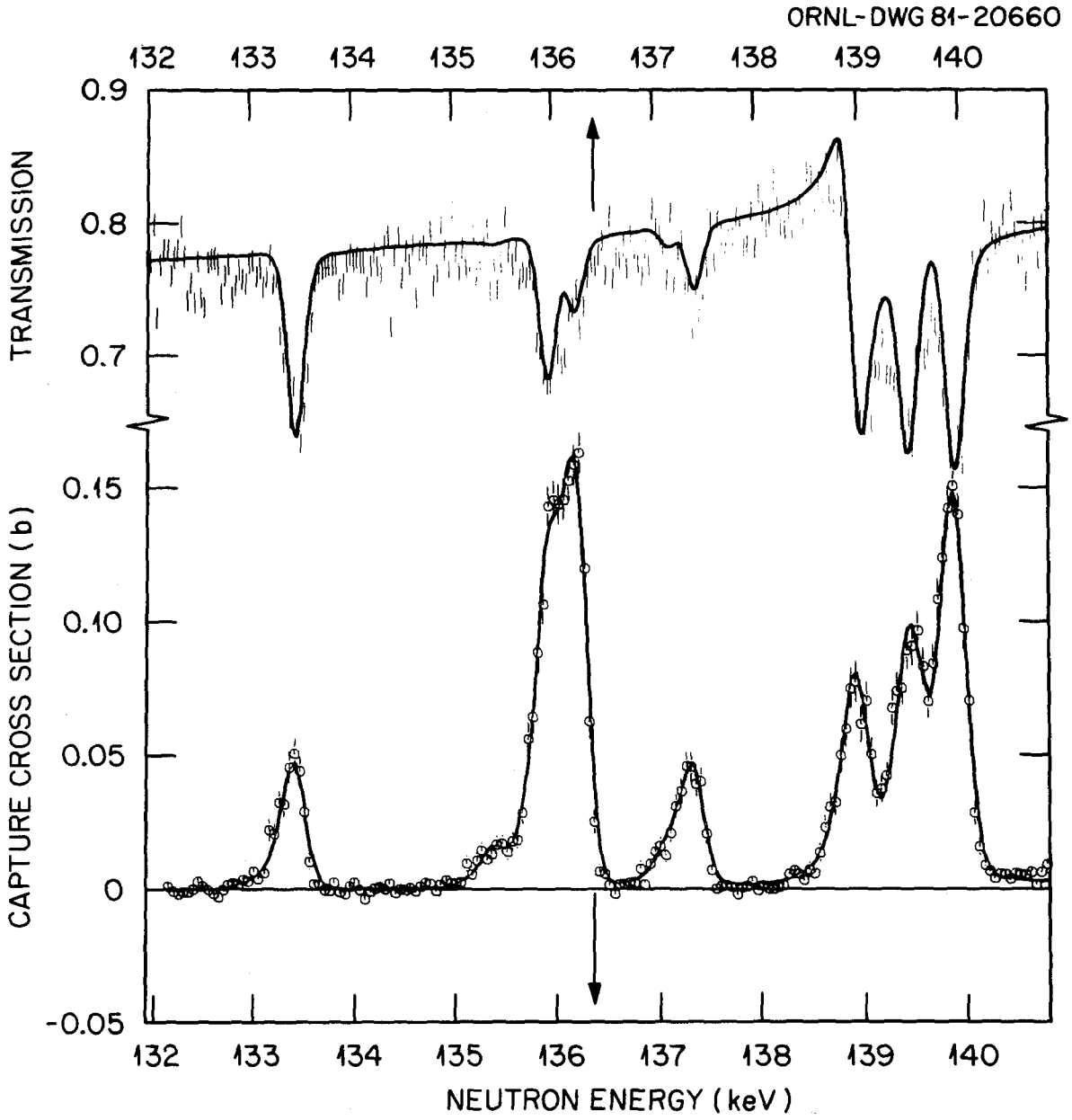

Fig. 11. Fits to the transmission and capture data in the 132- to 141-keV region. The shift between the two energy scales corresponds to the correction (E_T - E_c) discussed in Sect. 6.

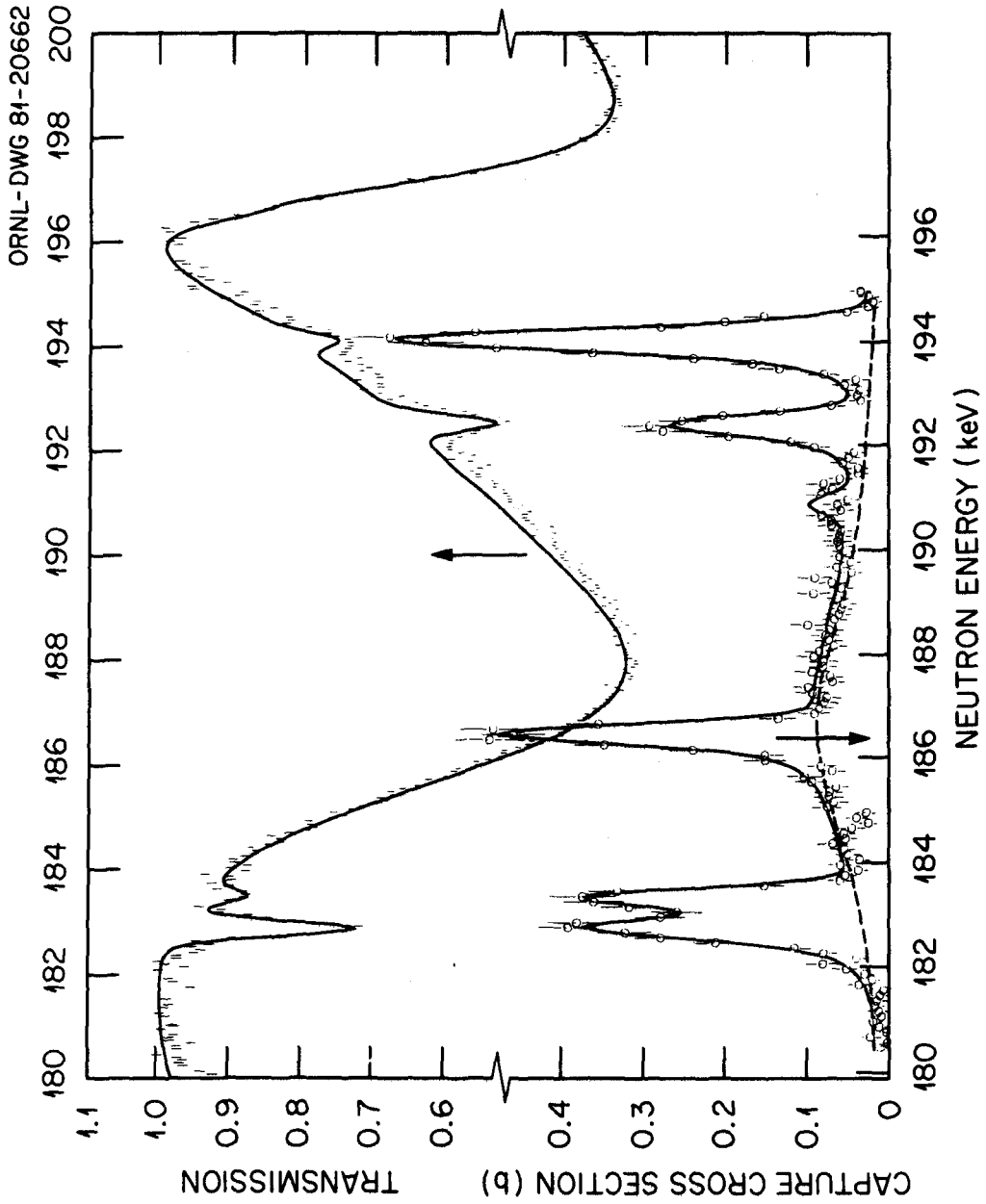

Fig. 12. Fits to the transmission and capture data in the region of the strong s-wave resonance at 186.51 keV. The dashed curve is the s-wave resonance contribution to the capture cross section. The shift between the two energy scales corresponds to the correction (E_T - E_c) discussed in Sect. 6.

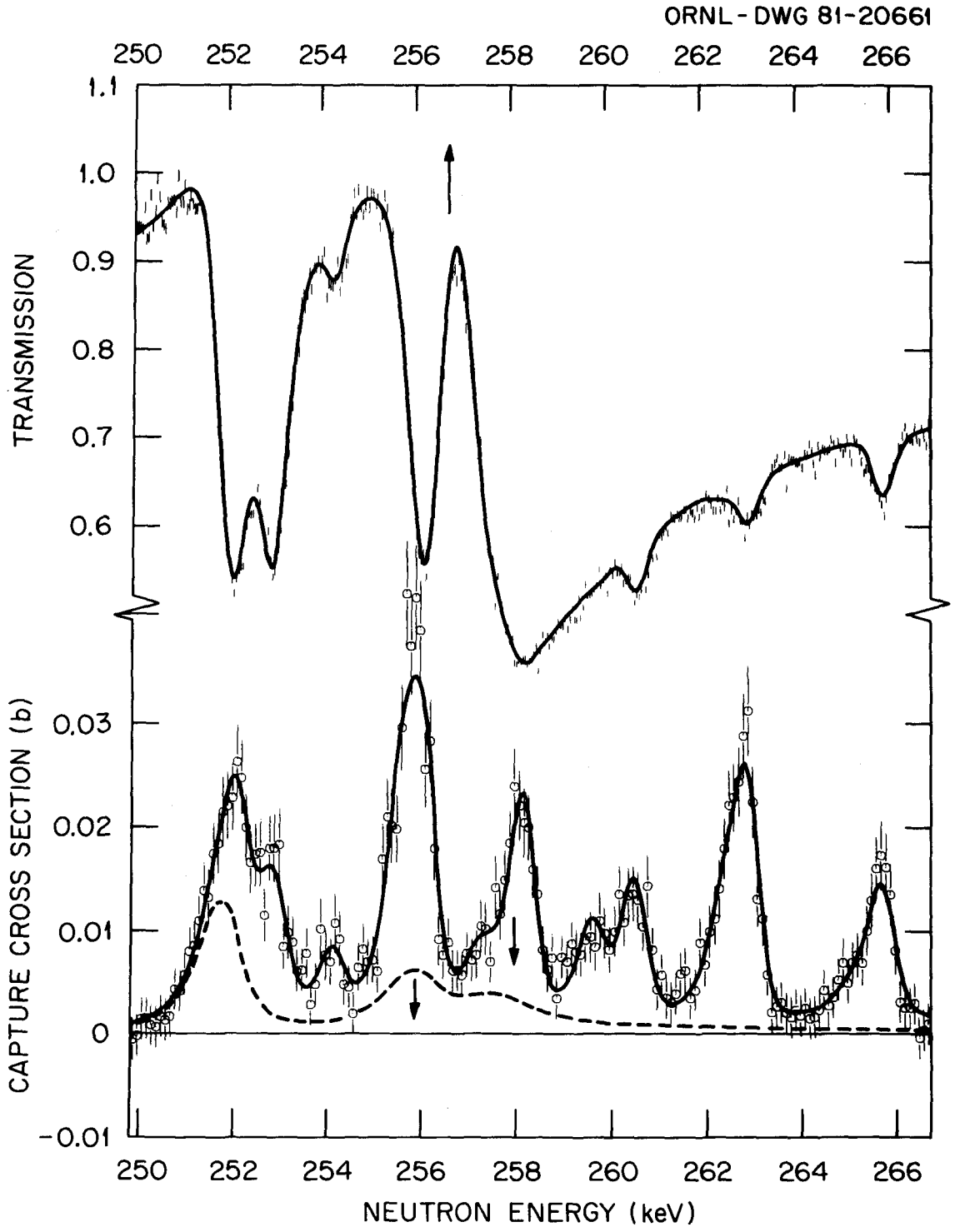

Fig. 13. Fits to the transmission and capture data in the 250- to 267-keV energy region. The dashed curve is the s-wave resonances contribution to the capture cross section. The shift between the two energy scales corresponds to the correction $(E_T - E_c)$ discussed in Sect. 6.

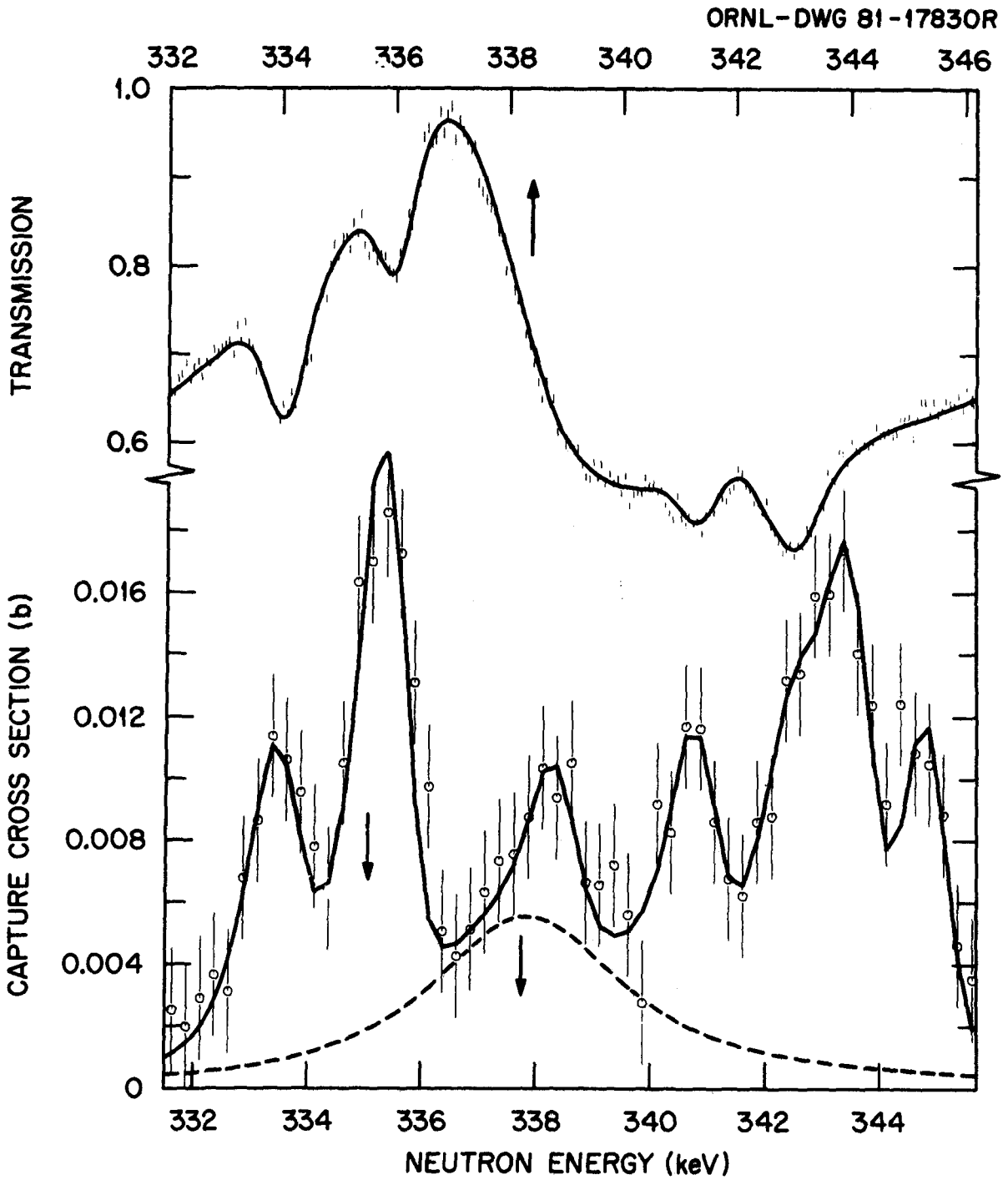

Fig. 14. Fits to the transmission and capture data in the 332- to 346-keV energy region. The dashed curve is the s-wave resonance contribution to the capture cross section. The shift between the two energy scales corresponds to the correction (E_T - E_c) discussed in Sect. 6.

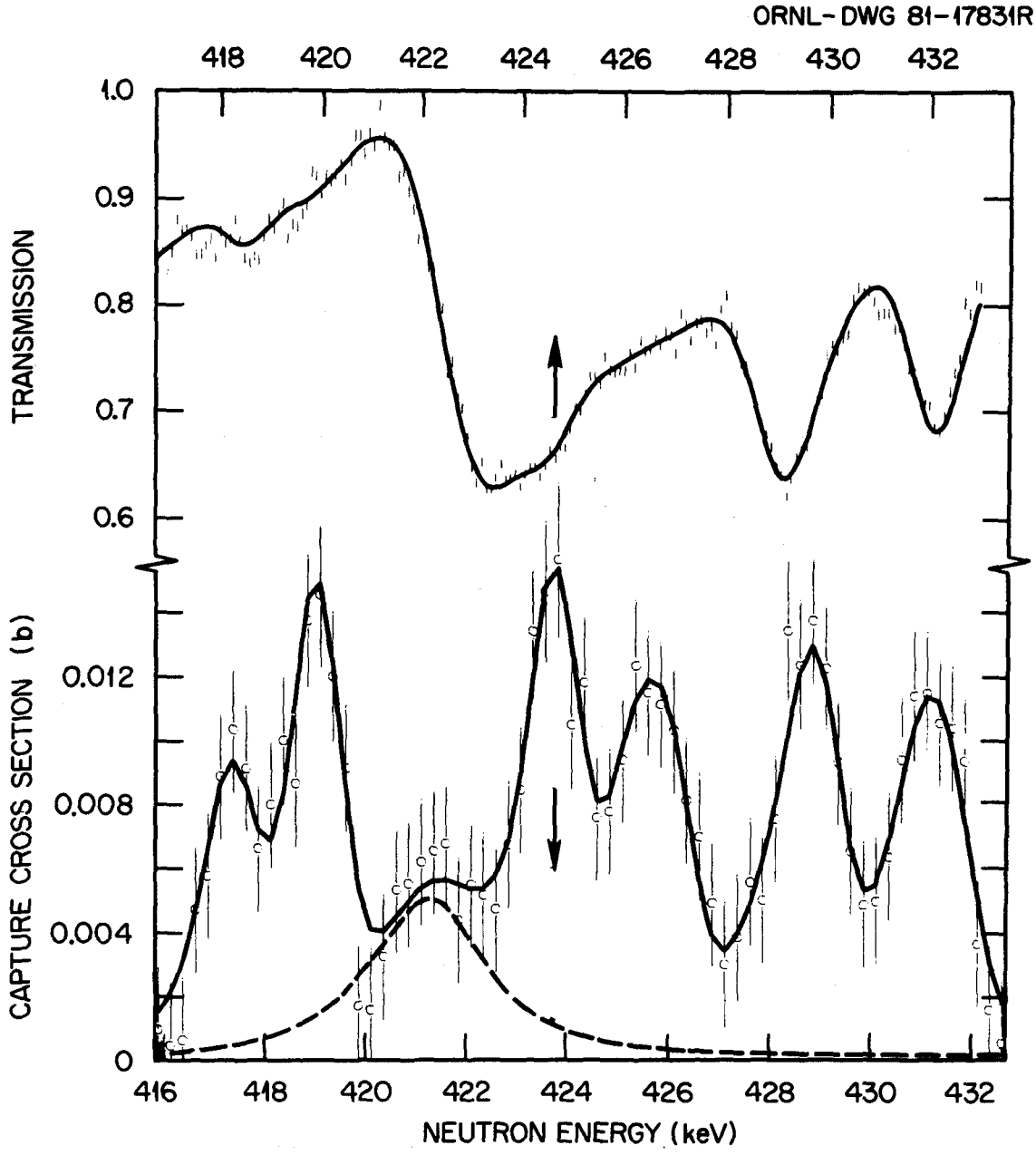

Fig. 15. Fits to the transmission and capture data in the 416- to 432-keV energy region. The dashed curve is the s-wave resonance contribution to the capture cross section. The shift between the two energy scales corresponds to the correction (E_T - E_c) discussed in Sect. 6.

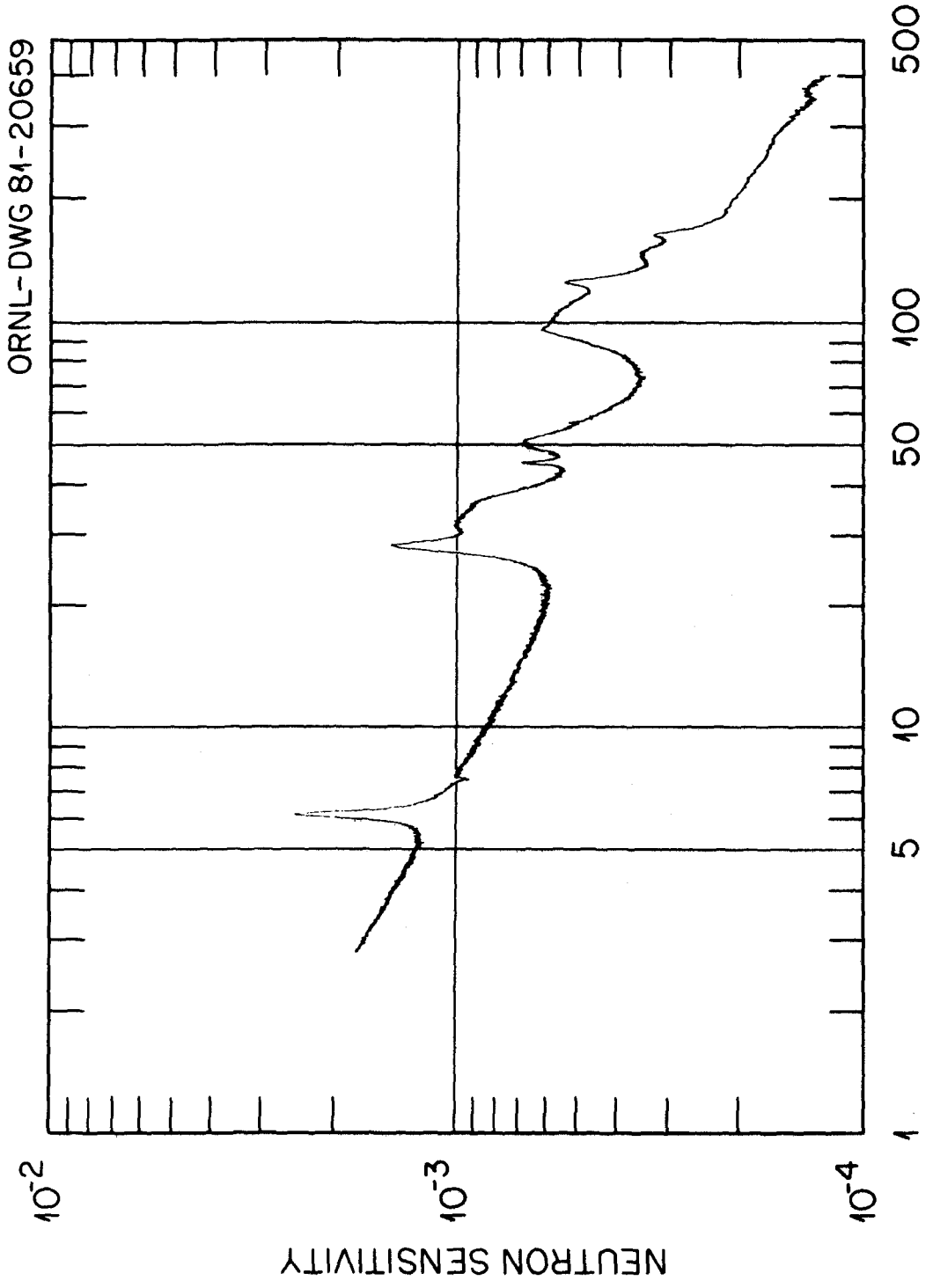

Fig. 16. Detector neutron sensitivity as a function of the incident neutron energy for the ^{60}Ni targets. The corrected radiation widths are given in the last column of Table 2. See Sect. 5.5 for details.

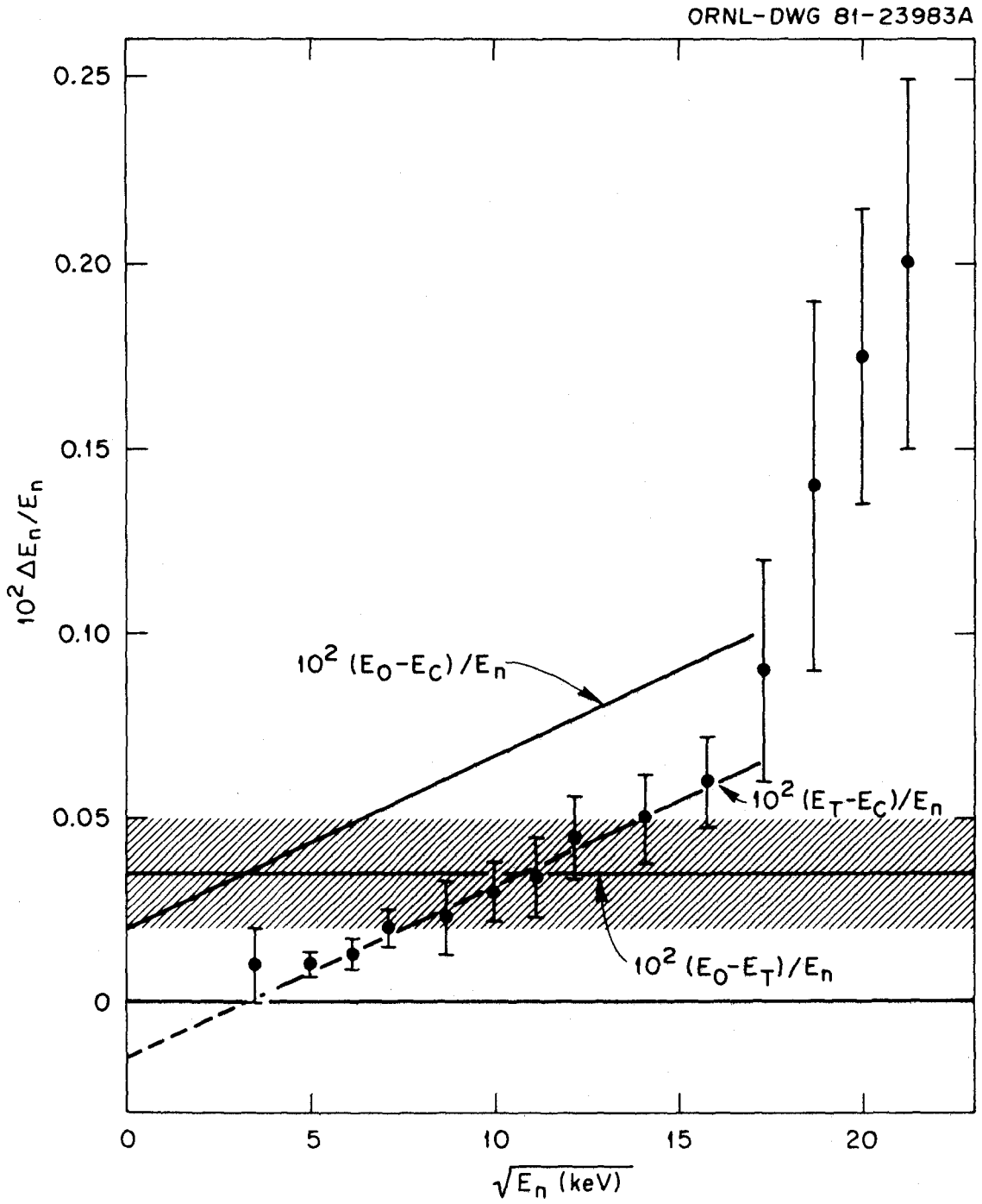

Fig. 17. Corrections in percent applied to the energy scales as a function of the square root of the incident neutron energy. E_c and E_T stand for the energy of resonances in the capture and transmission data respectively; E_o for the final energy scale given in Table 2. The shaded area shows the ±0.015% uncertainty on the 0.035% correction on the transmission data energy scale.

and in more detail in Figs. 11 and 12. The shift which must be applied to the energy, E_c, of a resonance observed in the capture data to match the energy, E_T, of the corresponding resonance in the transmission data is obtained from $\ell > 0$ resonances seen in both sets of data. The uncertainties associated with the points in Fig. 17 depend on how many resonances can be seen in both data sets in a given region and how well separated, and how sharp, these resonances are. For example, in the 75-keV region (Fig. 3) enclosed between the two s-wave resonances at 65.228 and 86.837 keV, eight sharp and well-separated resonances can be seen in the capture data. Only two of them are seen in transmission and only one, the resonance at 73.206 keV, has a well-defined energy in both sets of data. (The resonance at 86.170 keV is overlapping too much with the s-wave resonance.) Therefore, the point at 75 keV on Fig. 17 (plotted at 8.7 on the $\sqrt{E_n}$ scale) has an uncertainty of about 50%. Above 250 keV, the resonances in the transmission data are still fairly well separated but the resonances in the capture data become progressively more overlapping (Fig. 13). We start having difficulty in matching the resonances around 300 keV which explains the large uncertainties in the last four points plotted in Fig. 17. We were able to get fits similar to the ones shown in Figs. 14 and 15 only with a sharp increase in the difference between the two energy scales. Here we need again to stress the point that, especially above 300 keV, we do not claim that the fits and the corresponding set of resonance parameters are in any way unique. We probably could obtain satisfactory fits as well with a slightly different energy shift but we would need more resonances to fit the same data.

As reported earlier, the flight path and the burst width in the transmission experiment using the NE-110 detector are 78 m and 10 ns respectively, compared to a 40-m flight path and 4-ns burst width in the capture experiment. Therefore, the resolutions in both experiments are nearly the same and cannot justify the choice of one energy scale over the other. Typical values of the resolution (FWHM) are given in Table 1. Below 50 keV, the transmission data analyzed here are the data using the lithium glass detector with a burst width of 40 ns which explains the larger resolution of the transmission in this energy region.

A transmission experiment similar to the one analyzed in this report was conducted by D. C. Larson[11] on a natural nickel target at the 200-m flight-path station with an 8-ns burst width. Because of the better resolution and the attention paid to the energy calibration, we believe that the energy scale of these data is more accurate. Six well-separated $\ell > 0$ resonances in the natural nickel data can be identified with resonances in the presently analyzed ^{60}Ni data. In both sets of data, the energy of these resonances was determined by the first-moment method. This is reported in columns 1 and 2 of Table 6. These energy parameters are systematically larger in the natural nickel data by a percentage given in the third column. The average discrepancy is 0.033%.

In the transmission spectrum of the open neutron beam (through the overlap filter only), one can identify four resonances due to the sulfur content of the filter. These resonance energies are compared in Table 6 with values from an ENDF publication[18] and with neutron total and capture cross-section measurements on ^{32}S by Halperin et al.[19] Here it can be seen that the energy scale of the present transmission experiment is systematically too low by 0.037%.

A normalization factor of 0.035 $\pm$ 0.015% (shaded area in Fig. 17) was applied to the resonance energies of the transmission, E_T, to obtain the parameter E_o in Table 2. This correction is in good agreement with the 0.025% estimated systematic uncertainty on the transmission data energy scale given in ref. 19. Up to 300 keV, this renormalization factor is very similar to the corrections, (E_T - E_c), applied to the energy scale of the capture data to match the energy scale of the transmission data as shown in Fig. 17.

The difference between energy scales is associated primarily with the uncertainties on the time of flight and on the flight path. To find approximate values of these uncertainties, the following simple nonrelativistic relation between the neutron energy E_n in keV, the flight path L in mm, and the time of flight t in ns can be used:

Table 6. Energy scale calibration of the ^{60}Ni transmission data[a]

^{60}Ni Resonance energy (keV)			^{32}S Resonance energy (keV)			
Present work	Reference 11	Percent energy discrepancies	Present work (open beam)	Reference 18	Reference 19	Percent energy discrepancies
			30.365	30.376 (4)	30.380 (5)	0.036[b]
33.009	33.015	0.018				
33.380	33.387	0.021				
			97.463	97.498 (16)	97.500 (11)	0.036[b]
			112.122	112.175 (20)	112.180 (20)	0.047[b]
127.629	127.678	0.038				
214.045	214.118	0.034				
			288.30		288.38 (4)	0.028[c]
402.719	402.931	0.053				
516.056	516.244	0.036				

[a]The energies of six resonances are compared with energies of corresponding resonances in high-resolution natural-nickel measurements. The energies of five sulfur resonances seen with the open beam are compared with values given in two recent publications (see Sect. 6 for details). The uncertainties on the last significant figures are given in parentheses.

[b]Percent energy discrepancy between ref. 18 and present work.

[c]Percent energy discrepancy between ref. 19 and present work.

$$E_n = 10^{-3}(72.297\ L)^2 t^{-2} \quad , \tag{6.1}$$

from which

$$\frac{1}{t} = 0.4374\ \frac{1}{L}\ \sqrt{E_n} \quad . \tag{6.2}$$

From the partial derivative of Eq. (6.1) with respect to L and t, and using Eq. (6.2), we obtain

$$\frac{\Delta E_n}{E_n} \simeq 2\ \frac{\Delta L}{L} - 0.8748\ \frac{\Delta t}{L}\ \sqrt{E_n} \quad . \tag{6.3}$$

The correction, $(E_o - E_T)/E_n$, in percent, applied to the transmission data energy scale is shown in Fig. 17. Since the renormalization is independent of the energy, it should be associated entirely to a shift in the flight path. From Eq. (6.3), with $\Delta E_n/E_n = (0.035 \pm 0.015) \times 10^{-2}$ and $L = 78{,}203$ mm, we obtain

$$\Delta L = 14 \text{ mm} \pm 6 \text{ mm} \quad . \tag{6.4}$$

Although large, this correction is less than the NE-110 scintillator thickness which was 20 mm.

Recent Monte Carlo calculations of the ORELA moderator time distribution vs neutron energy[20] indicate a correction of 10 mm at 10 keV, rising to 29 mm at 400 keV for ^{60}Ni transmission data which used only the moderated flux. The flux for the 200-m flight path data is dominated by direct yield from the tantalum target rather than the water moderator.

The cumulative corrections, $(E_o - E_c)/E_n$, applied on the energy scale of the capture data are plotted in Fig. 17 as a function of $\sqrt{E_n}$. The slope of the straight line is positive since the energy of the capture data is systematically smaller than the final energy E_o. From Eq. (6.3), with $L = 40{,}123$ mm, the slope corresponds to a shift in the time of flight of -2.1 ± 0.3 ns and the intercept to a shift in the flight path of 4 ± 3 mm. These values are well within the range of the expected uncertainties in the capture experiment.

The Monte Carlo calculations of moderation time for ORELA[20] reproduce quite closely the observed slope of $(E_T - E_c)/E_n$ up to 250 keV. However, this slope disagrees with the calculations by two standard deviations at 400 to 450 keV. This suggests that there may be misidentifications of capture peaks with resonances seen in transmissions above 300 keV.

7. RESULTS AND DISCUSSIONS OF THE UNCERTAINTIES

7.1 RESONANCE PARAMETERS AND FITS

The final resonance parameters obtained in the combined analyses of the ^{60}Ni transmission and capture data from 1 to 450 keV are given in Table 2. Well-separated resonances are spaced by one blank line; strongly overlapping resonances are grouped; and resonances forming a multiplet are grouped and joined by a bracket. There is not a clear cut between what is called "strongly overlapping" resonances

and what is called a "multiplet"; therefore, this classification should not be taken too seriously. Nevertheless, it was adopted since we found it useful in spotting at a glance a group of resonances on the plots and the corresponding group of parameters in Table 2.

The resonance energy E_o reported in the first three columns is the corrected neutron energy as discussed in Sect. 6. The criteria for assigning an angular momentum of 1 or 2 to an $\ell > 0$ resonance were based only on the shape of the resonances as discussed in Sect. 3.1. Within parentheses are the statistical uncertainties on the energy parameters given by the search codes.

The capture kernels with their statistical uncertainties are given in the fourth column. When the capture area was adjusted by trial and error, the uncertainty was estimated from the sensitivity of the fit to the variation of this parameter and the subscript c is used.

Neutron widths and statistical uncertainties are given in column 5. For some small resonances, the neutron widths were adjusted by trial and error and the uncertainties quoted were estimated from the sensitivity of the fit to the variation of this parameter. The capture kernel is the only well-known parameter associated with the 89 resonances seen only in the capture data. However, the neutron and radiation widths of these resonances are not totally arbitrary. Estimated values of these parameters are given but without uncertainty.

The radiation widths reported in column 6 are defined only for resonances seen in both sets of data with the exception of the resonance at 2.253 keV. This small resonance, analyzed only in transmission because our capture data does not go below 2.5 keV, is best fitted with the set of parameters reported in Table 2. The calculated capture kernel corresponding to these parameters is 0.051 eV; therefore, this resonance would probably have been seen in capture if data were available since the resonance at 5.532 keV is well defined and has a capture kernel of only 0.043 eV.

The correction factor C for the neutron sensitivity of the detector and the corrected radiation widths, $\Gamma_{\gamma(cor)}$, are shown in the next two columns. The uncertainties associated with the corrected radiation widths are the quadratic combination of the 50% uncertainty on the correction factor C with the statistical uncertainties on Γ_γ.

In Figs. 1 to 7 the transmission data are compared to the theoretical transmission calculated with all the resonance parameters given in Table 2. The capture data (Figs. 1 to 7) show the many resonances seen in capture but not in transmission and show how the chosen neutron and radiation widths for these resonances affect the theoretical transmission. The fits to both kinds of data are shown in detail in Figs. 10 to 15 for six small energy regions. The theoretical transmission is the same as in Figs. 1 to 7. The fits to the capture data are typical of the fits obtained in the other energy regions. The top (E_T) and bottom (E_c) energy scales have been shifted by the proper correction (E_T - E_c), as discussed in Sect. 6, so that the resonances seen in both sets of data are aligned. Around 40 keV (Fig. 10), the correction is too small to be seen (less than 10 eV). The shift in Fig. 11 is 50 eV; 90 eV in Fig. 12; and 160 eV in Fig. 13. It jumps to about half of a keV around 340 keV (Fig. 14) and to almost 1 keV above 400 keV (Fig. 15).

The dashed lines in Figs. 10, 12, 13, 14, and 15 are the capture cross-section contributions of the large s-wave resonances present in these regions.

7.2 ESTIMATED UNCERTAINTIES AND THEIR CORRELATIONS

The search codes give us the statistical uncertainties and their correlations. Here some of the systematic uncertainties and, in a few examples, the various contributions to the covariance of the parameters of two resonances will be estimated.

The correlation matrix given by the code SAMMY at the end of the procedure described in Sect. 3.3 gives the correlations between the statistical uncertainty of all the 203 adjusted parameters inside and outside of the 1- to 450-keV energy range, whereas the correlation matrices for the parameters obtained in the capture analysis are relevant only to small energy ranges as shown in Figs. 10 to 15.

For conciseness, "correlations between parameters" will be referred to from now on instead of "correlations between statistical uncertainties of parameters" when this simplification does not lead to confusion.

7.2.1 *Resonance Energies*

The statistical uncertainties on the energies of the s-wave resonances given in Table 2 were determined by the code SAMMY from the transmission data analysis except for the three narrow resonances at 200.59, 418.3, and 443.9 keV which were better defined in the capture data. The systematic uncertainty of 0.015% on the renormalization of the energy scale discussed in Sect. 6 is the main source of uncertainty on the energies of the s-wave resonances as illustrated in Table 6. The contribution to the covariance due to the statistical uncertainties given by the code SAMMY will always be negligible compared to the contribution from the systematic uncertainties which are dominant and 100% correlated.

The statistical uncertainties of the energies of all the other resonances are obtained mostly from the LSFIT code used in the fitting of the capture data. Some energies of very small or very strongly overlapping resonances were adjusted by trial and error. In addition to the statistical uncertainties given in Table 2, the two sources of systematic uncertainties discussed in Sect. 6 must be considered. Final estimated uncertainties on E_o are given in Table 7 for six $\ell > 0$ resonances. This shows that up to 300 keV the three sources of uncertainties contribute about equally to ΔE_o, but above 300 keV the large uncertainty on the shift between the two energy scales, E_T - E_c, is the dominant factor.

The energy parameters of $\ell > 0$ resonances are correlated only in the case of strongly overlapping resonances. Take, for example, the doublet in Fig. 12. The energies of the resonances are 194.19 and 194.54 keV with statistical uncertainties of 10 and 30 eV, respectively. The correlation between these uncertainties is 0.26. The systematic uncertainties are 23 eV for $\Delta(E_T - E_c)$ and 29 eV for $\Delta(E_o - E_T)$, similar to what is given in Table 7 for the resonance at 192.59 keV. Therefore, the covariance of the energy parameters due to the statistical uncertainties is 78 eV^2 compared to 1370 eV^2 for the covariance due to the fully correlated systematic uncertainties. It can be seen that even for a doublet the contribution to the covariance of the energy parameters due to the statistical uncertainties is negligible.

7.2.2 *Neutron Widths*

Since the systematic uncertainties in the transmission experiment were not parameterized, they could not be included in the SAMMY input. Therefore, an estimate of the systematic uncertainties on the neutron widths cannot be given. The various sources of systematic uncertainties on fluorine transmission measurements were investigated and reported in ref. 2. A similar investigation on ^{60}Ni transmission measurements leads to an estimated 2% systematic uncertainty. This 2% systematic uncertainty should be added to the statistical uncertainties of cross sections calculated with the resonance parameters given in this report.

In the transmission data, most s-wave resonances are well separated. The largest correlation coefficient between the neutron widths of two s-wave resonances is -0.36. This is between the 256.12-keV resonance (Γ_n = 870 ± 6 eV) and the 257.63-keV resonance (Γ_n = 1826 ± 7 eV) which gives a covariance due to statistical uncertainties on neutron widths of -15 eV^2.

Table 7. Sample of uncertainties on the final energy parameter E_o

E_o (keV)	ℓ	ΔE_T or ΔE_c statistical (eV)	$\Delta(E_T - E_c)$ from Fig. 17 (eV)	$\Delta(E_o - E_T)$ 0.015% of E_o (eV)	ΔE_o (eV)
12.487	0	1		2	2.2
13.624	>0	1	(0.01%) 1.4	2	2.6
65.228	0	1		10	10
65.573	>0	2	(0.007%) 5	10	11
139.03	0	<10		21	21
139.56	>0	20	(0.011%) 15	21	33
186.51	0	<10		29	29
192.59	>0	20	(0.012%) 23	29	42
251.99	0	<10		38	38
252.32	>0	50	(0.012%) 30	38	63
422.49	0	<10		64	64
424.6	>0	100	(0.05%) 200	64	233

[a]In column 3 are the statistical uncertainties as given in Table 2. In columns 4 and 5 are systematic uncertainties from Fig. 17 and as discussed in Sect. 6. ΔE_o is the quadratic combination of the statistical and systematic uncertainties. E_T and E_c stand for the energy of resonances in the transmission and capture data respectively.

Covariances due to statistical uncertainties on the neutron widths of an $\ell > 0$ resonance on top of an s-wave resonance are also quite small. Take, for example, in Fig. 13 the p-wave resonance at 253.07 keV ($\Gamma_n = 264 \pm 3$ eV) on top of the s-wave resonance at 251.99 keV ($\Gamma_n = 536 \pm 4$ eV). These two resonances are strongly anti-correlated. The correlation coefficient between the two neutron widths given by the code SAMMY is -0.7 which leads to a covariance of -8 eV^2. Similar calculations applied to $\ell > 0$ resonance parameters forming a doublet also give very small covariances due to the small statistical uncertainties on the neutron widths. These small statistical uncertainties are due to the great number of data points and because the energy parameter of the $\ell > 0$ resonances were not adjusted in the code SAMMY.

7.2.3 *Capture Kernel*

A systematic uncertainty on the capture yield of 3.4 to 4% was reported in Sect. 4. An additional systematic uncertainty of 0.5% is associated with the multiple scattering and self-protection corrections in the data reduction.[21] This uncertainty is certainly larger than 0.5% for the large s-wave resonances. Finally two sources of systematic uncertainty arise from the data analysis. One is related to the fitting of the shape of the resonances by the code. This uncertainty is hard to estimate. The shape of a resonance is affected by the spin assignment and by the energy resolution. In ref. 21 this uncertainty is estimated to be less than 3%. All these uncertainties, when combined, add up to 4.6% below 100 keV

and 5% above 100 keV, which means 5% or less in the energy range considered in this analysis. Examples of these relative uncertainties are shown in the fourth column of Table 8 (Syst. 1). The other source of systematic uncertainty associated with the data analysis is in the subtraction of the background discussed in Sect. 5.4. Since the shape of the $\ell > 0$ resonances can be approximated by a triangle and the widths are given by the resolution function, the systematic uncertainty on the capture area due to the uncertainty on the background can easily be estimated for well-separated $\ell > 0$ resonances not on top of s-wave resonances. For $\ell > 0$ overlapping resonances, the total uncertainty on the capture kernel due to the uncertainty on the background is calculated with an estimated width at the base equal to the width due to the resolution plus the energy separation of the resonances.

This last relative systematic uncertainty increases with neutron energy and varies drastically from one resonance to another, depending on the capture area of the resonance. Examples of these relative systematic uncertainties are given in the fifth column of Table 8 (Syst. 2) and the total relative systematic uncertainties in the last column. Table 8 shows that the uncertainty due to the subtraction of the remaining background during the capture data analysis is the main source of systematic uncertainty above 250 keV.

Table 8. Uncertainties on the capture kernel K^a

E_o (keV)	K (eV)	$\Delta K/K$ statistical (%)	$\Delta K/K$ systematic (%)		
			Syst. 1	Syst. 2	Total syst.
21.274	0.022	10	4.6	2.7	5.3
23.788	0.24	4	4.6	0.3	4.6
136.03	1.34	4	5.0	0.9	5.1
226.28	0.65	6	5.0	7.5	9
341.4	1.0	10	5.0	25	26
431.9	1.3	15	5.0	20	21
432.4	1.2	17	5.0	20	21

$^a K = g\Gamma_n\Gamma_\gamma/\Gamma$.

To give an example of correlations between the uncertainties of two strongly overlapping resonances, we chose two resonances for which the neutron widths are much larger than the capture kernels. For such resonances the correlation coefficient between the radiation widths given by the code LSFIT is the same as the correlation coefficient between the capture kernels.

From Table 2 the resonance parameters of the doublet at 432 keV are:

$$E_{0_1} = 431.9 \text{ keV}, K_1 = 1.3 \pm 0.2 \text{ eV}, g\Gamma_{n_1} = 240 \pm 10 \text{ eV}$$

$$E_{0_2} = 432.4 \text{ keV}, K_2 = 1.2 \pm 0.2 \text{ eV}, g\Gamma_{n_2} = 180 \pm 8 \text{ eV}$$

where K denotes the capture kernel $g\Gamma_n\Gamma_\gamma/\Gamma$. The correlation coefficient given by the code is -0.88; consequently, the statistical contribution to the covariance of K_1 and K_2 is

$$<dK_1 dK_2>_{stat.} = -0.035 \text{ eV}^2 \quad .$$

The total relative systematic uncertainties are both 21% and are fully correlated. Therefore the systematic contribution to the covariance of K_1 and K_2 is

$$<dK_1 dK_2>_{syst.} = 0.068 \text{ eV}^2 \quad .$$

The two contributions to the covariance are of opposite signs; therefore, the total covariance of the capture kernels is equal to $+0.033$ eV^2. By definition the correlation coefficient C is given by

$$C(K_1,K_2) = \frac{<dK_1 dK_2>}{\sqrt{<dK_1^2><dK_2^2>}} \tag{7.1}$$

where $<dK_i^2>$ are the variances of the capture kernels. The final correlation coefficient for these resonances is $+0.31$.

This illustrates that the combined effect of the statistical and systematic uncertainties should be carefully studied before drawing a conclusion on the final correlation coefficient.

Some systematic uncertainties discussed earlier in this section apply only to narrow resonances. The 3% maximum contribution to the systematic uncertainty from the finite resolution and the lack of knowledge of the spin of the resonances does not apply to large s-wave resonances. On the other hand, the relative uncertainty associated with the multiple scattering and self-protection corrections can be as much as 5% (compared to an estimated 0.5% for narrow resonances). Also, for large s-wave resonances, even at low energy the subtraction of the background during the data analysis is a major source of systematic uncertainty.

8. COMPARISON WITH OTHER WORKS

Some resonance parameters in Table 2 will be compared with parameters reported in earlier publications referred to in Table 9. The range of energy analyzed is given for each reference. Up until now, there were no ^{60}Ni capture measurements above 200 keV and the total cross-section measurements of Farrel et al.[22] were the only data available above 340 keV.

8.1 s-WAVE RESONANCES

In Table 10, parameters for s-wave resonances are compared with values given in earlier publications. Resonance energies are generally in good agreement with ref. 23 but systematically higher than the two other works.[24,25] Above 150 keV, the discrepancies with the energy parameters of Fröhner[25] are as large as 2 keV. The neutron widths are in better agreement with ref. 24 than with ref. 23 for the first five s-wave resonances (up to 90 keV). Between 100 and 200 keV, it is the reverse. Above 200 keV, the uncertainties on the neutron widths given by Stieglitz et al.[23] are large but do not explain the factor of 2 to 3 found between their reported values and ours for three of the five s-wave resonances. Farrell et al.[22] neutron widths are compared with ours above 338 keV. The agreement is fair (better than 25%) only with the four larger resonances ($\Gamma_n > 1$ keV) above 370 keV.

Table 9. Ni-60 resonance parameter sources

Author	Ref.	Transmission data analysis range in keV	Capture data analysis range in keV
This work (ORELA)		$1 < E_n < 450$	$2.5 < E_n < 450$
Syme et al. (Harwell)	24	$\ell=0$, $10 < E_n < 200$ $\ell>0$, $30 < E_n < 300$	
Fröhner (KFK)	25		$10 < E_n < 200$
Stieglitz et al. (RPI)	23	$\ell=0$, $10 < E_n < 340$	$\ell=0$, $10 < E_n < 70$ $\ell>0$, $1 < E_n < 140$
Farrell et al. (Duke)	22	$\ell=0$, $10 < E_n < 600$ $\ell>0$, $120 < E_n < 600$	
Mughabghab et al.[a]	26	$1 < E_n < 600$	$10 < E_n < 200$

[a]Recommended neutron widths are based on refs. 22, 23, 24, 27, and 28. Recommended radiation widths are based on refs. 23, 25, 29, 30, and 31.

The radiation widths of the first two s-wave resonances at 12.487 and 28.709 keV are in good agreement with the values reported by Fröhner[25] because in this low-energy region the p-wave resonances on top of these two s-wave resonances are resolved in Fröhner's analysis as well as here. All other radiation widths for s-wave resonances reported in earlier publications are larger than the values obtained from this analysis. As illustrated by the first two examples in Table 11 at 43 and 65 keV, the unresolved $\ell > 0$ resonances on top of the s-wave resonances are responsible for these discrepancies. In each case two large $\ell > 0$ resonances were included in the s-wave resonance capture area reported in earlier works. Figure 10 illustrates how well these resonances are separated in the ORELA capture data in the 43-keV region.

In Table 11 the resonance parameters are also compared to the recommended values given in "Neutron Cross Sections" by S. F. Mughabghab et al.[26]

8.2 $\ell > 0$ RESONANCES

The level density of $\ell > 0$ resonances in this transmission data analysis is three times higher than in ref. 24 and six times higher than in ref. 22. Also, the capture data analyzed in this report made possible the separation of many levels which could not be resolved before. Since a detailed comparison of our resonance parameters of the $\ell > 0$ resonances with previously published results would be too cumbersome, comparison was made only for resonances below 40 keV (Table 12) and for two small energy regions shown in Fig. 11 (Table 11) and in Fig. 12.

Table 10. Ni-60 s-wave resonance parameters compared to other works

Present work			Stieglitz et al., ref. 23			Syme et al., ref. 24		Fröhner, ref. 25	
E_n (keV)	Γ_n (eV)	Γ_γ (eV)	E_n (keV)	Γ_n (eV)	Γ_γ (eV)	E_n (keV)	Γ_n (eV)	E_n (keV)	Γ_γ (eV)
12.487 (1)	2358 (3)	2.6 (9)	12.47 (6)	2660 (100)	3.3 (3)	12.22 (5)	2354 (1)	12.3 (2)	2.7 (5)
28.709 (1)	698 (1)	0.7 (5)	28.64 (10)	800 (50)	1.10 (10)	28.650 (1)	681.6 (2)	28.64 (10)	0.60 (15)
43.105 (1)	104.4 (6)	0.20 (4)	43.08 (23)	77 (15)	1.73 (18)	43.050 (4)	84.1 (1)	42.92 (11)	0.98 (16)
65.228 (1)	443.0 (8)	0.94 (9)	65.13 (40)	390 (30)	2.43 (25)	65.11 (2)	459.9 (8)	65.12 (16)	1.9 (3)
86.837 (1)	398 (1)	0.62 (10)	86.8 (6)	330 (25)		86.667 (7)	341 (2)	86.35 (22)	1.5 (3)
98.085 (1)	1002 (2)	0.9 (3)	98.1 (7)	870 (70)		97.85 (1)	835.6 (2)	96.79 (30)	1.20 (25)
107.85 (1)	649 (1)	0.8 (2)	107.8 (8)	610 (60)		107.479 (4)	265.3 (5)	107.77 (30)	1.35 (25)
139.03 (1)	30.7 (5)	1.18 (6)							
156.36 (1)	472 (1)	0.35 (13)	156.4 (12)	440 (50)		−156	−100	154.8 (7)	0.70 (12)
161.74 (1)	1325 (2)	0.46 (25)	162.1 (13)	1250 (130)		161.41 (2)	1010 (1)	160.9 (9)	2.2 (4)
186.51 (1)	5237 (6)	2.9 (8)	186.5 (15)	6000 (800)		185.41 (11)	9150 (2)	184.0 (15)	3.2 (8)
197.64 (1)	3025 (2)	1.2 (4)	198.0 (18)	3100 (350)		197.03 (5)	3692 (2)	195.0 (20)	4.1 (10)
200.59 (1)	9.8 (3)	0.6 (2)							
251.99 (1)	536 (4)	1.28 (13)							
256.12 (1)	870 (6)	0.56 (10)							
257.63 (1)	1826 (7)	0.38 (21)	257.8 (21)	3500 (600)					
278.93 (1)	225 (2)	0.41 (7)	279.6 (23)	750 (160)					

Table 10. (Continued)

Present work			Stieglitz et al., ref. 23			Syme et al., ref. 24		Fröhner, ref. 25	
E_n (keV)	Γ_n (eV)	Γ_γ (eV)	E_n (keV)	Γ_n (eV)	Γ_γ (eV)	E_n (keV)	Γ_n (eV)	E_n (keV)	Γ_γ (eV)
291.92 (1)	140 (3)	0.69 (6)							
317.02 (1)	2788 (9)	1.1 (3)	316.8 (31)	3200 (600)					
325.52 (1)	7084 (17)	1.5 (7)	326.3 (33)	6800 (1100)					
338.48 (1)	3563 (14)	2.5 (6)	339.5 (35)	7500 (1500)					
			338.0	5250[a]					
			346.0	250[a]					
357.65 (1)	1619 (10)	2.8 (5)	357.2	1000[a]					
376.84 (1)	3865 (18)	3.0 (6)	375.5	4000[a]					
383.13 (5)	370 (5)	1.82 (13)							
413.44 (5)	344 (6)	0.93 (15)	412.3	750[a]					
418.3 (1)	68 (3)	1.30 (11)							
422.49 (1)	1861 (15)	2.1 (3)	421.0	2000[a]					
			426.5	500[a]					
437.73 (1)	1219 (4)	1.35 (30)	436.0	1000[a]					
443.9 (2)	177 (7)	2.0 (2)							
448.00 (1)	2733 (36)	1.7 (5)	446.0	3000[a]					

[a] From ref. 22.

Table 11. Comparison of parameters obtained in this work for some overlapping resonances with parameters reported in earlier publications (a, b, c, d, and parentheses, same as in Table 2.)

E_n [a] (keV)		$g\Gamma_n$	$g\Gamma_n\Gamma_\gamma/\Gamma$	Γ_γ	
$s_{1/2}$	$p_{1/2}$	(eV)	(eV)	(eV)	Reference
	42.705 (1)	1.6 (2)[c]	0.35 (5)	0.45 (3)	This work
	42.985 (2)[b]	2	0.37 (4)	0.50[d]	and Fig. 10
43.105 (1)		104.4 (6)	0.26 (2)	0.20 (4)	
			0.98 (7)		
43.050 (4)		84.1 (1)			24
42.92 (11)				0.98 (16)	25
43.08 (23)		77 (15)		1.73 (18)	23
43.050 (15)		90 (4)		1.4 (3)	26
	64.918 (10)[b]	0.05	0.05 (2)[c]	0.50[d]	
	65.053 (6)[b]	0.47	0.24 (7)	0.50[d]	
65.228 (1)		443.0 (8)	1.10 (5)	0.94 (9)	This work
	65.573 (2)[b]	≤2.4	1.09 (8)	2.0	
			2.4 (1)		
65.11 (2)		459.9 (8)			24
65.12 (16)			1.9 (3)		25
65.13 (40)		390 (30)		2.43 (25)	23
65.110 (13)		460 (30)		2.3 (3)	26
	135.46 (2)[b]	0.16	0.12 (2)	0.50[d]	
	136.03 (1)	15.5 (4)	1.34 (5)	1.45 (8)	This work
	136.29 (1)	6.7 (3)	1.93 (8)	2.7 (1)	and Fig. 11
			3.4 (1)		
	135.7 (5)		3.3 (5)		25
	136.5 (14)		4.3 (9)		23
	136.8 (5)			3.1 (6)	26
139.03 (1)		30.7 (5)	1.14 (6)	1.18 (6)	This work
	139.56 (2)	26.2 (5)	1.22 (6)	1.28 (7)	and Fig. 11
	140.01 (1)	31.6 (5)	2.23 (6)	2.4 (1)	
			4.6 (1)		
	141.9	41.5 (2.6)			24
	139.0 (6)		3.0 (5)		25
	139.6 (14)		4.0 (9)		23
	139.7 (6)		3.0 (6)		26

Table 12. Ni-60 $\ell > 0$ resonance parameters compared to other works below 40 keV

Present work			Stieglitz et al., ref. 23		Fröhner, ref. 25		Syme et al., ref. 24	
E_n (keV)	$g\Gamma_n\Gamma_\gamma/\Gamma$ (eV)	$g\Gamma_n$ (eV)	E_n (keV)	$g\Gamma_n\Gamma_\gamma/\Gamma$ (eV)	E_n (keV)	$g\Gamma_n\Gamma_\gamma/\Gamma$ (eV)	E_n (keV)	$g\Gamma_n$ (eV)
2.253 (1)	0.051[a]	0.053 (1)	2.257 (9)	0.068 (11)				
5.532 (1)	0.043 (3)	0.045 (3)	5.53 (2)	0.056 (9)				
12.220 (1)	0.201 (4)		12.2 (4)	0.042 (7)	12.23 (3)	0.22 (5)		
13.624 (1)	0.353 (6)		13.6 (5)	0.090 (13)	13.62 (3)	0.34 (5)		
					17.20 (5)	0.06 (2)		
21.274 (2)	0.022 (2)							
23.788 (1)	0.24 (1)	4.5 (2)	23.8 (1)	0.92 (14)	23.89 (6)	0.72 (12)		
23.898 (1)	0.54 (1)	1.17 (4)						
28.458 (2)	0.04 (2)				28.47 (7)	0.10 (3)		
28.497 (2)	0.11 (2)							
29.480 (2)	0.061 (5)				29.46 (8)	0.04 (1)		
30.262 (1)	0.39 (1)	1.0 (3)	30.1 (1)	0.32 (5)	30.25 (8)	0.34 (5)		
33.017 (2)	0.56 (1)	7.7 (3)	32.9 (1)	0.35 (6)	33.04 (8)	0.40 (7)	33.03	7 (2)
33.393 (2)	0.29 (1)	10.0 (3)	33.3 (1)	0.19 (3)	33.42 (8)	0.23 (4)	33.55	3.6 (13)
39.534 (1)	0.57 (1)	2.3 (1)	39.4 (2)	0.57 (10)	39.52 (10)	0.43 (7)		

[a]Calculated with the parameters obtained from the transmission data analysis.

The capture kernels reported by Stieglitz et al.[23] for the two first resonances at 2.25 and 5.53 keV are higher than our values but almost within the uncertainties. For the two resonances at 12.22 and 13.62 keV, which are on top of a large s-wave resonance, the capture kernels found in this analysis are in good agreement with the values reported by Fröhner[25] but are in complete disagreement with the reported values of Stieglitz. No resonance around 17 keV (reported by Fröhner) could be seen either in our transmission or in our capture data obtained with the thick or the thin sample. Above 23 keV our values are systematically higher than those of Fröhner.

Resonance parameters of the 132- to 140-keV region are given in Table 11. In this energy region (Fig. 11), neither the resonances at 133.52 keV nor the doublet around 137.4 keV were seen in any other total cross sections or capture measurements, even though Syme et al.[24] claim a better energy resolution (0.075 ns/m) than the one obtained at ORELA in this transmission experiment (0.12 ns/m). Around 136 keV, the small resonance followed by the two large overlapping resonances were seen, in earlier publications, as a single resonance in capture data and not at all in any total cross-section measurements. It is shown in Table 11 that the sum of the capture kernels of the three resonances reported in this work is equal to the capture kernel given by Fröhner[25] and is smaller than but in the range of the possible values given by Stieglitz.[23] Even the three resonances around 139 keV, which are separated by half a keV, were not resolved before. In the present work, these three resonances are fairly well separated in both sets of data. The sum of the capture kernels is slightly higher than the single value given in refs. 23 or 25. The large discrepency between the energy parameters reported in refs. 24 and 25 could lead to confusion if more resonances were identified, but this resonance around 140 keV is the only one reported between 128 and 154 keV in ref. 24 and the only one between 136 and 148 keV in ref. 25.

In the 180- to 195-keV energy region, shown in Fig. 12, none of the five $\ell > 0$ resonances clearly seen in the capture data (four of which are also identified in the transmission data) were reported in any previous publications.

8.3 RESONANCE PARAMETERS STATUS IN ENDF/B-V

In the most recent documentation on the nickel neutron-induced reaction cross-section evaluation for ENDF/B-V,[1] it is reported that "From 1.0×10^{-5} eV to 690.0 keV, the resonance parameters along with the smooth background cross sections have been taken from the ENDF/B-IV Ni evaluation (MAT=1190), which, in turn, were adopted from ENDF/B-III Ni (MAT=1123) evaluation."

The ENDF/B-III ^{60}Ni resonance parameter evaluation was based on an evaluation by Stieglitz et al.[32] which made use of refs. 22, 31, and 33. Garg's paper[28] on natural nickel became available after this evaluation was completed but confirmed some s-wave resonance energy assignments. This means that, in the ^{60}Ni resonance region, ENDF/B-V is based on experiments prior to 1971. The evaluation above 340 keV is based on ref. 22 which reports measurements of neutron total cross sections up to 650 keV, but the data were analyzed only up to 600 keV. Nevertheless, resonance parameters for ^{60}Ni in ENDF are given up to 652 keV. Forty-one s-wave resonances are reported from 12 to 652 keV but only 49 $\ell > 0$ resonances from 1 to 553 keV. The radiation widths given in ENDF/B-V are average values based, for s-wave resonances, on the four values of Γ_γ obtained for resonances between 12 and 65 keV and given in Table 8.[23] For $\ell > 0$ (or p-wave) resonances $\overline{\Gamma}_\gamma$ is based on an unspecified number of radiation widths of resonances below 140 keV. The average radiation width of 2.14 eV given for s-wave resonances is large compared to our average value of 1.30 ± 0.07 eV. The reason for this discrepancy is shown in the first two examples in Table 11 which were discussed earlier. On the other hand, the average value of 0.6 eV given for the radiation width of the $\ell > 0$ resonances is only half of our average Γ_γ calculated with all the non s-wave resonances reported in Table 2 and seen in both data sets.

This new set of resonance parameters between 1 and 450 keV with the set of outside resonances necessary to describe the smooth background cross section is a definite improvement over the resonance parameters given presently in ENDF/B-V.

9. DISCUSSION AND AVERAGE PARAMETERS

9.1 REDUCED NEUTRON WIDTH DISTRIBUTION OF S-WAVE RESONANCES

Thirty s-wave resonances were identified in the range of energies analyzed, but some s-wave resonances of small widths could have been missed. On the assumption that the reduced neutron widths of s-waves follow a Porter-Thomas distribution,[34] an estimate of missed s-wave resonances was made.

The reduced neutron width at 1 eV for s-wave resonances is

$$\Gamma_n^o = \Gamma_n \sqrt{1\text{eV}/E_n} \tag{9.1}$$

where Γ_n^o, Γ_n, and E_n are in eV.

The normalized Porter-Thomas density function is

$$P(x) = (2\pi x)^{-1/2} e^{-x/2} \tag{9.2}$$

where $x = \Gamma_n^o/\overline{\Gamma}_n^o$ and $\overline{\Gamma}_n^o$ is the average reduced neutron width.

The average of the 30 identified s-wave resonances reduced neutron widths is equal to 3.6 ± 0.4 eV. Since only resonances of small widths could have been missed, the value of $\overline{\Gamma}_n^o$ is possibly too large and the number of missed levels could be underestimated. The histogram giving the normalized reduced neutron widths, $\Gamma_n^o/\overline{\Gamma}_n^o$, for 29 of the 30 resonances identified as s-waves in the analyzed region is given in Fig. 18. ($\Gamma_n^o/\overline{\Gamma}_n^o$ of the first s-wave resonance at 12.487 keV is equal to 5.9 and is not shown.) The smooth curve in Fig. 18 is the Porter-Thomas density function normalized to give the same number of levels under the curve as the observed number of levels in the range of values of x from 0.1 to 3.6. The normalization factor for the Porter-Thomas density function is 7.1 and, as it should be, is insensitive to the cut-off value of x used since when it is raised by a factor of 4 to 0.4, this normalization factor is 7.2. Comparing the number of levels observed with x values below 0.1 or below 0.4 with the corresponding area under the normalized Porter-Thomas density function yields the estimate that between three and four s-wave resonances having small neutron widths could have been missed.

9.2 LEVEL DENSITIES

It is of some interest to determine within the framework of a model of level densities the consistency between the number of levels of different angular momentum observed in these experiments at high excitation energies in ^{61}Ni and the number of low-lying levels. The model used is the one of Gilbert and Cameron[35] where the Fermi-gas constant a and the energy shift parameter Δ are treated as free parameters.

Gilbert and Cameron started from a Fermi-gas model of the nucleus which was modified to take into account the pairing energy and possibly shell model effects, using an effective excitation energy U instead of the actual excitation energy E. The density of levels of total angular momentum J at an effective excitation energy U is given by

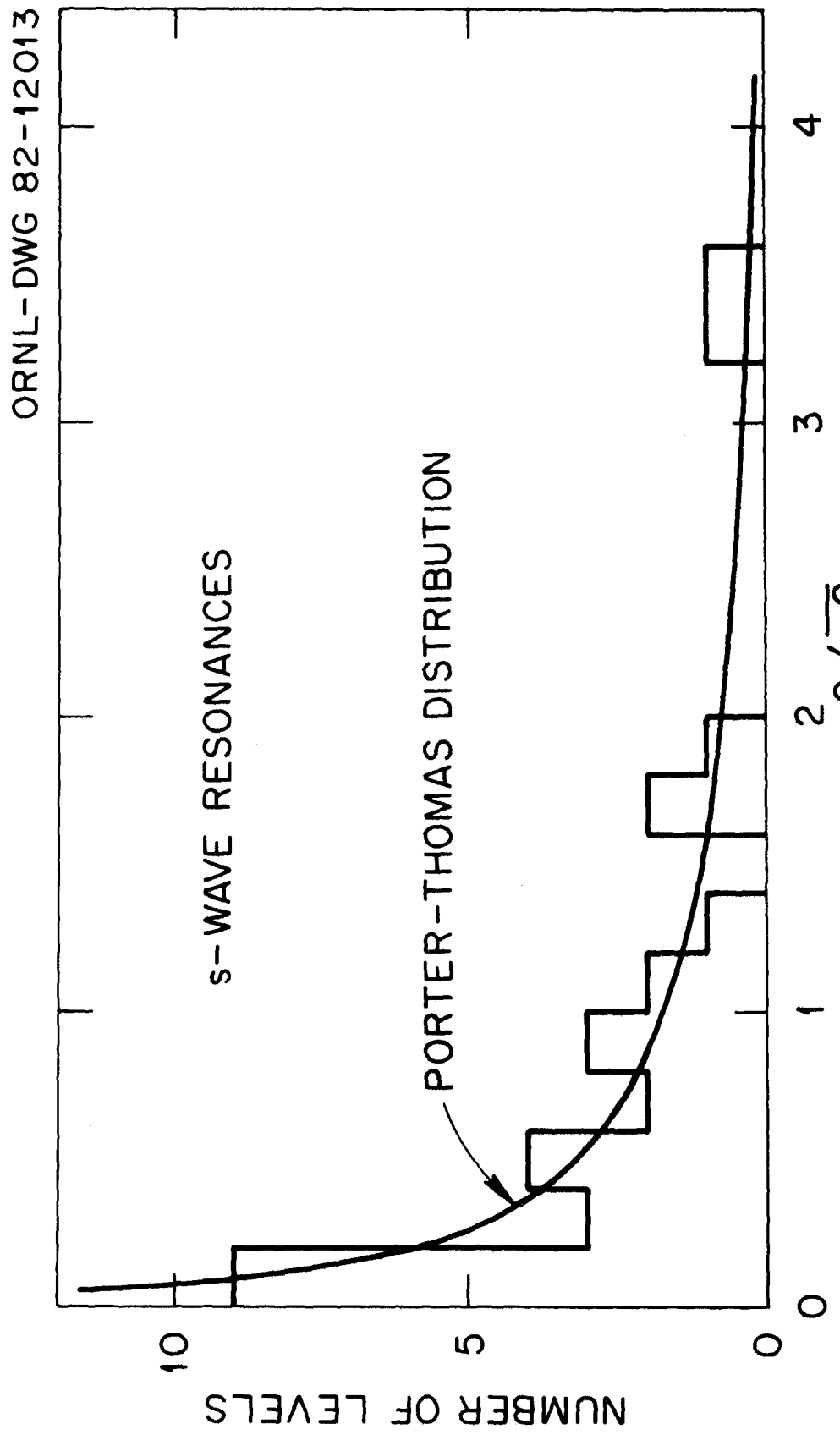

Fig. 18. The neutron reduced widths distribution for the observed s-wave resonances. The smooth curve is the Porter-Thomas distribution normalized to the area of the histogram between $\Gamma_n^o/\Gamma_n^o = 0.1$ and 3.6.

$$\rho(U,J) = \frac{\exp[2\sqrt{aU}]}{12a^{1/4}U^{5/4}} \frac{(2J+1)}{2\sqrt{2}} \frac{\exp[-(J+1/2)^2/2\sigma^2]}{\sigma^3} , \quad (9.3)$$

where a is the Fermi-gas constant and σ^2 is called the spin cut-off parameter. The effective excitation energy U is measured from a fictitious ground state shifted by an amount Δ, the energy shift parameter, from the actual ground state of the compound system. Thus, the effective excitation energy U is related to the actual excitation energy E above the ground state by the relation $U = E - \Delta$.

The spin cut-off parameter σ^2 is not a free parameter in the Fermi gas model since it is related to the distribution of the projections of the total angular momentum J. More specifically, the spin cut-off parameter is given by

$$\sigma^2 = \frac{6}{\pi^2} <m^2> \sqrt{aU} , \quad (9.4)$$

where $<m^2>$ is the mean-square magnetic quantum number for single-particle states. From the shell model it is expected that

$$<m^2> \simeq 0.146 A^{2/3} , \quad (9.5)$$

where A is the atomic mass number of the compound system. This value of $<m^2>$ will fluctuate somewhat due to shell effects. Combining those results we obtain

$$\sigma^2 \simeq 0.0888 A^{2/3}\sqrt{aU} . \quad (9.6)$$

This value of σ^2 corresponds approximately to the compound system having a moment of inertia equal to 75% of its rigid moment of inertia.[36]

If one adopts the above expression for σ^2, the Gilbert and Cameron level-density formula contains only two parameters: the Fermi-gas constant a and the energy shift factor Δ. The derivation of the above level density formula contains a number of approximations, and it is customary to treat the parameters a and Δ as free parameters which are adjusted to fit the data. It is within this framework that the level density formula above is being used.

Because of barrier penetrability effects we cannot use the number of $\ell > 0$ resonances observed in this experiment in the fitting process to determine if there are values of a and Δ that are consistent with all the data since one does not know which J values they correspond to. However, one can use the number of s-wave resonances observed in the experiment together with the known[37] low-lying levels of ^{61}Ni. Then using these values of a and Δ in the level density formula, one can compare its prediction for various ℓ values with the observations made in this experiment for levels with $\ell > 0$.

In the range of neutron energy from 10 to 450 keV, 30 s-wave resonances were observed, but, due to the possibly missed levels discussed in the previous section, this number of resonances is considered uncertain by three to four levels. We cannot expect that the level-density formula will reproduce correctly the density of very low-lying levels in ^{61}Ni due to the energy gap and collective effects which were not incorporated into the formula. Since the energy gap in ^{60}Ni extends to at least 2.1 MeV of excitation,

we did not consider the levels below 2.1 MeV in ^{61}Ni as data that should be reproduced by the level-density formula. Also as the excitation energy in ^{61}Ni increases it is more likely that levels have been missed. On the basis of the data in the *Nuclear Data Sheets*,[37] it was decided that the level density formula should only be constrained to match the 13 levels observed in the range of 2.4 to 2.9 MeV with an uncertainty of ± 2 levels.

The values of the Fermi-gas constant a and the energy shift parameter Δ were obtained using the computer code LEVDEN.[38] LEVDEN is a fitting code that solves Bayes' equation. Using as prior values 6 ± 20 MeV^{-1} for the Fermi gas constant and 0 ± 2 MeV for the energy shift parameter, the code was required to produce 13 ± 2 levels of all values of J in the excitation energy interval 2.4 to 2.9 MeV above the ground state of ^{61}Ni and 30 ± 3 s-wave levels in the energy interval 10 to 450 keV above the neutron binding energy of 7.817 MeV in ^{61}Ni. This corresponds to a mean observed level spacing for s-wave resonances, D_o, equal to 15.2 ± 1.5 keV. The posterior values for the Fermi-gas constant and the energy shift parameter, with their standard deviations, were found to be

$$a = 5.88 \pm 0.24 \text{ MeV}^{-1} \tag{9.7}$$

$$\Delta = -0.77 \pm 0.34 \text{ MeV}$$

with a correlation coefficient of 0.93.

The integral of the theoretical level density formula from 10 to 450 keV for $\ell = 0$ with the above parameter values and their uncertainties is shown compared to the observed cumulative sum for s-wave resonances in Fig. 19 (bottom staircase and curve). Using the above parameter values and assuming that due to centrifugal barrier penetrabilities only $\ell = 1$ and $\ell = 2$ resonances were observed, the predictions of the model are compared to the cumulative sum of observed levels with $\ell > 0$ also in Fig. 19. More $\ell > 0$ levels have been observed than were predicted by the model using the above parameter values. We should not conclude that this disagreement indicates that we must be observing many resonances for which $\ell > 2$ because it is possible to fit simultaneously the s-wave cumulative sum and the cumulative sum for $\ell > 0$ resonances assuming that they contain only $\ell = 1$ and $\ell = 2$ levels at the expense of the fit to the number of low-lying levels in ^{61}Ni. For instance, the set of parameter values $a = 6.5$ MeV^{-1} and $\Delta = 0$ MeV in the level-density formula gives a very good fit to the observed cumulative sum of $\ell > 0$ levels and gives 34 s-wave resonances from 10 to 450 keV, which is consistent with the observations if one includes the estimated missing levels. But it gives only nine levels in the energy range 2.4 to 2.9 MeV above the ground state of ^{61}Ni instead of 13. It is not clear to which extent one should reproduce the low-lying levels in ^{61}Ni due to collective effects that are ignored in the level density formula used. Another set of parameter values that reproduces well the cumulative sum of $\ell > 0$ levels, assuming that they are only $\ell = 1$ and $\ell = 2$ levels, is $a = 6.8$ MeV^{-1} and $\Delta = 0.5$ MeV. This set of parameters also gives 34 s-wave resonances in the energy range from 10 to 450 keV but reduces to seven the number of levels in the 2.4 to 2.9 MeV energy range above the ground state of ^{61}Ni.

In view of the above, there seems to be little that one can conclude on the basis of the data obtained in these experiments concerning the validity of the Gilbert and Cameron level-density formulae treated as an empirical model.

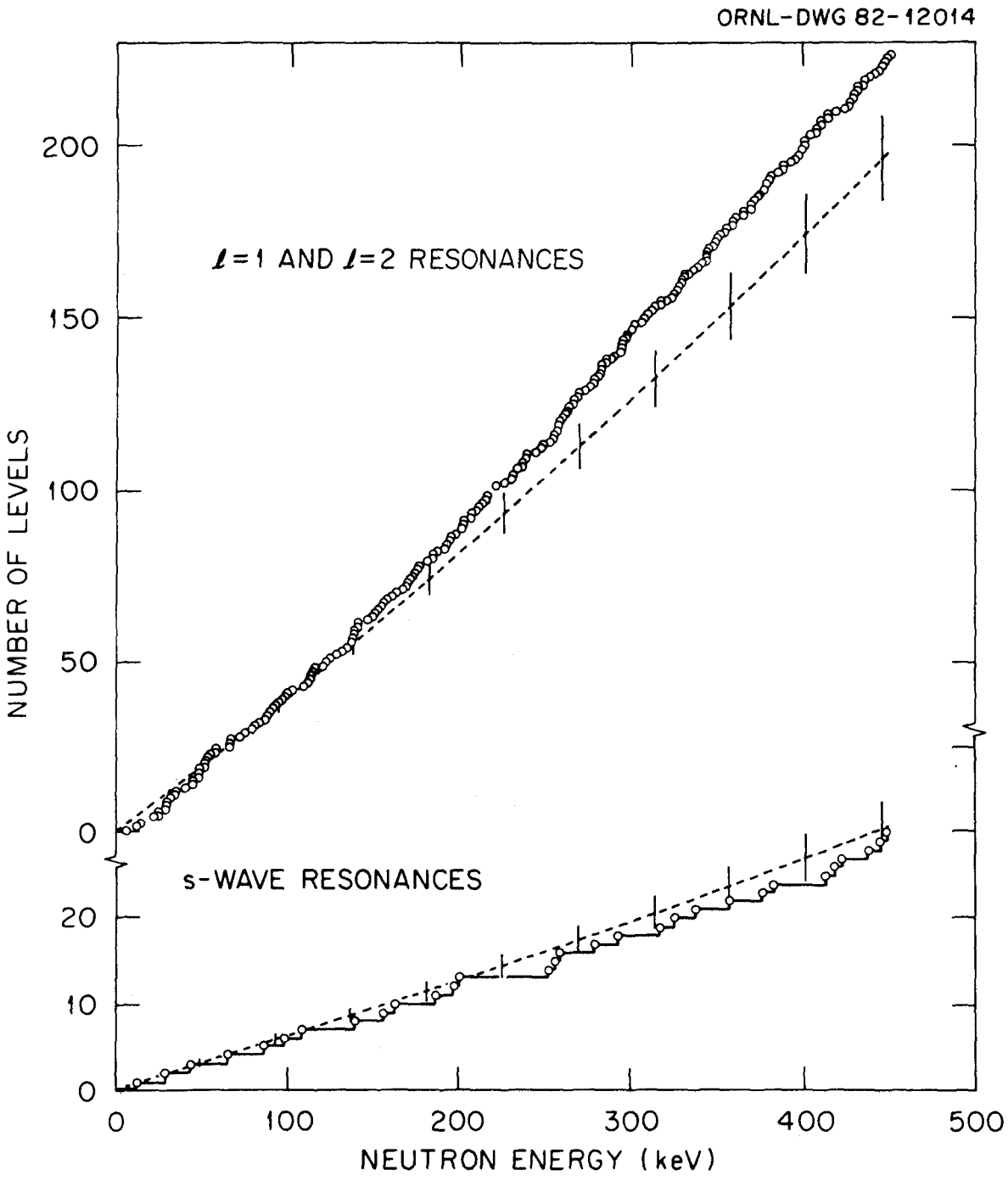

Fig. 19. Cumulative number of resonances for $\ell = 0$ and $\ell = 1$ and 2 as a function of the neutron incident energy. The dashed lines are fits to the data using the Fermi-gas model as discussed in Sect. 9.2.

9.3 s-WAVE STRENGTH FUNCTION AND DOORWAY STATES

When discussing strength functions, it is useful to look at a plot of the cumulative sum of the reduced neutron widths of the observed resonances as a function of energy since the strength function defined as

$$S_o = \frac{\overline{\Gamma}_n^o}{D_0} \tag{9.8}$$

is the slope of such a plot. A plot of the cumulative sum of the s-wave resonances as a function of energy is shown in Fig. 20.

There is no ambiguity in obtaining the s-wave strength function from a staircase plot such as the one in Fig. 20 when it can be reasonably well approximated by a straight line over the complete energy range analyzed. When this is the case, the cumulative strength of the resonances being a linear function of the energy, the strength function is a very well defined entity and is independent of any method used for averaging. However, in many instances, as is the case for ^{60}Ni, the staircase plot shows considerable structure and it is necessary to consider the averaging procedure in some detail.

In Sect. 9.1, the distribution of the s-wave resonance reduced widths was analyzed within the framework of the Porter-Thomas distribution. It was found that for the 30 s-wave resonances observed up to 450 keV, the reduced widths were consistent with such a distribution. In Sect. 9.2, the level density from 0 to 450 keV was found to be consistent with a Fermi-gas model. The above indicate that the data are not inconsistent with the statistical assumptions that underlie these models. Assuming the validity of these statistical assumptions, the structure of the staircase plot in Fig. 20 is to be interpreted in terms of statistical fluctuations. A likelihood estimate could be made for the distribution of strength among pairs of nearest levels that are observed, for instance using a runs test. Although such a test was not made since the structure is clearly evident to the naked eye, it seems quite likely that a small probability would be found for the actual distribution observed. However, because the widths of these structures are rather small, the probability for the occurrence of these structures would not be so small as to compel us to reject the hypothesis of the statistical assumption with a null test.

In view of the above, the usual procedure for extracting the s-wave strength function could be followed. One notes that

$$\overline{\Gamma}_n^o = \frac{1}{N} \sum_{i=1}^{N} \Gamma_{n,i}^o \quad , \tag{9.9}$$

and

$$D_o = (E_N - E_1)/(N-1) \quad , \tag{9.10}$$

where E_1 is the energy of the first resonance analyzed and E_N the energy of the last one. From these observations, one obtains

$$S_o = \frac{N-1}{N} \frac{\sum_{i=1}^{N} \Gamma_{n,i}^o}{E_N - E_1} \quad . \tag{9.11}$$

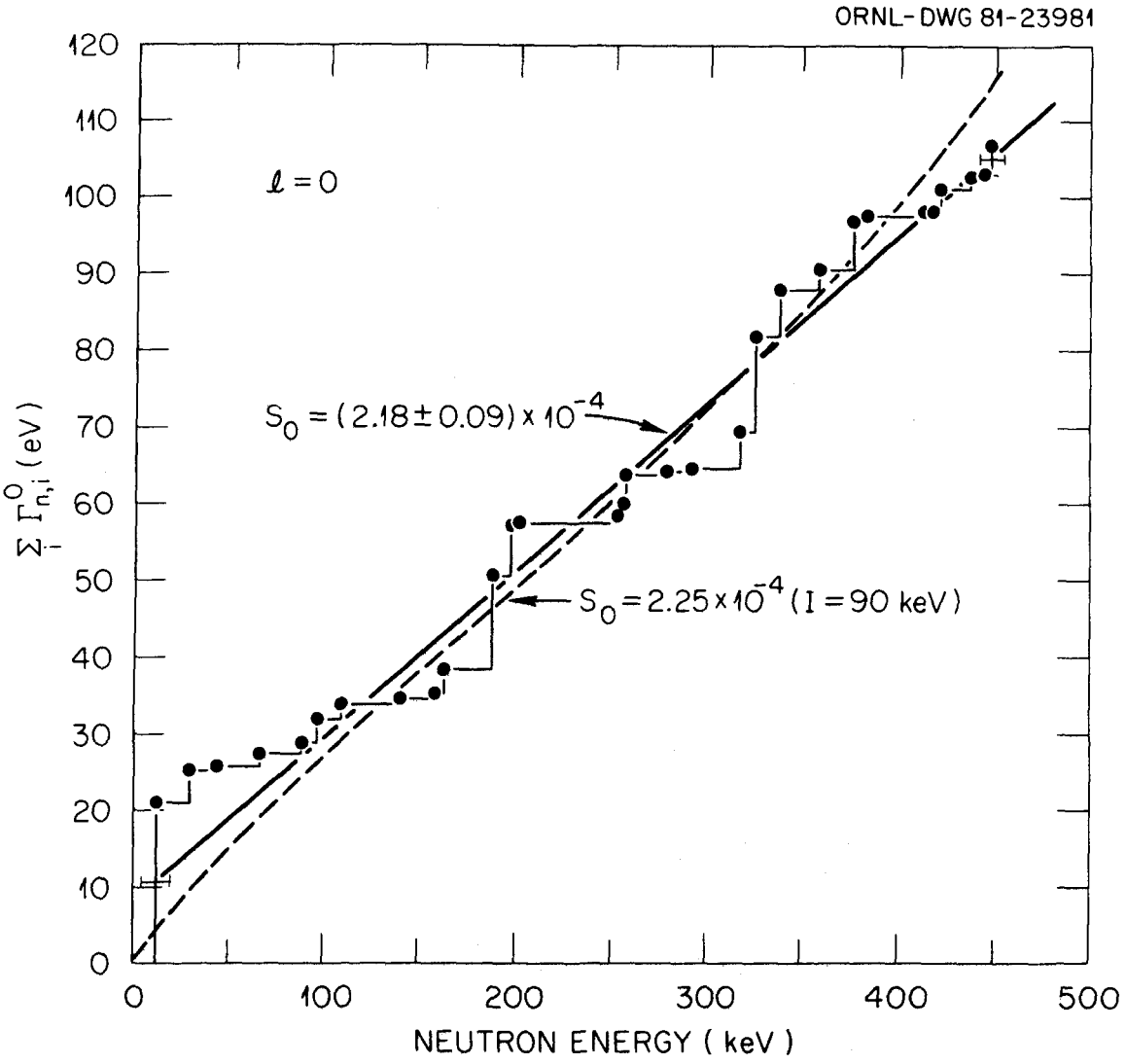

Fig. 20. The sum of the reduced neutron widths for s-wave resonances as a function of the neutron incident energy. The strength function is given by the slope of the full straight line or by the slope of the straight portion of the dashed line obtained by integrating, from 0 to 450 keV, the Lorentzian-averaged strength function, S_{TOT}, with I = 90 keV.

If one considers the uncertainties in the quantities that appear on the right-hand side of the expression, there is a very small uncertainty in the value of S_o from the analysis of the data. However, as is well known,[39] if N levels are drawn randomly from a Porter-Thomas distribution having mean value $\overline{\Gamma_n^o}$, the expectation value in the sum of these N levels is $N\overline{\Gamma_n^o}$ and the variance in this sum is $2N(\overline{\Gamma_n^o})^2$. Therefore, even though we may have obtained with great accuracy the total strength in the energy interval 0 to 450 keV, there is a relative standard deviation of $\sqrt{2/N}$ or 26% in the numerator of S_o. In comparison the uncertainty in $E_N - E_1$ is small even though one could argue that since the full strength of the first and last resonances is taken in the summation of the reduced neutron widths, half of the average level spacing, D_o, should be added at each end of the energy interval $E_N - E_1$. The maximum uncertainty on the denominator would still be only 3%. The strength function calculated with relation (9.11) is equal to $(2.38 \pm 0.62) \times 10^{-4}$.

Relation (9.11) can be considered as determining the average value of the strength function at the energy which is the midpoint of the energy range analyzed, and a rectangular weighting function is used whose width is equal to the energy range analyzed. As is well known, such sharp weighting functions have very unpleasant mathematical properties. This can be illustrated in our case by eliminating the lowest and highest resonance analyzed. One now obtains a nominal value for S_o of 1.9×10^{-4}. It can be observed from Fig. 20 that subsequent reductions in the width of the rectangular weighting function will produce much smaller changes. A compromise value is suggested for the nominal value of the "statistical" strength function. It is given by the slope of the "best line" fit that goes through two rectangular boxes centered at the energies of the lowest and highest resonance analyzed as shown in Fig. 20. The widths of these boxes are equal to the average level spacing and the heights to the reduced widths of these resonances. The value so found is 2.18×10^{-4} with a standard deviation of 0.09×10^{-4}. This line appears suggestively to be a good straight-line approximation to the staircase plot over the complete energy range. This value of 2.18×10^{-4} represents a minimal attempt at mitigating the sharpness of the weighting function.

The s-wave neutron strength function recommended in ref. 26 for ^{60}Ni in the 0 to 600 keV energy range is $(2.7 \pm 0.6) \times 10^{-4}$. Fröhner[25] reports a value of $(2.6 \pm 0.8) \times 10^{-4}$ and Stieglitz et al.[23] a value of $(2.95 \pm 1.04) \times 10^{-4}$ from their analyses up to 340 keV.

There are three conspicuous large steps in the staircase plot in Fig. 20 occurring at 15, 190, and 325 keV. They arise because two consecutive levels have relatively large reduced widths in the first two steps and three in the third step. These steps account for 63% of the total s-wave strength in the energy region analyzed but span only about 10% of the energy range. Although as pointed out, it is not unlikely that these steps arise from purely statistical sources, they could be the manifestation of some physical mechanism modulating the strength of the levels in this energy region. They could indicate the presence of particle vibration doorway states and, if this were so, one should find such modulations of the s-wave strength function in the nuclides of this mass region. Such modulations have been observed before. In ^{54}Fe where the level spacing is also large[40] - of the order of 20 keV - two large steps occur in the cumulative s-wave strength as a function of energy. They are located around 192 and 330 keV. In the zinc isotopes, ^{66,68,70}Zn, where level spacing is of the order of 5 keV, these modulations also occur but are spread over many more levels.[41] Preliminary calculations[42] indicate that these modulations could be due to particle vibration doorway states.

If one is interested in studying modulations of the strength function in terms of doorway states, it is convenient to average the reduced R-function with a Lorentzian weighting function.[43] The poles of the Teichman-Wigner reduced R-function[44] are necessarily below the energy axis, and we have

$$R(E) = \sum_i \frac{\gamma_{n,i}^2}{E_i - E - i\gamma_{c,i}^2/2} \quad , \tag{9.12}$$

where in our case $\gamma^2_{e,i}$'s are the effective reduced level widths for the eliminated channels: the capture channels. It should be noted that the sum is to be carried over all the poles of the R-function, that is to say, should include the poles outside the energy region analyzed. Because the poles of the reduced R-function are below the real axis, if one calculates the R function at an energy $E + iI$, where I is a positive number, one is calculating an average value of the R functions at the energy E. The amount of averaging that one performs is controlled by the size of I. In the statistical model, one makes I every large compared to the average level spacing in order to completely average over the statistical fluctuations. If the level widths have a Porter-Thomas distribution, I must also be very large in order to effectively average over the fluctuations. The value of the R function at a complex energy $E + iI$ where $I >> \gamma^2_{e,i}$ is usually denoted by

$$R(E+iI) = \bar{R}(E,I) + i\pi S(E,I) \quad , \tag{9.13}$$

where

$$\bar{R}(E,I) = \sum_i \frac{\gamma^2_{n,i}\,(E_i - E)}{(E_i - E)^2 + I^2} \tag{9.14}$$

and

$$S(E,I) = \frac{I}{\pi} \sum_i \frac{\gamma^2_{n,i}}{(E_i - E)^2 + I^2} \quad . \tag{9.15}$$

Because of the factor E_i - E in the numerator, $\bar{R}(E,I)$ is often called the contribution of the distant levels, away from the value of E, to the average. The absence of such a factor in the numerator of $S(E,I)$ means that its value at the energy E is more strongly dominated by the levels near the energy E and $S(E,I)$ is often called the Lorentzian averaged strength function.

We show in Fig. 21 the value of $S(E,I)$ for several values of I, from twice the average level spacing D_o to six times D_o over the range of energy the data were analyzed. The cumulative sum of the reduced level widths and the reduced level widths for the levels in the region analyzed are also shown for comparison. In Fig. 22, the contributions of the levels inside the energy region analyzed, S_{INT}, and those of the levels outside of the energy region, S_{EXT}, are shown. In Fig. 21, only the total sums, corresponding to S_{TOT} in Fig. 22, are shown. It should be noted that the levels outside the energy region analyzed are not "physical levels" in the sense that we expect actual resonances or states to be observed there. These external levels are merely an expansion of the contribution of the levels outside the energy region to the R-function inside the energy range analyzed. These contributions must be included in any analysis in order to fit the data but are often not represented by a pole expansion except for a single negative energy resonance. Frequently the statistical assumption is made concerning the levels outside the energy range analyzed. That is to say, one assumes that in the external regions there is a uniform density of states having the same average strength as in the region analyzed. If such were the case, the contribution to $S(E,I)$ of these levels would give the curve labelled S_{COR} in Fig. 22 which, added to S_{INT}, gives the total estimated strength S_{EST}. As is seen in Fig. 22, since S_{COR} is smaller than S_{EXT} there seems to be more strength in the levels just outside the energy region analyzed than such a model would predict. This was investigated and will be discussed later.

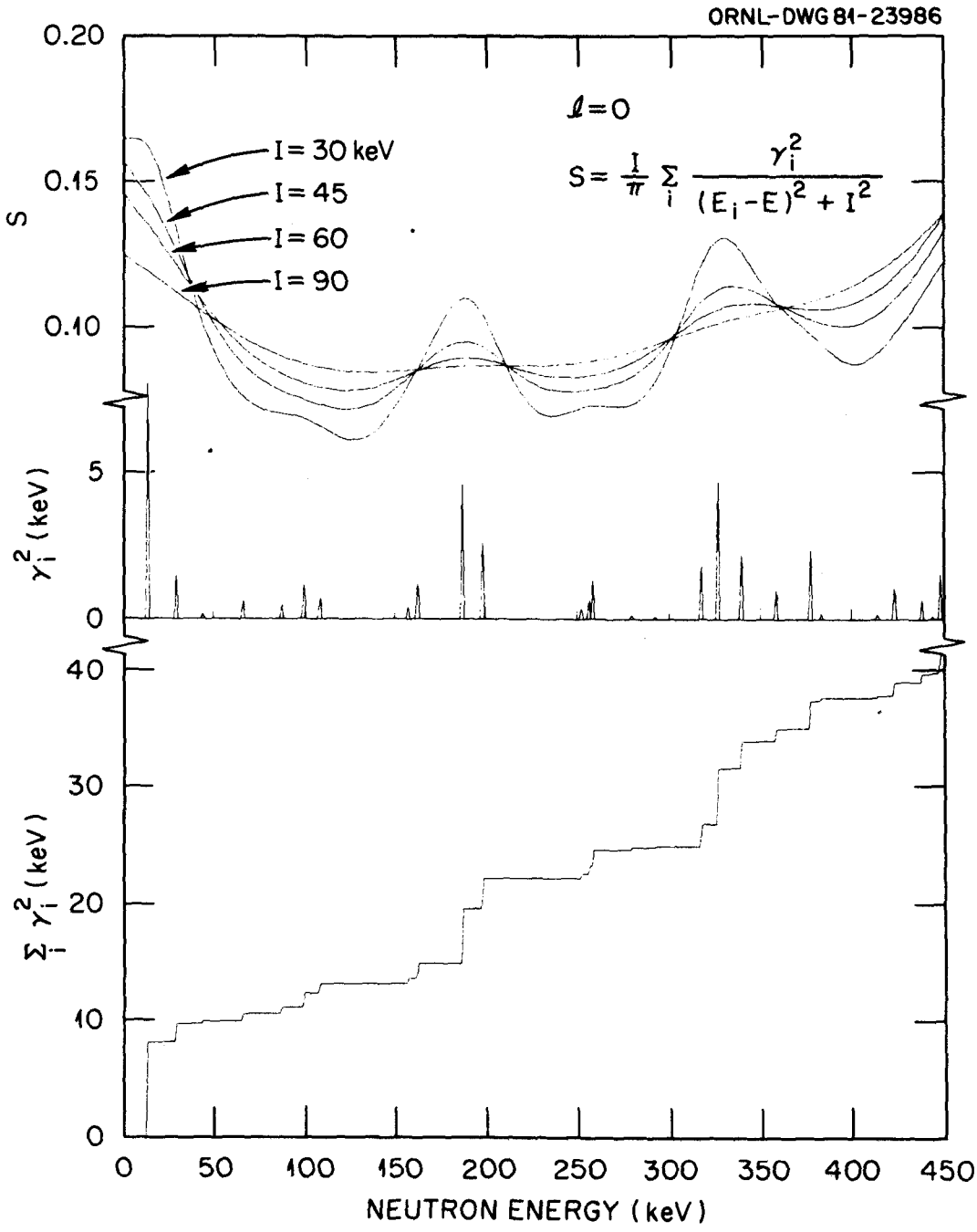

Fig. 21. From top to bottom: the Lorentz-weighted strength function of the reduced level widths of the observed s-wave resonances averaged over various energy intervals; the reduced level widths of the observed s-wave resonances; summations of the reduced level widths of the s-wave resonances as a function of the neutron incident energy. The three doorway states are clearly seen on each of these representations of the s-wave resonances reduced level widths.

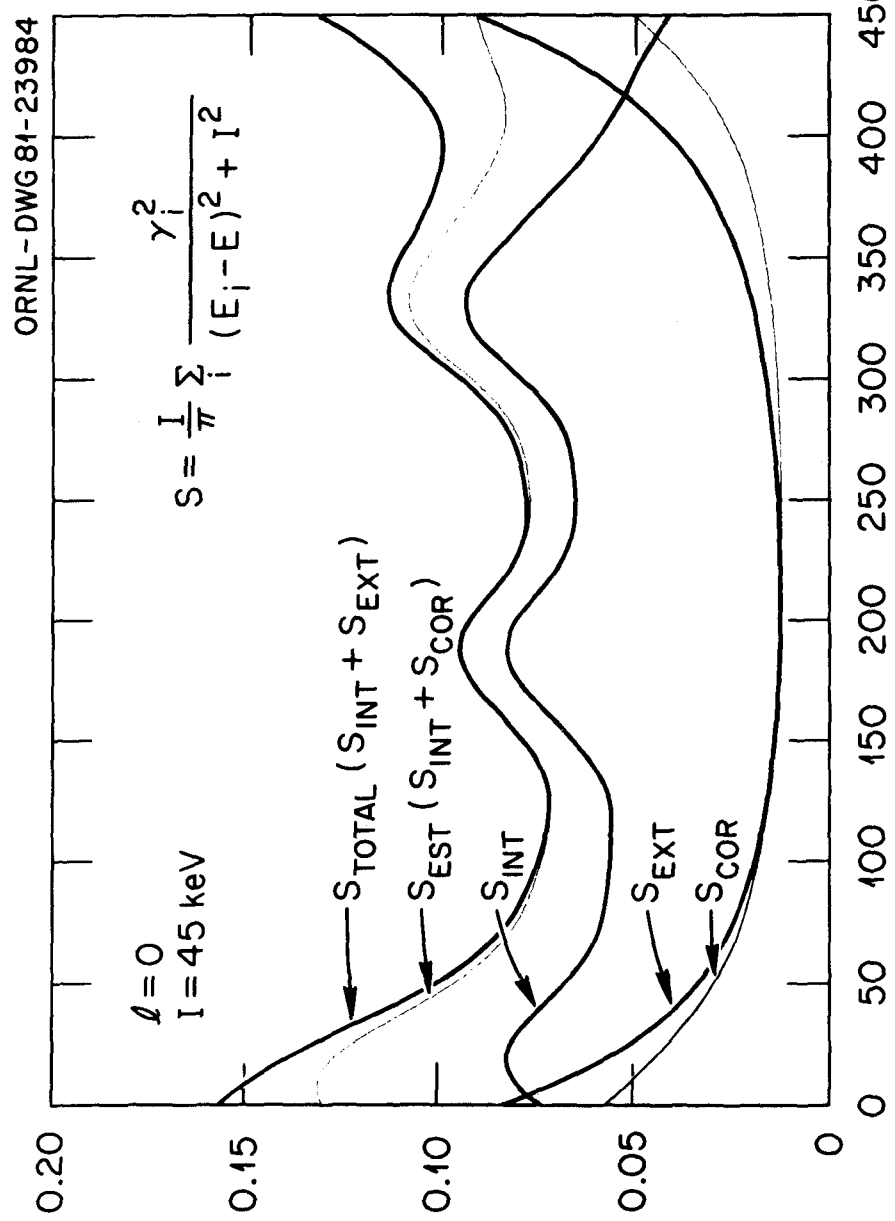

Fig. 22. Lorentz-weighted *s*-wave strength function of the reduced level widths averaged with $I = 45$ keV between 0 and 450 keV. S_{INT} is the contribution of the 30 observed *s*-wave resonances inside the 0- to 450-keV region. S_{EXT} is the contribution of the ten outside dummy resonances. S_{TOTAL} is the sum of S_{INT} and S_{EXT}. S_{COR} is the estimated contribution assuming a uniform average value of γ_i^2 outside the 0- to 450-keV region. S_{EST} is the sum of S_{INT} and S_{COR}.

The integral from 0 to 450 keV of the total Lorentz-weighted strength function averaged with I = 90 keV (six times the average level spacing) is given by the dashed line in Fig. 20. The slope of the straight part of this line gives also an estimate of S_o in the middle of the range of energy analyzed and is found to be equal to 2.25×10^{-4}.

In Fig. 23, the value of $\bar{R}(E,I)$ corresponding to the value of $S(E,I)$ in Fig. 22 is shown. However, because $\bar{R}(E,I)$ is more sensitive to far away levels, due to the term $(E_i - E)$ in the numerator, there is very little that one can infer about its behavior. The pole expansion used for the contribution of the levels outside the energy region analyzed is largely insensitive to the faraway levels.

Figure 21 displays very graphically the modulation of strength of the levels in the energy region analyzed and is suggestive of possible doorway states at least around 190 and 325 keV. There is very little that can be done with our data to investigate the possibility that there may be additional structure below the energy range analyzed. However, this can be done above 450 keV. In our preliminary analysis using the code MULTI (Sect. 3.1), the analysis of the transmission data had been carried out to 550 keV. As is evident from the capture data above 450 keV, there is a high density of levels in this region, and it is judged that a large part of subjectivity entered in the analysis, in particular concerning the smaller levels. However one can be fairly confident in this analysis above 450 keV concerning the large s-wave resonances. In Fig. 24, we give the cumulative sum of the reduced level widths for s-wave resonances up to 550 keV and the corresponding integral of $S(E,I)$ for I = 45 keV. It is quite clear from this figure that there is another structure in this staircase plot around 510 keV. For comparison purposes, we show in Fig. 25 the values of $S(E,I)$, for a value of I = 45 keV, for the two analyses. In the region of overlap these two analyses are fairly consistent and if some s-wave resonances above 450 keV were missed, as is now more likely, the differences in the two analyses in the region of overlap are in the right direction.

We conclude that even though the distribution of reduced level widths follows the Porter-Thomas distribution, there may be particle-vibration doorway states responsible for the modulation as a function of energy of the strengths of the s-wave levels. This will be investigated theoretically and an attempt made to see if such particle-vibration doorway states can provide a coherent explanation of the behavior of the reduced level width distributions as a function of energy observed for nuclides in this mass region.

9.4 CORRELATION BETWEEN Γ_n^o AND Γ_γ FOR S-WAVE RESONANCES

Because a correlation between the reduced neutron widths and the radiative capture widths of the observed resonances might indicate nonstatistical effects, such correlation coefficients are frequently calculated for s-wave resonances.

A survey of correlation coefficients for nuclei in the mass region $40 < A \leq 64$ was made by Beer and Spencer[45] in 1975. Only a few resonances were available for each isotope. For ^{60}Ni the reported correlation coefficient of 0.8 ± 0.28 was based on nine s-wave resonances below 170 keV, and it was shown that this correlation was due entirely to the single large resonance at 12.5 keV.

Since then analyses of high-resolution ORELA data for medium-range nuclei were completed and correlation coefficients were calculated for a large number of resonances. These correlation coefficients are given in Table 13 for eight nuclei in the mass region $54 \leq A \leq 68$ for a total of 223 resonances. The correlation coefficients given for the iron isotopes were calculated from the recommended parameter values of ref. 47. The uncertainties quoted include uncertainties in the neutron and radiation widths and the effect of finite sample size.

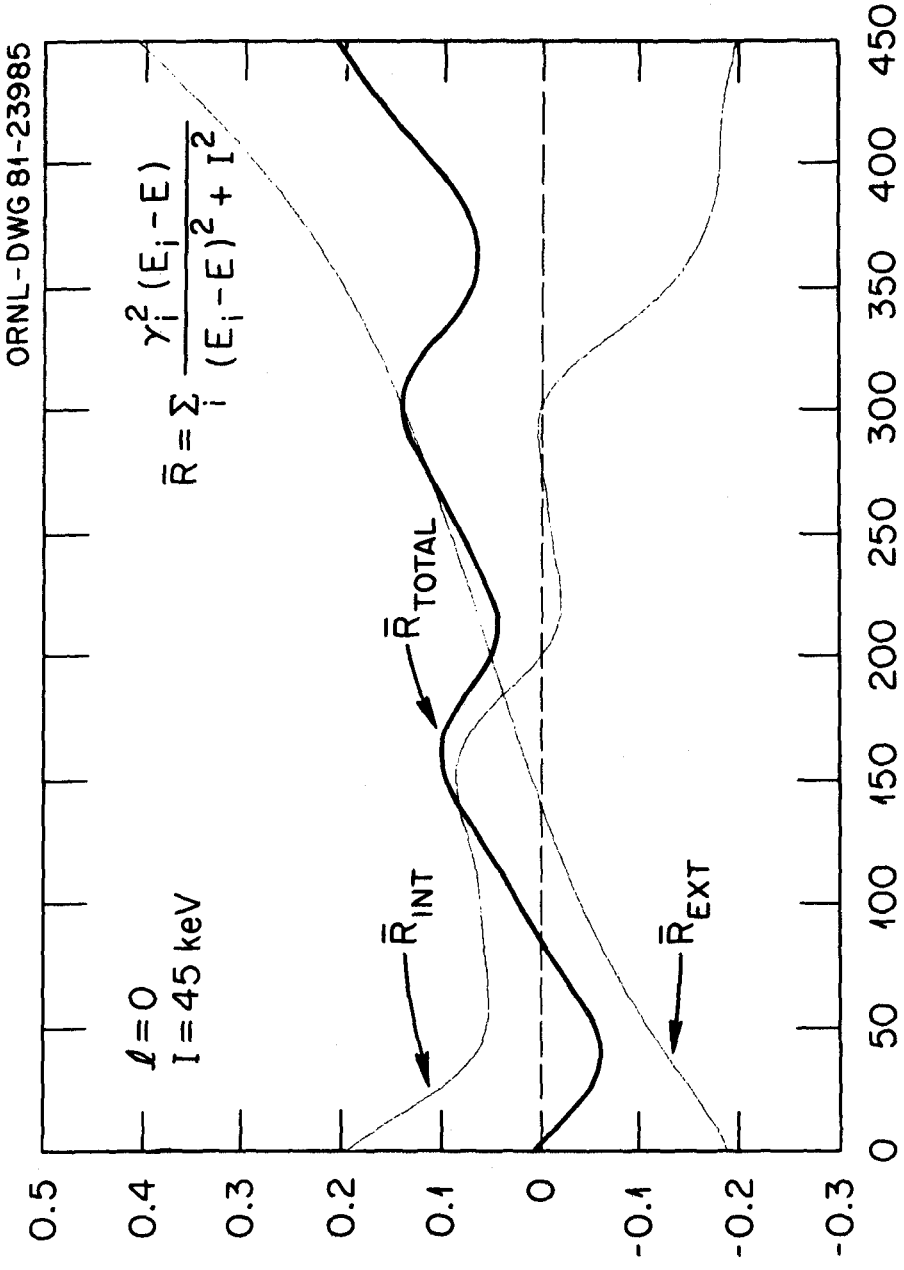

Fig. 23. Lorentz-weighted R-function of the s-wave reduced level widths averaged with $I = 45$ keV between 0 and 450 keV. $\bar{R}_{INT}$ is the contribution of the observed 30 s-wave resonances inside the 0- to 450-keV region. $\bar{R}_{EXT}$ is the contribution of the ten outside dummy resonances. $\bar{R}_{TOTAL}$ is the sum of $\bar{R}_{INT}$ and $\bar{R}_{EXT}$.

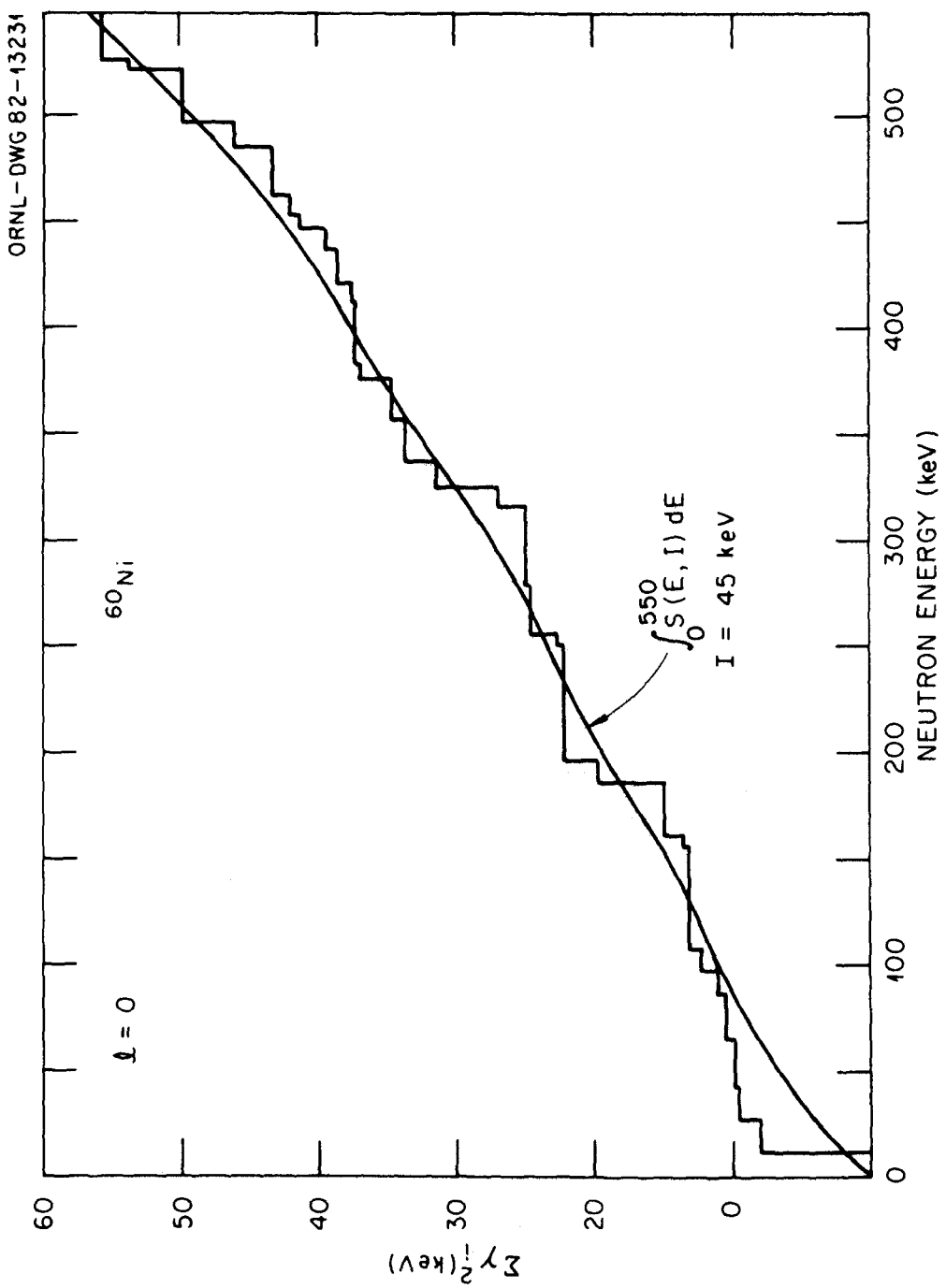

Fig. 24. The sum of the reduced level widths for s-wave resonances as a function of energy from 0 to 550 keV. The parameters used in this figure are from a preliminary analysis of the transmission data which was conducted up to 550 keV. The smooth curve is the integral from 0 to 550 keV of the Lorentzian-averaged strength function with $I = 45$ keV.

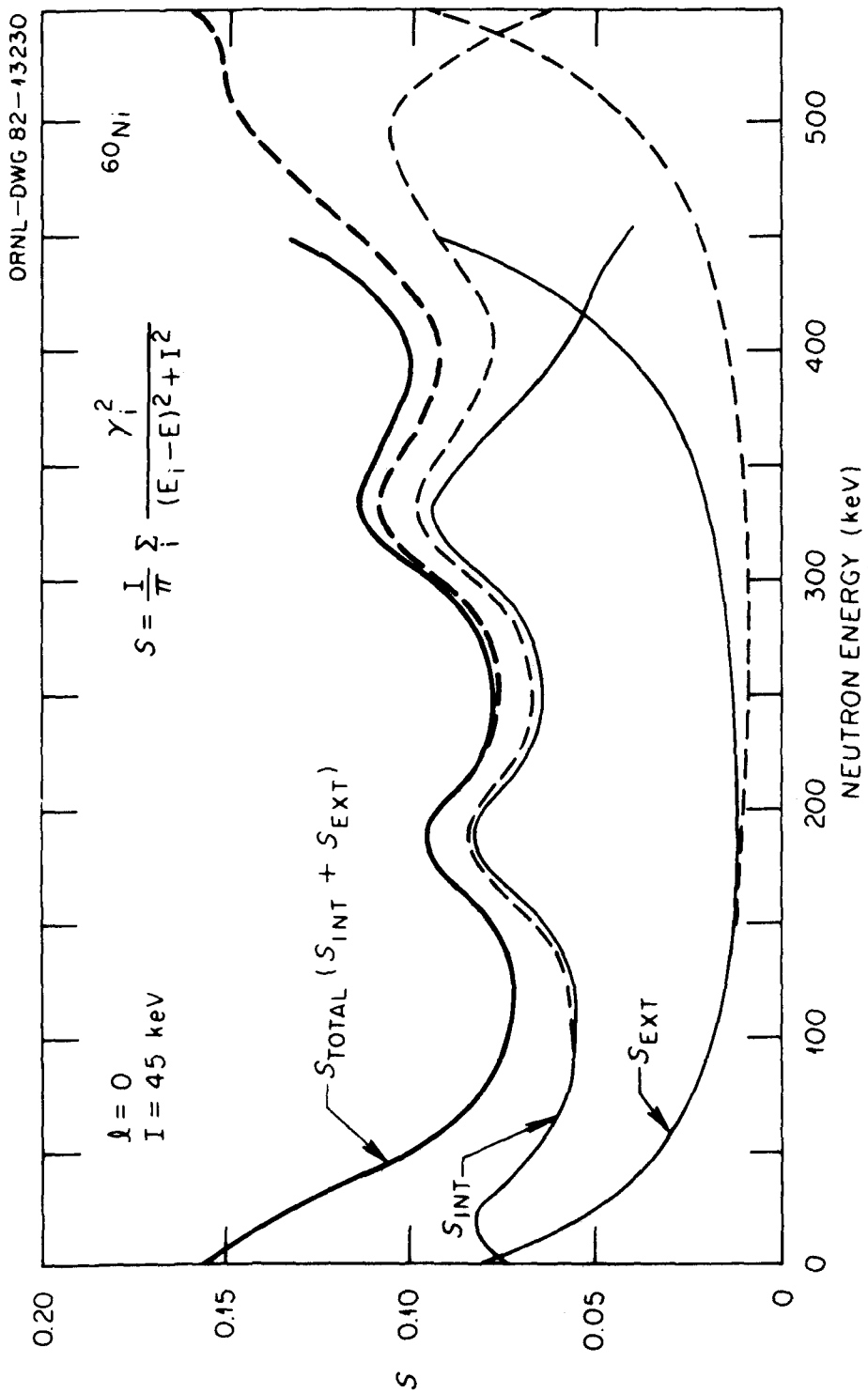

Fig. 25. Lorentz-weighted s-wave strength function of the reduced level widths averaged with I = 45 keV between 0 and 450 keV (full lines) and between 0 and 550 keV (dashed lines). S_{INT} is the contribution of the observed s-wave resonances inside the analyzed energy regions. S_{EXT} is the contribution of the outside dummy resonances. S_{TOTAL} is the sum of S_{INT} and S_{EXT}.

Table 13. Correlation coefficients, $\rho(\Gamma_n^o, \Gamma_\gamma)$, for some medium range nuclei

Element	J	No. of s-wave resonances	$\rho(\Gamma_n^o, \Gamma_\gamma)$	Reference
^{55}Mn	2,3	47	0.64 ± 0.14	46
^{54}Fe	1/2	16	0.94 ± 0.49	47
^{56}Fe	1/2	15	0.34 ± 0.20	47
^{59}Co	3,4	35	0.33 ± 0.06	48
^{60}Ni	1/2	30	0.53 ± 0.18	This work
^{64}Zn	1/2	32	0.47 ± 0.08	49
^{66}Zn	1/2	26	0.59 ± 0.10	41
^{68}Zn	1/2	22	0.5	41

The correlation coefficient for the 30 s-wave resonances of ^{60}Ni analyzed in this report is now 0.53 ± 0.18. As expected the parameters of the large resonance at 12.487 keV are no longer dominant. Without the parameters of this resonance the correlation coefficient is 0.48 ± 0.15.

The 50% uncertainty on the neutron sensitivity correction factor is the major source of uncertainty on the radiation widths of large s-wave resonances as discussed in Sect. 5.5. In other publications[41,46,48,49] smaller uncertainty on this correction factor was assumed which explains the smaller uncertainties on the correlation coefficients reported for ^{55}Mn, ^{59}Co, and zinc isotopes than we have for ^{60}Ni.

We investigated the sensitivity of the correlation coefficient to the absolute normalization of the neutron sensitivity curve used for the detector in the capture measurements (Fig. 16). If the neutron sensitivity coefficients, C, in Table 2 are lowered systematically by a factor of 2, the correlation coefficient would increase from 0.53 to 0.68 ± 0.17. If they are systematically increased by a factor of 1.5, then the correlation coefficient decreases to a value of 0.38 ± 0.18.

It seems that in this mass region the correlation coefficients are of the order of 0.5. This result could be considered evidence for nonstatistical effects in these nuclei as well as the structure observed in the reduced width staircase plots.

9.5 AVERAGE CAPTURE CROSS SECTIONS

The average capture cross sections given in Table 14 in lethargy intervals up to 450 keV were obtained by summing the capture areas of the resonances in each interval. The "narrow resonance" approximation was made; that is to say, that all the capture area of the resonance was assumed to fall in the energy interval where the resonance energy lies. This approximation is very poor only for the

Table 14. Average capture cross sections[a]

Energy range (keV)	Average capture cross sections (mb)	Energy range (keV)	Average capture cross sections (mb)	Energy range (keV)	Average capture cross sections (mb)
2.0 - 2.51	188 ± 4				
5.0 - 6.3	25.3 ± 0.6	50.1 - 63.1	9.8 ± 0.1	400 - 500	8.5 ± 0.1
6.3 - 7.9		63.1 - 79.4	13.7 ± 0.5	500 - 600	7.8 ± 0.1
7.9 - 10.		79.4 - 100.	19.4 ± 0.8	600 - 700	8.0 ± 0.1
10 - 12.6	366 ± 114	100 - 126	12.8 ± 0.3	700 - 800	7.4 ± 0.1
12.6 - 15.8	34.3 ± 0.6	126 - 158	13.6 ± 0.2	800 - 900	8.4 ± 0.1
15.8 - 20		158 - 200	14.2 ± 0.4	900 - 1000	7.8 ± 0.1
20. - 25.1	28.0 ± 0.5	200 - 251	9.3 ± 0.2	1000 - 1100	8.0 ± 0.2
25.1 - 31.6	29 ± 11	251- 316	10.0 ± 0.2	1100 - 1200	9.6 ± 0.2
31.6 - 39.8	20.7 ± 0.4	316 - 398	11.8 ± 0.3	1200 - 1300	10.6 ± 0.2
39.8 - 50.1	19.4 ± 0.9	398 - 450	9.6 ± 0.2		

[a]Up to 450 keV, the average capture cross sections were calculated from the resonance parameters obtained in this analysis. Uncertainties due to the prompt neutron sensitivity of the detector combined with the statistical uncertainties are given. From 400 keV and up to the inelastic threshold, $\bar{\sigma}_\gamma$ was estimated directly from the thick sample capture data. Statistical uncertainties are given. Corrections applied to the data in this energy range and systematic uncertainties are discussed in Sect. 9.5.

large s-wave resonance at 12.487 keV. The uncertainties given in Table 14 include the statistical uncertainties as well as the uncertainties from the correction for the detector neutron sensitivity. The uncertainties in the correction for the detector neutron sensitivity were treated as uncorrelated, a poor approximation when the correction curve is smooth. To the uncertainties given in Table 14, the systematic uncertainties discussed in Sect. 7.2.3 should be added and treated as fully correlated. The average capture cross section given in the 2.0 to 2.5 keV interval was calculated from the resonance parameters obtained in the transmission data analysis of the 2.253-keV resonance.

From 400 keV to the threshold of the inelastic scattering to the first 2^+ state in ^{60}Ni (1355 keV), the thick sample data were corrected for average resonance self-protection and scattering of neutrons in the sample before capture using strength functions. While this is admittedly a poor substitute for individual resonance parameterization as was done below 450 keV, the corrections to the data were small, 2.4% at 450 keV dropping to 0.4% at 1250 keV. The 2.5-mb background found between resonances at lower energies, discussed in Sect. 5.4, was subtracted. The uncertainty in this background correction is the dominant uncertainty and should be considered fully correlated. The average capture cross sections above 400 keV are also given in Table 14 and the uncertainties in the table are the statistical uncertainties only.

The average cross sections up to 1 MeV are shown in Fig. 26, together with a theoretical calculation. The theoretical calculation was provided by C. Y. Fu and obtained using the code TNG.[50] The code TNG calculates the capture cross sections by using transmission coefficients for gamma rays derived from the width of the E1 giant dipole resonance.[51] Only E1 transitions were considered and the gamma ray partial widths are only functions of the gamma-ray energy E_γ, the initial level spin and the final level spin. Level densities and their spin distributions were obtained from the Gilbert and Cameron formula. The parameters of the giant dipole resonance for ^{60}Ni were taken from the photonuclear reaction data[52] (σ_o = 90 mb,E_o = 19.0 MeV, and the Lorentzian width of 5.5 MeV). This model usually predicts the capture cross sections within a factor of two.[51] In this case, the capture cross section was overpredicted and the theoretical predictions in Fig. 26 were normalized by a factor of 0.40.

For comparison with our results, the average capture cross section was calculated with the parameters given in ENDF/B-V. Since ENDF/B-V does not have an isotopic evaluation of ^{60}Ni, the resonance parameters were taken from the elemental evaluation of nickel. In ENDF, the capture cross section is calculated using the resonance parameters to which is added a smooth background. In the evaluation of elemental nickel, the smooth background is of the order of 6 mb. If we assume that this 6-mb background is to be added to all the isotopes of nickel, we can calculate the ENDF/B-V average capture cross section which when compared to our results indicates that the ENDF/B-V infinitely dilute capture cross section for ^{60}Ni above 20 keV is approximately 20 to 25% smaller than our results shown in Fig. 26.

The first s-wave resonance at 12.487 keV contributes 1.5 $\pm$ 0.5 b to the thermal capture cross section. Summing the contributions of the other 29 s-wave resonances at positive energies, we have obtained up to 450 keV gives only 0.03 b. The latest evaluation of the thermal capture cross section[26] gives 2.9 $\pm$ 0.2 b. The difference could be attributed to the direct capture component and to bound levels but the data analyzed in this report are not sensitive to these contributions.

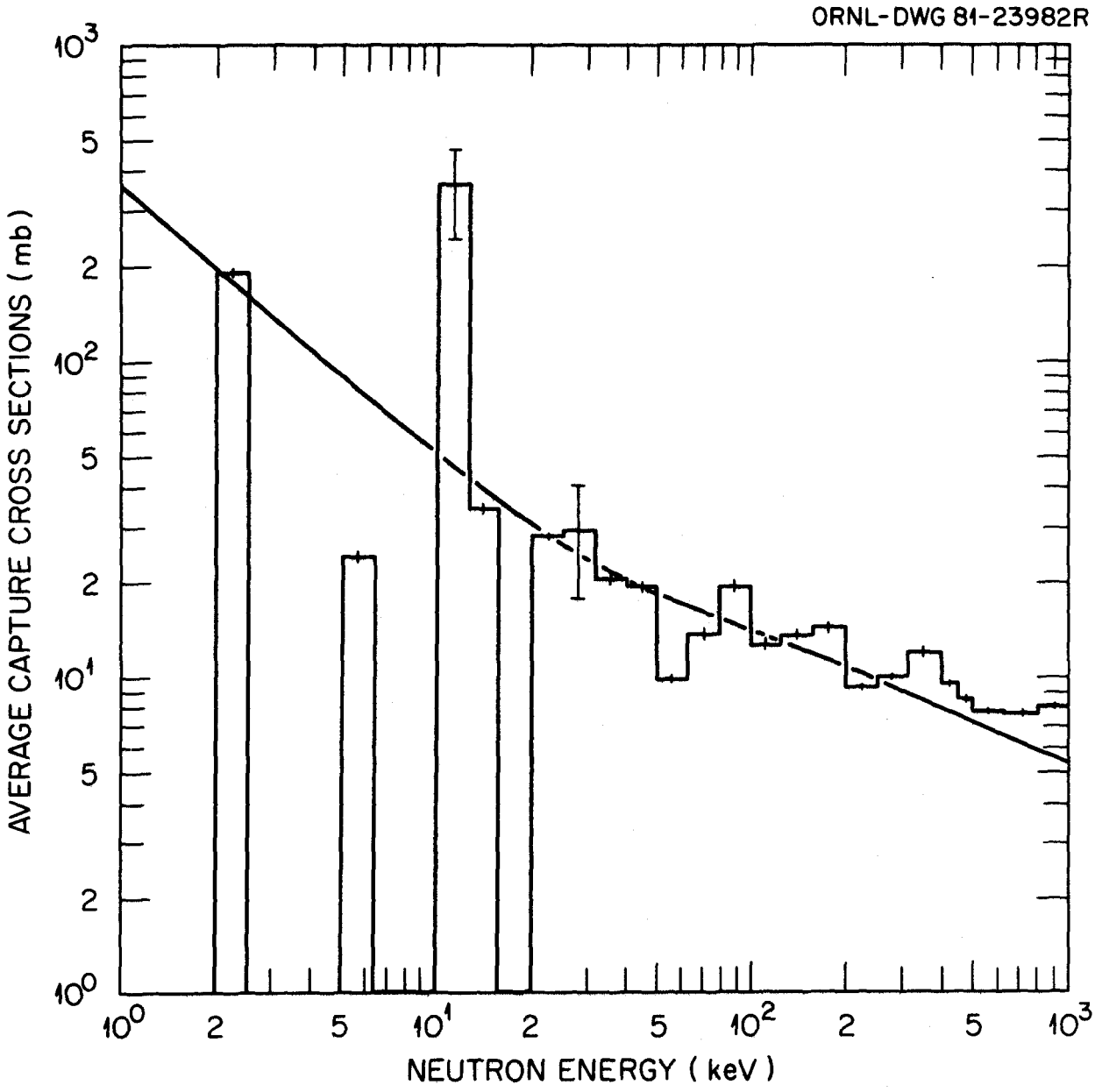

Fig. 26. Ni-60 average capture cross section from 2 keV to 1 MeV as a function of the neutron incident energy. The smooth curve is given by the tail of the giant dipole at 19 MeV normalized by 0.40.

10. CONCLUSIONS

The complete set of resonance parameters from this analysis, including those outside the energy region analyzed, is consistent with both the transmission and the capture data between 2.5 and 450 keV. Although the distribution of the s-wave resonance reduced neutron widths is in good agreement with a Porter-Thomas distribution, the strength of the s-wave resonances from 2.5 to 450 keV is modulated in a way that is suggestive of doorway states as observed in other nuclides in this mass region.

ACKNOWLEDGEMENTS

We gratefully acknowledge the valuable assistance of N. W. Hill in the experimental aspects of the transmission measurements and the extensive help of N. M. Larson during the analysis of the transmission data with the code SAMMY. We thank W. M. MacDonald and D. J. Horen for providing the codes used to perform the Lorentzian averaging of the R-function. We also thank C. Y. Fu for performing the average capture cross-section prediction calculations and R. R. Spencer for helpful discussions on the correlation coefficient between the resonance widths.

REFERENCES

1. M. Divadeenam, *Ni Elemental Neutron Induced Reaction Cross-Section Evaluation*, BNL-NCS-51346, Brookhaven National Laboratory, Upton, N.Y., 1979.

2. D. C. Larson, C. H. Johnson, J. A. Harvey, and N. W. Hill, *Measurement of the Neutron Total Cross Section of Fluorine from 5 eV to 20 MeV*, ORNL/TM-5612, Oak Ridge National Laboratory, Oak Ridge, Tenn., 1976. Also see ref. 11.

3. N. W. Hill, J. A. Harvey, G. S. Slaughter, and A. St. James, *Bull. Am. Phys. Soc.* **17**, 901 (1972). [Also in *Physics Div. Ann. Prog. Rep. 1971*, ORNL-4743, Oak Ridge National Laboratory, Oak Ridge, Tenn., pp. 137.]

4. M. S. Pandey, J. B. Garg and J. A. Harvey, *Phys. Rev.* **C15**, 600 (1977).

5. N. A. Betz, J. W. Reynolds, and G. G. Slaughter, "Rapid Data Acquisition into more than 10^5 channels at ORELA," p. 218 in *Proc. Conf. Computer Systems in Experimental Nucl. Phys.*, Skytop, Pennyslvania, March 2, 1969, Columbia University Report No. CONF-69030.

6. G. F. Auchampaugh, *MULTI, A FORTRAN Code for Least-Squares Shape Fitting of Neutron Cross-Section Data Using the Reich-Moore Multilevel Formalism*, LA-5473-MS, Los Alamos Scientific Laboratory, Los Alamos, N.M., 1974.

7. N. M. Larson and F. G. Perey, *User's Guide for SAMMY: A Computer Model for Multilevel R-Matrix Fits to Neutron Data Using Bayes' Equations*, ORNL/TM-7485, Oak Ridge National Laboratory, Oak Ridge, Tenn., 1980. See also *SAMMY Users Notes of March, April, and May 1981* (unpublished).

8. J. C. Craven, *SELAVG A Selective Data Averaging Program for ORELA Data Formatted Files*, (unpublished, 1975).

9. F. G. Perey, G. T. Chapman, W. E. Kinney, and C. M. Perey, "Recent Results for ^{58}Ni and ^{56}Fe at ORELA," p. 530 in *Neutron Data of Structural Materials for Fast Reactors*, Geel, Belgium, 1977 .

10. D. J. Horen, J. A. Harvey, and N. W. Hill, *Phys. Rev.* **C20**, 478 (1979).

11. D. C. Larson, J. A. Harvey, N. W. Hill, and C. H. Johnson, *Measurement of Neutron Total Cross Section of Natural Nickel from 2 keV to 20 MeV*, ORNL/TM-8203, Oak Ridge National Laboratory, Oak Ridge, Tenn., 1982.

12. R. L. Macklin and B. J. Allen, *Nucl. Instrum. Methods*, **91**, 565 (1971).

13. R. L. Macklin, N. W. Hill, and B. J. Allen, *Nucl. Instrum. Methods*, **96**, 509 (1971).

14. R. L. Macklin, R. W. Ingle, and J. Halperin, *NSE* **71**, 205 (1979).

15. R. L. Macklin, J. Halperin, and R. R. Winters, *Nucl. Instrum. Methods* **164**, 213 (1979).

16. R. L. Macklin, *LSFIT - A Least Squares Computer Program to Fit Neutron Capture Cross Section Resonance Data from ORELA*, ORNL/TM-4810, Oak Ridge National Laboratory, Oak Ridge, Tenn., 1975.

17. B. J. Allen, A. R. de L. Musgrove, R. L. Macklin, and R. R. Winters, "Neutron Sensitivity of Capture Gamma Ray Detectors," p. 506 in *Neutron Data for Structural Materials for Fast Reactors*, Geel, Belgium, 1977.

18. F. G. Perey, "Neutron Energy Standards", p. IX.1 in *Standard Reference and Other Important Nuclear Data by CSEWG*, ENDF-300, 1979.

19. J. Halperin, C. H. Johnson, R. R. Winters, and R. L. Macklin, *Phys. Rev.* **C21**, 545 (1980).

20. C. Coceva, R. Simonini and D. K. Olsen, "Calculation of the ORELA Neutron Moderator Spectrum and Resolution Function," to be published in *Nucl. Inst. Meth.* (1982).

21. H. Beer and R. L. Macklin, "^{178,179,180}Hf and ^{180}Ta(n,γ) Cross Section and Their Contribution to Stellar Nucleosynthesis," to be published in *Phys. Rev. C.* (1982).

22. J. A. Farrell, E. G. Bilpuch, and H. W. Newson, *Ann. Phys.* **37**, 367 (1966).

23. R. G. Stieglitz, R. W. Hockenbury, and R. C. Block, *Nucl. Phys* **A163**, 592 (1971).

24. D. B. Syme, P. H. Bowen and A. D. Gadd, "Resonance Analysis Analysis of Nickel Transmission Data," p. 703 in *Neutron Data of Structural Materials for Fast Reactors*, Geel, Belgium, 1977.

25. F. Fröhner, "Evaluation of Resonance Data for Cr, Fe, Ni below 300 keV with special regard to Doppler effect calculation," p. 138 in *Neutron Data of Structural Materials for Fast Reactors*, Geel, Belgium, 1977.

F. Fröhner, "Resonance Cross Sections for Structural Material," p. 268 in *Neutron Physics and Nuclear Data for Reactors*, Harwell, 1978.

26. S. F. Mughabghab, M. Divadeenam, and N. E. Holden, *Neutron Cross Sections, Vol. 1: Neutron Resonance Parameters and Thermal Cross Sections*, Academic Press, 1981, p. 28-8. 1973.

27. H. Beer et al., KFK Report 1271/3, Kernforschungszentrum Karlsruhe, Germany, 1971.

28. J. B. Garg et al., *Phys. Rev.* **C3**, 2447 (1971).

29. F. Fröhner, Kernforschungszentrum Karlsruhe, Germany, personal communication to S. F. Mughabghab and D. I. Garger, Brookhaven National Laboratory, Upton, N.Y., 1972.

30. A. Ernst, D. Kompe, and F. H. Fröhner, "High Resolution Measurements of Radiative Neutron Capture in ^{47}Ti, ^{56}Fe, ^{58}Ni, ^{60}Ni, and ^{61}Ni between 7 and 200 keV", p. 633 in *Second Int. Conf. on Nucl. Data for Reactors*, Helsinki, 1970.

31. R. W. Hockenbury et al., *Phys. Rev.*, **178**, 1746 (1969).

32. R. G. Stieglitz, J. T. Reynolds, C. J. Slavik, and C. R. Lubitz, *Evaluated Neutron Cross Sections for Chromium, Iron, and Nickel*, KAPL-M-7156, Knolls Atomic Power Laboratory, Schenectady, N.Y., 1973.

33. R. G. Stieglitz, unpublished PhD Thesis, RPI, 1970.

34. C. E. Porter and R. G. Thomas, *Phys. Rev.* **104**, 483 (1956).

35. A. Gilbert and A. G. W. Cameron, *Can. J. Phys.* **43**, 1446 (1965).

36. W. Dilg, W. Schantl, H. Vonach, and M. Uhl, *Nucl. Physc.* **A217**, 269 (1973).

37. *Nuclear Data*, B2-5-85, Nuclear Data Group, Oak Ridge National Laboratory, Oak Ridge, Ten., 1968.

38. N. M. Larson, *LEVDEN: A Level Density Code Using the Fermi-Gas Model*, (unpublished, 1982).

39. J. E. Lynn, *The Theory of Neutron Resonance Reactions*, Clarendon Press, Oxford, 1968.

40. M. S. Pandey, J. B. Garg, J. A. Harvey, and W. M. Good, p. 748 in *Proc. Conf. Nuclear Cross Sections and Technology*, Vol. II, NBS Special Publ. 425, 1975.

41. J. B. Garg, V. K. Tikku, J. A. Harvey, R. L. Macklin, and J. Halperin, *Phys. Rev.* **C24**, 1922 (1981).

J. B. Garg, V. K. Tikku, J. A. Harvey, J. Halperin, and R. L. Macklin, *Phys. Rev.* **C25**, 1808 (1982).

J. B. Garg, V. K. Tikku, and J. A. Harvey, to be published in *Phys. Rev. C.*

42. J. A. Harvey, M. Divadeenam, J. B. Garg, and V. K. Tikku, *Bull. Am. Soc.* **26**, 1138 (1981).

J. B. Garg, V. K. Tikku, J. A. Harvey, R. L. Macklin, and M. Divadeenam, *Bull. Am. Soc.* **26**, 1138 (1981).

43. C. Mahaux and H. A. Weidenmuller, *Nucl. Phys.* **A91**, 241 (1967).

W. M. MacDonald and A. Z. Mekjian, *Phys. Rev.* **160**, 730 (1967).

A. K. Kerman and A. F. R. de Toledo Piza, *Ann. Phys.* **48**, 173 (1968).

44. T. Teichmann and E. P. Wigner, *Phys. Rev.* **87**, 123 (1952).

45. H. Beer and R. R. Spencer, *Nucl. Phys.*, **A240**, 29 (1975).

46. J. B. Garg, R. L. Macklin, and J. Halperin, *Phys. Rev.*, **C18**, 2079 (1978).

47. C. M. Perey and F. G. Perey, *Evaluation of Resonance Parameters for Neutron Interaction with Iron Isotopes for Energies up to 400 keV*, ORNL/TM-6405, Oak Ridge National Laboratory, Oak Ridge, Tenn., 1980.

48. R. R. Spencer and R. L. Macklin, *Nucl. Sci. Eng.* **61**, 346 (1976).

49. J. B. Garg, V. K. Tikku, J. Halperin, and R. L. Macklin, *Phys. Rev.*, **C23**, 683 (1981).

50. C. Y. Fu, "Development of a Two-Step Hauser-Feshbach Code with Precompound Decays and Gamma-Ray Cascades - A Theoretical Tool for Cross Section Evaluations," p. 328 in *Conf. on Nucl. Cross Sections and Technology, March 3-7, 1975*, Washington, D. C., Vol. I, NBS Special Pub. 425, CONF-750303-14, October 1975.

51. P. Axel, *Phys. Rev.* **126**, 671 (1962).

52. E. G. Fuller, H. M. Gerstenberg, H. Vander Molen, and T. C. Dunn, *Photo Nuclear Reaction Data*, NBS Special Pub. 380, 1973.

ORNL-5893
ENDF-330

INTERNAL DISTRIBUTION

1-2.	Central Research Library	24-28.	N. M. Larson
3.	Document Reference Section	29-33.	R. L. Macklin
4-6.	Laboratory Records Department	34.	F. C. Maienschein
7.	Laboratory Records-RC	35.	D. K. Olsen
8.	ORNL Patent Section	36.	R. W. Peelle
9-10.	L. S. Abbott	37-41.	C. M. Perey
11.	G. T. Chapman	42-46.	F. G. Perey
12.	G. de Saussure	47.	R. R. Spencer
13.	J. K. Dickens	48.	L. W. Weston
14.	C. Y. Fu	49-53.	R. R. Winters
15-19.	J. A. Harvey	54.	A. Zucker
20.	N. W. Hill	55.	P. W. Dickson, Jr. (consultant)
21.	D. J. Horen	56.	H. J. C. Kouts (consultant)
22.	C. J. Johnson	57.	W. B. Loewenstein (consultant)
23.	D. C. Larson	58.	R. Wilson (consultant)

EXTERNAL DISTRIBUTION

59. Office of Assistant Manager for Energy Research and Development, Department of Energy, Oak Ridge Operations, Oak Ridge, TN 37830
60. S. L. Whetstone, Division of Nuclear Sciences, Office of Basic Energy Sciences, U.S. Department of Energy, Rm G-355, Washington, D.C. 20545
61. B. J. Allen, AAEC Research Establishment, Private Mail Bag, Sutherland 2232, NSW, Australia
62. G. F. Auchampaugh, Los Alamos Scientific Laboratory, MS 442, P-3, Los Alamos, NM 87545
63. H. Beer, Kernforschungszentrum Karlsruhe, Institut für Angewandte Kernphysik, D7500 Karlsruhe 1, Germany
64. R. F. Carlton, Middle Tennessee State University, Physics Department, Box 407, Murfreesboro, TN 37132
65. M. Divadeenam, National Nuclear Data Center, 197D, Brookhaven National Laboratory, B197d, Upton, NY 11973
66. F. Fröhner, INR, Kernforschungszentrum, Postfach 3640, D-75 Karlsruhe, West Germany
67. J. B. Garg, Department of Physics, New York State University, Albany, NY 12203
68. Prof. Claude Mahaux, Institut de Physique, Sart Tilman, 4000 Liege 1, Belgium
69. W. M. Macdonald, Physics Department, University of Maryland, College Park, MD 20740

EXTERNAL DISTRIBUTION (Contd)

70. N. Moxon, Nuclear Physics Division, Atomic Energy Research Establishment, Harwell, Didcot, Oxon. OX11 ORA, United Kingdom
71. M. G. Sowerby, Nuclear Physics Division, Bldg. 418, Atomic Energy Research Establishment, Harwell, Didcot, Oxon, OX11 ORA, United Kingdom
72. D. B. Syme, Nuclear Physics Division, Atomic Energy Research Establishment, Harwell, Didcot, Oxon. OX11 ORA, United Kingdom
73. H. Weigman, Bureau Central de Mesures Nucleaires, Steenweg Naar Retie, B-2440, GEEL
74. K. Wisshak, Kernforschungszentrum Karlsruhe GmbH, Postfach 3640, D7500, Karlsruhe 1, Germany

75-101. Technical Information Center (TIC)

102-207. National Nuclear Data Center, ENDF Distribution, Brookhaven National Laboratory, Upton, Long Island, NY 11973